Prepared for:

Rijkswaterstaat / RIKZ

Sensitivity analysis of numerical aspects of SWAN

Geographical and spectral grid resolution and convergence behaviour

Report

December 2007

H4918.39

WL | delft hydraulics

Prepared for:

Rijkswaterstaat / RIKZ

Sensitivity analysis of numerical aspects of SWAN

Geographical and spectral grid resolution and convergence behaviour

Ivo Wenneker and Jacco Groeneweg

Report

December 2007

WL | delft hydraulics

Client:	Rijkswaterstaat / RIKZ
Title:	Sensitivity analysis of numerical aspects of SWAN

Abstract:

Within the framework of het project 'Uitvoering Plan van Aanpak SBW-RVW Waddenzee' (Plan of Action on the Boundary Conditions for the Wadden Sea) a sensitivity analysis of numerical aspects in SWAN has been performed and reported in WL / RIKZ / Alkyon / NRL (2007). Focussing on the Amelander Zeegat insight was obtained in the discretisation errors, convergence behaviour and requirements to curvi-linear grids. The latter study left three unresolved issues with respect to discretisation errors in geographical space, required directional resolution in spectral space and the convergence behaviour of the computations. The aim of the present study is to resolve these issues.

The main conclusions of the present study are:

- For simulations in the Amelander Zeegat the original gradient-based convergence criterion yields solutions that have not sufficiently converged. More accurate results have been obtained with the curvature-based convergence criterion. Nevertheless, convergence errors appear in some local areas.
- Taking into account the full action density balance, i.e. including all source terms, errors due to geographical grid resolution were at most 10 - 20 cm in significant wave height and 0.2 - 0.3 s in mean wave period for a mesh size of 100m, and 2 - 5 cm and 0.1 - 0.2 s respectively for a 20 m mesh. The discretisation errors on the 20 m grid resolution are smaller than the physical representation errors (5 - 10 cm resp. 1 - 2 s), in contrast to the errors with the 100 m grid resolution. Therefore a 20 m grid is preferred over a 100 m grid.
- Especially, the prediction of the mean wave direction detoriates significantly in regions with strong refraction, when the directional resolution is decreased. For values smaller than 6° effects due to scintillation strongly affects the accuracy, mainly in the lee side of the islands. Based on the single test in the Amelander Zeegat we conclude that an optimal value for the directional resolution is 6^0.

References:

Ver	Author		Date	Remarks	Review		Approved by	
1	I. Wenneker et al..		December 2007	draft	M.J.A. Borsboom		M.R.A. van Gent	
2	I. Wenneker and J. Groeneweg		December 2007	final	M.J.A. Borsboom		M.R.A. van Gent	

Project number:	H4918.39
Keywords:	Numerical analysis, SWAN, SBW, hydraulic boundary conditions
Number of pages:	26
Classification:	None
Status:	Final

Contents

1 Introduction

1.1 Background

The spectral wind wave model SWAN plays a key role in the estimation of the Hydraulic Boundary Conditions (HBC) for the primary sea defences of the Netherlands. Since some uncertainty remains with respect to the reliability of SWAN for application to the geographically complex area of the Wadden Sea, a number of activities have been initiated under project 'Uitvoering Plan van Aanpak SBW-RVW Waddenzee' (Plan of Action on the Boundary Conditions for the Wadden Sea) to devise a strategy for the improvement of the model. This activity is carried out in parallel with a measurement campaign that is being undertaken in the Wadden Sea to assist in the establishment of the boundary conditions ('SBW-Veldmetingen').

In this context, hindcast and sensitivity studies carried out with SWAN for the Amelander Zeegat in the Wadden Sea (WL 2006; Royal Haskoning 2006; WL 2007) have shown that the performance of SWAN in the Wadden Sea is quite good. Some physical shortcomings within SWAN, in applying the model to the Wadden Sea, have been identified and will be investigated next year. Also several numerical aspects have been highlighted. The present study will focus on the numerical aspects.

1.2 Previous numerical study

In report WL / RIKZ / Alkyon / NRL (2007) results of a numerical sensitivity study with respect to the SWAN model, again with application to the Wadden Sea, were reported. The following conclusions are drawn in that report:

- With respect to the convergence behaviour of the simulations of the Amelander Zeegat, the presently used convergence criteria (default in SWAN) are not robust enough, i.e. too few iterations are employed. By means of the curvature-based convergence criteria of Zijlema and Van der Westhuysen (2005) more accurate, converged solutions for the significant wave height H_{m0} and T_{m01} are obtained. Even more iterations are needed when also converged directional parameters are required.

- Non-uniform and curvi-linear grids for wave model applications should be denser in areas where physical processes cause strong variations in the wave conditions. Based on this principle a non-uniform curvi-linear grid for the Amelander Zeegat was constructed.

- Implementations of physical processes, mainly quadruplet interactions, strongly depend on the presently used exponential frequency distribution and the optimal choice of 1.1 as relative frequency step. The lowest model frequency is determined by the peak frequency on the offshore boundary. The highest model frequency can be based on peak frequencies that occur about 1 km from the coast. In practice an upper limit of 1 Hz suffices for the Wadden Sea.

In WL / RIKZ / Alkyon / NRL (2007) also error estimates due to geographic grid discretisations are presented as well as accuracy estimates due to spectral grid discretisations. The approach of the research was questioned by the external reviewer. In a discussion between the executor (Marcel Zijlema, at that time employed at RIKZ), the external reviewer (Mart Borsboom of WL | Delft Hydraulics, who was hired by the client RIKZ, Rijkswaterstaat) and the client (Martin Verlaan of RIKZ, Rijkswaterstaat) no final solution could be obtained. A summary of the discussion was made by the client and is added here in Appendix A. The summary is in Dutch.

The minor discussion points have been processed in WL / RIKZ / Alkyon / NRL (2007). Nevertheless, it was concluded that some issues needed further research:

- With respect to the estimation of errors due to geographical grid discretisations conclusions were based on computations in which source terms were neglected, and thus pure wave propagation was considered. It is not a priori evident whether the physical accuracy of the source terms affects the numerical accuracy of the solution. Therefore, the computations in WL / RIKZ / Alkyon / NRL (2007, Section 2.2) should be repeated, but with the source terms activated. Because the quadruplet interaction term might strongly affect the accuracy, the same computations should be repeated with the quadruplet term deactivated.

- The estimates of the errors due to spectral grid discretisation are based on quasi-Courant numbers, which is conceptually incorrect. Therefore, the conclusions drawn have to be recalled. By performing computations as was done for swell (see WL / RIKZ / Alkyon / NRL, 2007, Section 4.3), insight in the errors due to grid discretisations in directional space can be obtained. For that purpose computations should be carried out in which the number of directional bins varies.

- In the study on convergence behaviour (WL / RIKZ / Alkyon / NRL, 2007, Chapter 3) the computations were performed with a maximum number of iterations equal to 30. Inspection of the iteration behaviour shows that the wave period has not converged after 30 iterations. The computations should be repeated with a higher maximum number of iterations.

1.3 Aim of the present study

The aim of the present study is to resolve the remaining three issues mentioned above with respect to discretisation errors in geographical space, required directional resolution in spectral space and the convergence behaviour of the computations.

1.4 Contents of the report

By means of some SWAN computations in the Amelander Zeegat the convergence behaviour is studied in Chapter 2. In Chapter 3 the analysis on the grid resolution is described. The geographical resolution is discussed in Section 3.2, the spectral resolution in Section 3.3, with the focus on the directional resolution. Conclusions on the results in this

report are mentioned in Section 4.1, whereas a comparison with the previous study on numerical aspects in SWAN (WL / RIKZ / Alkyon / NRL, 2007) is made in Section 4.2.
The present study has been carried out by Ivo Wenneker and Jacco Groeneweg. The external review was carried out by Mart Borsboom.

2 Convergence behaviour

2.1 Introduction

Because the action balance equation is solved implicitly, nonlinear terms within that balance have been linearised, and non-linear four-wave interactions and refraction may propagate energy from one quadrant to another, the (stationary) SWAN solution is determined iteratively (Zijlema and Van der Westhuysen, 2005). In general, the iterative process can be stopped as soon as the approximate solution is accurate enough. A good termination criterion is very important, because if the criterion is too weak the solution obtained may be too inaccurate and perhaps even useless, whereas if the criterion is too severe the iteration process may cost too much computational time or in the worst case may never stop.

In the hindcasts performed by WL (2006) the original *gradient-based convergence criterion* is used. This means that the iteration process is terminated if the maximum number of iterations, in this report denoted as *n,max*, is reached (*n,max* was taken as 50 in WL, 2006) or the following criteria for the significant wave height H_{m0} and mean relative wave period T_{m01} are satisfied in at least *npnts* = 99% of all wet grid points (i,j), see SWAN User Manual (2006) [1]:

$$\frac{\left|H_{m0}^{n}(i,j)-H_{m0}^{n-1}(i,j)\right|}{H_{m0}^{n-1}(i,j)}<drel \quad \text{or} \quad \frac{\left|H_{m0}^{n}(i,j)-H_{m0}^{n-1}(i,j)\right|}{\overline{H_{m0}}}<dhoval \tag{2.1}$$

and

$$\frac{\left|T_{m01}^{n}(i,j)-T_{m01}^{n-1}(i,j)\right|}{T_{m01}^{n-1}(i,j)}<drel \quad \text{or} \quad \frac{\left|T_{m01}^{n}(i,j)-T_{m01}^{n-1}(i,j)\right|}{\overline{T_{m01}}}<dtoval\ . \tag{2.2}$$

Here, $\overline{H_{m0}}$ and $\overline{T_{m01}}$ are the average significant wave height and wave period respectively, where the average is taken over all wet grid points. For each of the parameters *drel*, *dhoval* and *dtoval*, the value 0.01 is taken.

Recently, an alternative for the gradient-based convergence criterion was developed by Zijlema and Van der Westhuysen (2005), the so-called *curvature-based convergence criterion*. In this criterion not only the relative error in significant wave height (2.1) is considered, but also the second derivative or curvature of the curve traced by the series of iterates (iteration curve). Since the curvature of the iteration curve must tend towards zero as convergence is reached, terminating the iteration process when a certain minimum curvature has been reached would be a more robust break-off procedure. The resulting curvature-based termination criterion is given by

1 Enabled by means of the keyword NUM ACCUR [*drel*] [*dhoval*] [*dtoval*] [*npnts*] STAT MXITST=[*n,max*]

$$\frac{\left|H_{m0}^{n}-(H_{m0}^{n-1}+H_{m0}^{n-2})+H_{m0}^{n-3}\right|}{2H_{m0}^{n}}<\varepsilon_C, \qquad n=3,4,\cdots \tag{2.3}$$

where ε_C is a given maximum allowable curvature. The curvature measure is made non-dimensional through normalization with H_{m0}^{n}. Conditions (2.1) and (2.3) must be satisfied in at least *npnts* = 99% of all wet grid points before the iterative process stops. This curvature requirement is the primary criterion. The weaker criterion (2.1) is retained in addition to the stricter criterion (2.3). Note that criterion (2.2) has been abandoned in the curvature-based convergence criterion. The new stopping criteria[2] have been applied with the default curvature parameter of ε_C = 0.001.

In order to assess the two convergence criteria, we have carried out several simulations. The results have been compared to results of benchmark computations, in which a sufficiently large number of iterations are performed.

2.2 Results

The calculations of the Amelander Zeegat are carried out with (nested) areas, see Figure 2.1. The basis grid used for the largest area (*area1*) has a mesh size of 100 m, while for the other nested area (*area2*) a basis mesh size of 20 m is employed. The remaining nested areas, south and south-east of *area2*, have not been considered. Further details on these grids can be found in WL (2006, Section 3.4.1 and Figure 3.25). Here we perform three computations:

- *area1*, with a uniform water level and no currents;
- *area2*, with a uniform water level and no currents;
- *area2*, with spatially varying water level and currents.

We have considered the storm situation of January 2, 2005 at 10:00 hr, see also WL (2006, Section 3.4). At this instant the tidal stage is flood. A uniform wind field is imposed based on measurements at Vlieland: the wind speed is 17 m/s and the wind direction is 274 degrees. In WL/Alkyon (2007) for the same area a more representative wind was deduced from the HIRLAM model, with a wind speed of 20 m/s and direction of 277 degrees. For the present study the difference in wind speed is not relevant. The water level at NES (see Figure 2.1 for its location) is 1.04 m. For the computations with uniform water level field this value has been used. Spatially varying water level and current fields have been obtained with WAQUA. These have been taken from WL (2006). The offshore boundary conditions have been obtained from the so-called Kuststrook model. Offshore boundaries for this model were obtained from the directional waveriders at the locations SON and ELD (see Figure 2.1 for their locations). At the instant considered the significant wave height, mean period T_{m01}, mean wave direction and directional spreading were equal to 5.3m, 7.2s, 293 degrees and 33 degrees, respectively, at station ELD, and 6.0m, 7.3s, 296 degrees and 33 degrees, respectively, at station SON.

Simulations have been performed with *n,max* = 80 iterations. The reason for choosing this large number is to ensure convergence. As we will see, no changes in significant wave

2 Enabled by means of the keyword NUM STOPC 0.00 [*drel*] [ε_C] [*npnts*] STAT MXITST=[*n,max*]

height H_{m0} and almost no changes in mean wave period T_{m01} are found after already about 20 to 30 iterations.

In the simulations, all physical processes are included. In contrast to the present study triads were not activated in WL / RIKZ / Alkyon / NRL (2007), which explains the small differences between our results and theirs. For wind generation the formulation of Yan (1987) and for whitecapping the adapted formulation of Alves and Banner (2003) were employed, respectively[3], as described in Van der Westhuysen et al. (2006). The SWAN solution after *n,max* iterations are shown in Figures 2.2a, 2.3a and 2.4a for the three simulations (*area1* and *area2*; the latter with uniform and spatially-varying model input for water level and current).

2.3 Analysis of convergence behavior

Figures 2.2b, 2.3b and 2.4b depict the convergence behaviour of H_{m0} and T_{m01} for the three simulations. This is done by showing the ratio of the 'error' and the converged solution at several buoys in Amelander Zeegat for the three computations. The converged solution is the solution after *n,max* = 80 iterations, and the error is the difference between the solution after *n* iterations and the converged solution.

Using results of previous section, we can now determine at which iteration convergence criteria (2.1), (2.2) and (2.3) are satisfied. The errors given by (2.1) (2.2) and (2.3) are presented in the upper left, upper right and lower left panels respectively of Figures 2.2c, 2.3c and 2.4c. The number of required iterations for convergence, indicated by *n,conv*, is given in Table 2.1. For the three computations both the gradient-based and the curvature-based criterion have been considered.

	Gradient-based convergence criterion (2.1) and (2.2)	**Curvature-based convergence criterion (2.1) and (2.3)**
Δx = 100m	7	19
Δx = 20m (constant water level, no current)	10	16
Δx = 20m (space-varying water level and current)	9	19

Table 2.1 Number of required iterations for convergence, *n,conv* obtained with difference convergence criteria

2.3.1 Analysis of gradient-based convergence criteria

Comparing the presented values with the convergence behaviour shown in Figures 2.2b, 2.3b and 2.4b, it may be concluded that the gradient-based convergence criterion is not at all strict enough to obtain accurate results. Figures 2.2b, 2.3b and 2.4b show that the iteration process can converge so slowly that at a certain iteration level the difference between

3 Enabled by means of the keyword "GEN3 WESTH".

successive iterates can be small enough to meet the convergence criteria, causing the iteration process to stop, even though the converged solution has not yet been found. In particular, this happens when convergence is non-monotonic such that the process is terminated at local maxima or minima that may not coincide with the converged solution. These conclusions are similar to those in earlier studies of Alkyon (2007) and WL / RIKZ / Alkyon / NRL (2007), in which the same test computations were considered.

2.3.2 Analysis of curvature-based convergence criterion

The curvature-based convergence criterion yields solutions that are more accurate, i.e. that are closer to the converged solution. This is a consequence of the curvature-based convergence criterion being stricter than the gradient-based convergence criterion, as can be deduced from Figures 2.2c, 2.3c and 2.4c. In these figures also the non-dimensional curvature of the mean wave period $T_{m\text{-}1,0}$ (defined as for the significant wave height in (2.3)) is shown.

The convergence behaviour is rather similar for the three simulations. This is beneficial, since it implies that the same convergence criterion can be used regardless of grid cell size and the presence of currents and water level variations. In other words, the curvature-based convergence criterion is robust.

To determine whether the curvature-based convergence criterion yields truly converged solutions (=grid-converged solutions, i.e. solutions that are converged given the grid), two types of relative error have been computed over the entire computational domain:

- The first type of relative error concerns the relative difference between the grid-converged solution (after *n,max* iterations) and the converged solution based on the curvature-based convergence criterion (after *n,conv* iterations). In other words, this type of error indicates how far the converged solution is from the grid-converged solution, i.e. the 'exact' SWAN solution on a given grid.
- The second type of relative error concerns the relative difference between the subsequent iterates of the grid-converged solution, i.e. the solutions after (*n,max* – 1) and *n,max* iterations. In other words, this type of error quantifies the 'wiggly' behaviour between the grid-converged solutions at subsequent iterations. This wiggly behaviour is due to energy transfer back and forth between adjacent frequency and directional bins at subsequent iterates.

The relative errors pertaining to the 'wiggly' behaviour, see Figures 2.2d, 2.3d and 2.4d, are over the entire domain (much) smaller than 1%. This is acceptable.

On the other hand, the relative errors pertaining to the difference between the curvature-based converged solution and the grid-converged are much larger, see Figures 2.2e, 2.3e and 2.4e. The relative errors go up to 10%, in particular at the ebb-tidal delta, in between and at the lee side of the islands, and at the coastline of the islands. This indicates that the curvature-based criterion with the given curvature setting is not strict enough, and that more iterations are required to get converged solutions. This can be achieved by reducing the maximum allowable curvature ε_C . Note that the premature convergence with the considered criterion has also been recognized in WL (2007). In that report, it has been proposed to add a curvature-based termination criterion based on the period T_{m01}, besides the existing

criterion based on H_{m0}. Since this issue has been elaborated on in more detail in WL (2007), we leave it here as it is.

2.4 Conclusions

Considering the convergence behaviour of the simulations of the Amelander Zeegat, it appears that the original gradient-based convergence criterion is not robust enough, i.e. too few iterations are employed. By means of the curvature-based convergence criterion of Zijlema and Van der Westhuysen (2005), more accurate wave parameters are obtained. However, the default settings of the curvature-based convergence criterion are not strict enough, since the relative errors in the wave height and wave period are up to 10%. These large errors occur in regions with strong depth-induced breaking and triad interaction, such as the North Sea coast of the barrier islands and the ebb tidal delta, as well as in the regions immediately downwind of the barrier islands, where young wind sea is generated. Since this issue has been elaborated on in more detail in WL (2007), we leave it here as it is.

3 Analysis of errors in wave parameters due to geographic and spectral grid resolution

3.1 Introduction

To verify the SWAN model results for e.g., Amelander Zeegat, it is important to get insight in the numerical accuracy of the computations, which is determined among other things by the resolution of the geographical and spectral grid. In Sections 3.2 and 3.3, we estimate global errors in the significant wave height H_{m0}, mean wave period $T_{m-1,0}$, mean wave direction θ and directional spreading σ due to the use of:

- geographic grid resolution and
- spectral grid resolution,

respectively, of the model for the Amelander Zeegat. For details about the latter model we refer to WL (2006).

3.2 Analysis of global error due to geographic grid resolution

3.2.1 Introductory remarks

In this section the global error due to geographic grid resolutions is studied in a similar manner as was done in WL / RIKZ / Alkyon / NRL (2007). In that report it was assumed that the geographic space discretisation does not affect the accuracy of the source terms and that the effect of the source terms on the accuracy of energy transport in geographical space may be negligible. Therefore, all physical processes including refraction were disabled in that study. However, the drawn conclusions may not necessarily pertain to practical SWAN applications, since in the latter all physical processes are included. In the present study the computations of WL / RIKZ / Alkyon / NRL (2007) have been repeated with the source terms activated.

The present formulation for quadruplet interaction in SWAN by means of the DIA (discrete interaction approximation) might affect the geographic grid convergence. Therefore, two sets of computations are performed: one set with all source terms activated, and one set with all source terms except the quadruplets activated. Note that in all computations the source terms include the triads.

The global error is the error occurring in the numerical approximation. Let ϕ be the exact solution of the continuous model problem and ϕ_h the numerical approximation obtained with a discretised model with mesh size h, then the global error is defined as:

$$\varepsilon_h = \phi - \phi_h \tag{3.1}$$

To get insight in the global error, we make computations with three different mesh sizes: h, $2h$ and $4h$. Next, we calculate the following mesh differences in the solution of subsequent mesh sizes:

$$\Phi_h = \phi_{2h} - \phi_h$$
$$\Phi_{2h} = \phi_{4h} - \phi_{2h} \tag{3.2}$$

By means of the so-called *Richardson correction* we may obtain an estimate of order p for the global error. The estimate of the global error is

$$\phi - \phi_h \approx \frac{1}{1-2^p}\left(\phi_{2h} - \phi_h\right) = \frac{\Phi_h}{1-2^p} \tag{3.3}$$

Thus, we have

$$p = \log\left(\frac{\Phi_{2h}}{\Phi_h}\right) \Big/ \log 2 \tag{3.4}$$

For smooth solutions, it is generally true that the higher the order of accuracy of an approximation, the better it is able to produce a numerical solution that is closer to the exact solution on a given geographic grid.

3.2.2 Description of test case

The calculations of the Amelander Zeegat are carried out with four (nested) areas, see Figure 2.1. All areas are covered with uniform grids. The basis grid used for the largest area (*area1*) has a mesh size of 100 m, while for the other nested areas (*area2*, *area3* and *area4*) a basis mesh size of 20 m is employed. Further details on these grids can be found in WL (2006, Section 3.4.1 and Figure 3.25). Here we repeat the calculations twice for *area1* with mesh sizes 200 m and 400 m and for *area2* with sizes 40 m and 80 m. The computations with three resolutions on the two areas have been performed both with quadruplets activated and with quadruplets de-activated. This leads to a total of 2x3x2=12 simulations.

We consider the storm situation of January 2, 2005 at 10:00 hr. The environmental conditions in terms of wind, water level, current and offshore boundary conditions have been described in Section 2.2. Details on model settings can be found in the WL (2006, Section 3.4). The computations for *area1* have been performed with constant water level and no current, while the computations for *area2* have been performed with currents and a nonuniform level. All the calculations are carried out with 80 iterations, which is enough to obtain converged solutions (see Chapter 2). Now the errors are not partly diffused by convergence errors.

The SWAN solution on *area1* (h = 100m) and on *area2* (h = 20m) are shown in Figures 2.2a and 2.4a.

3.2.3 Global errors of wave parameters computed for *area1*

Figures 3.1, 3.2, 3.3 and 3.4 depict the mesh differences Φ_h and Φ_{2h} of wave parameters H_{m0}, $T_{m-1,0}$, θ and σ with and without quadruplets at domain *area1* with basis mesh size of h = 100 m. All buoy locations are indicated in the figures. The largest differences due to grid discretisation are found on the ebb-tidal delta between the islands Terschelling and Ameland and, to some lesser extent, between the islands and the mainland. For each wave parameter the overall patterns of Φ_h and Φ_{2h} are very similar. The mesh differences become smaller as the mesh sizes become smaller. At h = 100 m, the largest mesh difference in H_{m0}, $T_{m-1,0}$, θ and σ are in order of 10 – 20 cm, 0.2 – 0.3 s, 5 – 10^0 and 5 – 10^0, respectively. By comparing Figures 3.1 with 3.3, and 3.2 with 3.4, we conclude that activation of the quadruplets by means of the DIA has hardly an effect on the mesh differences.

Looking more specifically, the mesh differences of H_{m0}, $T_{m-1,0}$, θ and σ in some wave buoys in the Amelander Zeegat have been determined. These are displayed in Tables 3.1 and 3.2. As expected, the smallest differences can be found near the outer boundary (AZB11 and AZB12). The largest differences are on the ebb-tidal delta and between the islands (AZB21, AZB22, AZB31 and AZB32), and are in the order 5 cm (wave height), 0.25 s (wave period) for h=100 m. For h=200 m these errors are of the order 10 cm respectively 0.5 s. The differences in mean wave direction and directional spreading are less than 1^0.

From Figures 3.1a-3.4a and Table 3.1 we observe that doubling the grid resolution roughly doubles the mesh difference for the significant wave height and the mean wave period. According to (3.4), it appears that roughly p=1. For small coastal regions, a global error of order 1 is good enough. The resulting consequence is that the global error in the wave parameters is roughly equal to the value of the corresponding mesh difference Φ_h, since (3.3) implies that $\phi - \phi_h \approx = -\Phi_h$.

location	h=100 m				h=200 m			
	$\Phi(H_{m0})$ [m]	$\Phi(T_{m-10})$ [s]	$\Phi(\theta)$ [°]	$\Phi(\sigma)$ [°]	$\Phi(H_{m0})$ [m]	$\Phi(T_{m-10})$ [s]	$\Phi(\theta)$ [°]	$\Phi(\sigma)$ [°]
AZB11	-0.0111	0.0101	-0.141	0.053	0.0004	-0.0129	0.097	-0.035
AZB12	-0.0032	0.0039	-0.010	0.095	-0.0008	0.0106	-0.080	-0.004
AZB21	0.0686	0.2835	0.922	-0.090	0.0984	0.4358	-0.018	0.573
AZB22	0.0550	0.2618	-0.389	-0.702	0.1213	0.5834	0.928	0.926
AZB31	-0.0698	-0.1764	-0.229	0.422	-0.0743	-0.1876	0.857	2.150
AZB32	-0.0842	-0.2320	0.260	0.700	-0.0501	-0.1907	0.534	1.441
AZB41	0.0151	-0.0589	-0.217	-0.842	0.0817	0.0454	1.270	-2.006
AZB42	0.0114	-0.0434	-0.975	-0.518	0.0926	0.0574	3.097	-3.342
AZB51	-0.0037	-0.0184	-0.101	0.230	0.0191	0.0232	0.991	-1.199
AZB52	-0.0044	-0.0205	-0.456	-0.396	-0.0035	-0.0008	-2.512	-1.043

Table 3.1 Mesh differences in Amelander Zeegat buoys for *area1* for h = 100m and 200m, with quadruplets.

location	h=100 m				h=200 m			
	$\Phi(H_{m0})$ [m]	$\Phi(T_{m-10})$ [s]	$\Phi(\theta)$ [°]	$\Phi(\sigma)$ [°]	$\Phi(H_{m0})$ [m]	$\Phi(T_{m-10})$ [s]	$\Phi(\theta)$ [°]	$\Phi(\sigma)$ [°]
AZB11	0.0001	-0.0003	-0.023	0.006	-0.0036	-0.0018	-0.022	-0.030
AZB12	0.0047	0.0033	-0.023	0.041	0.0092	0.0034	-0.159	0.054
AZB21	0.0706	0.2441	0.155	-0.067	0.1106	0.4367	-1.347	0.486
AZB22	0.0557	0.2334	-1.180	-0.659	0.1386	0.6503	-0.690	0.878
AZB31	-0.0553	-0.1533	-0.048	0.020	-0.0861	-0.1597	0.595	1.471
AZB32	-0.0507	-0.2405	0.162	-0.296	-0.0613	-0.1573	0.548	0.604
AZB41	0.0279	-0.0271	0.116	-0.243	0.0993	0.0516	-0.134	-1.056
AZB42	0.0214	-0.0087	-0.610	0.352	0.1250	0.0653	0.477	-2.067
AZB51	0.0282	0.0415	2.343	1.376	0.0158	0.0293	0.091	0.571
AZB52	-0.0445	-0.0187	-0.907	2.110	-0.0104	-0.0154	-2.531	-0.505

Table 3.2 Mesh differences in Amelander Zeegat buoys for *area1* for h = 100m and 200m, without quadruplets.

3.2.4 Global errors of wave parameters computed for *area2*

The results obtained with *area2* are shown in Figure 3.5 to 3.8. Compared to the results of *area1* (cf. Figure 3.1 to 3.4) the region with largest differences is significantly smaller. Moreover, the mesh differences are also smaller. The largest differences in H_{m0}, $T_{m-1,0}$, θ and σ are in order of 2 – 5 cm, 0.1 – 0.2 s, 5 – 10^0 and 2 – 5^0, respectively.

In Tables 3.3 and 3.4, mesh differences of wave parameters in the wave buoys AZB21, AZB22, AZB31 and AZB32 (all in *area2*) are shown. For *h*=20 m the differences in significant wave height and mean wave period are in the order of 1 cm and 0.05 s respectively. For *h*=40 m these differences are 2 cm and 0.05 – 0.1 s respectively. The mesh differences in mean wave direction and directional spreading are less than 1^0. Also here the order of accuracy roughly equals 1. We note that in particular the error behaviour for θ and σ is rather irregular. This may be due to its dependency on the spectral resolution, which is not particularly fine (see also Section 3.3).

location	h=20 m				h=40 m			
	$\Phi(H_{m0})$ [m]	$\Phi(T_{m-10})$ [s]	$\Phi(\theta)$ [°]	$\Phi(\sigma)$ [°]	$\Phi(H_{m0})$ [m]	$\Phi(T_{m-10})$ [s]	$\Phi(\theta)$ [°]	$\Phi(\sigma)$ [°]
AZB21	0.0174	0.0471	-0.080	0.204	0.0231	0.0402	-0.271	0.006
AZB22	0.0065	0.0323	-0.985	0.126	0.0169	0.0362	-0.769	0.197
AZB31	-0.0162	-0.0642	0.313	0.809	-0.0182	-0.1297	-0.405	0.223
AZB32	-0.0065	-0.0314	0.334	0.490	-0.0317	-0.1087	-0.066	0.156

Table 3.3 Mesh differences in Amelander Zeegat buoys for *area2* for h = 20m and 40m, with quadruplets.

location	h=20 m				h=40 m			
	$\Phi(H_{m0})$ [m]	$\Phi(T_{m-10})$ [s]	$\Phi(\theta)$ [°]	$\Phi(\sigma)$ [°]	$\Phi(H_{m0})$ [m]	$\Phi(T_{m-10})$ [s]	$\Phi(\theta)$ [°]	$\Phi(\sigma)$ [°]
AZB21	0.0190	0.0395	-0.239	0.415	0.0189	0.0355	-0.489	0.155
AZB22	0.0068	0.0254	-1.025	0.310	0.0123	0.0295	-0.887	0.420
AZB31	-0.0062	-0.0716	0.161	0.858	-0.0185	-0.0999	-0.327	0.148
AZB32	-0.0020	-0.0370	0.437	0.628	-0.0218	-0.1182	-0.012	-0.080

Table 3.4 Mesh differences in Amelander Zeegat buoys for *area2* for h = 20m and 40m, without quadruplets.

3.2.5 Conclusions concerning geographic grid resolution

The global errors in the significant wave height H_{m0}, the mean period $T_{m-1,0}$, the mean wave direction θ and directional spreading σ due to geographic grid discretisation have been quantified. For the largest area with a mesh size of h = 100 m, the largest difference in H_{m0}, $T_{m-1,0}$, θ and σ are in order of 10 – 20 cm, 0.2 – 0.3 s, 5 – 10^0 and 5 – 10^0 respectively. For the smallest area with a mesh size of h = 20m, the largest difference in H_{m0}, $T_{m-1,0}$, θ and σ are in order of 2 – 5 cm, 0.1 – 0.2 s, 5 – 10^0 and 2 – 5^0. It is made plausible that the difference values just given are representative of the error due to geographic grid discretisation.

The mesh differences and the resulting global errors are considered to be small bearing in mind that the errors due to the physical modelling of different processes (generation, dissipation and interactions) used in SWAN are relatively larger. In hindcast studies Royal Haskoning (2003) and WL/Alkyon (2003) showed that these model errors are of the order 5-10 cm for the significant wave height and 1-2 s for the wave period. In this respect the 100 m resolution would yield grid discretisation errors that are larger than physical representation errors. The discretisation errors based on the 20 m grid resolution are smaller than the physical representation errors. With respect to the hindcasts of the Amelander Zeegat, grids with a resolution of the order 20 m are preferred over those of the order 100 m. Moreover, the fine grids are better in representing the large gradients in the bottom at relative short distances.

Activation of the quadruplets has hardly an effect on the mesh differences, as can be concluded from comparison of Figures 3.5 with 3.7, and 3.6 with 3.8. This study does not provide any indication for the assumption that the DIA hinders the geographic grid convergence.

It must be stressed that this study is based on stationary simulations and thus provides steady-state error estimates. The above conclusions may not be valid for other type of applications like non-stationary simulations. However, the above conclusions are expected to hold also for simulations with slow temporal variations in the forcing (quasi stationary cases), since there is no apparent reason why these conclusions should not be applicable.

3.3 Analysis of global error due to spectral resolution

3.3.1 Introductory remarks

The spectral resolution concerns the discrete frequencies and the directions that have to be specified in SWAN. The frequency range and the distribution of the discrete frequencies is investigated in WL / RIKZ / Alkyon / NRL (2007). Summarizing, the lowest model frequency should be about 0.4 times the peak frequency on the offshore boundary. The highest model frequency can be based on the peak frequency that occurs at about 1 km from the coast. In practice, an upper limit of 1 Hz suffices. The distribution of succeeding frequencies needs to be done according to the relation $f_{i+1} = (1+x)f_i$, where x is equal to 0.1. This is a consequence of the discrete interaction approximation (DIA) of the quadruplet interaction. In the calibration of the DIA the parameter x in the geometric frequency distribution was one of the tunable parameters (see e.g. Van Vledder et al., 2000). If a different frequent resolution of the wave spectrum is used, unexpected and undesired results appear. Therefore, without a new calibration of the DIA or an alternative formulation for quadruplet interactions, there is no point in investigating the issue of frequency resolution.

According to the SWAN user manual (2006), the directional resolution should reflect the directional spreading of the incident wave conditions. In WL / RIKZ / Alkyon / NRL (2007), the directional resolution for computing the penetration of long period waves (swell) through the tidal inlet is investigated. It was demonstrated that the directional resolution affects the penetration of swell into the Wadden Sea, but no convergence was obtained with respect to the directional resolution.

In the present section, the issue of directional resolution is investigated again, but now for a situation involving wind waves.

3.3.2 Description of test case

As a test case a similar storm situation is taken as was considered in the directional resolution study for swell waves (see Section 4.3 of WL / RIKZ / Alkyon / NRL, 2007). This concerns the storm of 8 February 2004 (22:30 MET) in the Amelander Zeegat, see also WL/Alkyon (2007). Note that this is not exactly the same as in WL / RIKZ / Alkyon / NRL (2007), where 22:20 MET was considered. In WL/Alkyon (2007) the model settings and model input were expanded and optimised. Therefore the latter was chosen here.

The wind field was obtained from the HIRLAM model. The wind speed and direction at buoy AZB11 are 16.6 m/s and 325°N respectively. The water level and current fields were obtained from the WAQUA model. For reference, the water level at NES measured 2.60 m + NAP. The offshore wave conditions at AZB11 were 5.3 m, 9.5 s and 319°N in terms of significant wave height H_{m0}, mean wave period T_{m-10} and mean wave direction.

The computations were carried out on the curvi-linear grid AZG3A, see Figure 3.9. This grid was applied in the hindcast study of WL/Alkyon (2007) and is embedded in a larger grid covering a coastal strip along the northern part of the Netherlands. The larger grid is not used in the present study. For more details on wave model settings and model input we refer

to WL/Alkyon (2007). Whereas in WL/Alkyon (2007) the curvature-based convergence criterion was applied, all calculations in this section have been carried out with 80 iterations. In this way convergence errors are assumed to be negligible.

For the sensitivity analysis, the following values for the directional resolution were used:

$$\Delta\theta = 2^0, 2.5^0, 4^0, 5^0, 6^0, 8^0, 10^0, 15^0, 20^0 .$$

Note that $\Delta\theta = 10^0$ is the value for the directional resolution applied in WL/Alkyon (2007).

3.3.3 Approach

The solution for the wave height, wave period, wave direction (in Nautical convention) and directional spreading, obtained with the SWAN default value for the directional resolution ($\Delta\theta = 10^0$), are shown in Figure 3.10. A strong decrease in wave height as well as wave period takes place at the ebb tidal delta. The wave direction is more or less aligned with the wind direction (pointing south-east), apart from the refraction zones near the islands. The directional spreading varies largely over the domain, primarily behind the islands, where the wave height and wave period are small.

The computed wave field, obtained with the smallest applied value for the directional resolution ($\Delta\theta = 2^0$), is shown in Figure 3.11. It appears that the results show unrealistic features. They are due to a phenomenon called scintillation, see Holthuijsen and Booij (1994), which is similar to the 'blinking' appearance of the stars due to slight variations in the earth's atmosphere.

The origin of scintillation can be understood as follows. If we insert homogeneous wave conditions in the spectral balance equation:

$$\frac{\partial N}{\partial t} + \frac{\partial (c_x N)}{\partial x} + \frac{\partial (c_y N)}{\partial y} + \frac{\partial (c_\sigma N)}{\partial \sigma} + \frac{\partial (c_\theta N)}{\partial \theta} = \frac{S}{\sigma},$$

where the symbols have their usual meaning (see SWAN user manual, 2006), the conventional wave ray model is obtained:

$$\frac{\partial \theta}{\partial s} = -\frac{1}{c}\frac{\partial c}{\partial n}.$$

Here, *s* is a local coordinate in the wave direction, *n* is a local coordinate along the wave crest and *c* is the local phase velocity. In the conventional wave ray model, only the local gradient in the water depth and the depth itself are relevant for refraction. Conventional wave ray models are known to suffer from scintillation, i.e. unrealistically large gradients in the computed wave field. These are a consequence of the crossing or non-crossing of rays. The cause for this non-physical behaviour lies in the absence of diffraction in the model: when the wave field varies significantly, diffraction should be taken into account. Important in this respect is the numerical differencing of the direction term in the spectral balance

equation. The smaller the directional resolution $\Delta\theta$ becomes, the closer the *discrete* spectral balance equation resembles the *analytical* wave ray model (still assuming homogeneous wave conditions). In other words, the numerical solution as computed by SWAN converges, in the limit of $\Delta\theta$ to zero, to the solution of the conventional wave ray model. This solution can, as mentioned before, suffer from scintillation. And, since SWAN does not account for diffraction, SWAN results are prone to contain scintillation as well. The reason that scintillation does not occur for the more commonly used values of $\Delta\theta$ (say, around 10^0), is that numerical diffusion in the direction space smears the wave field sufficiently. The reasoning given above can, as may be inferred also from Holthuijsen and Booij (1994), be carried over to non-homogeneous wave conditions, which are described by the spectral balance equation.

Summarizing the findings above, there are two opposing requirements determining the choice for the directional resolution $\Delta\theta$. On the one hand, $\Delta\theta$ should be taken as small as possible to resolve the various wave directions most accurately. On the other hand, $\Delta\theta$ cannot be chosen too small, since this leads to the occurrence of scintillation. Unfortunately, there is no theory available (yet) that supports us in selecting an optimal value for $\Delta\theta$. This means that the only way to determine an optimal value for $\Delta\theta$ is by close inspection of the numerical results. The reason followed here is that, for sufficiently large values of $\Delta\theta$, the mesh differences $\Phi_{\Delta\theta} = \phi_{2\Delta\theta} - \phi_{\Delta\theta}$ should decrease for decreasing values of $\Delta\theta$. When $\Delta\theta$ drops below a certain threshold (we call this the scintillation threshold), the appearance of scintillation is expected to cause mesh differences to increase. Note that SWAN does include a formulation for diffraction. However, this formulation may lead to instabilities and yields inaccurate results in practical situations. Therefore, in the present computations diffraction is not activated. It is unclear whether scintillation occurs when SWAN computations are performed with (sufficiently accurate formulations for) diffraction activated.

3.3.4 Results

Computations were carried out for the 9 directional resolutions mentioned in Section 3.3.2: $\Delta\theta = 2°, 2.5°, 4°, 5°, 6°, 8°, 10°, 15°, 20°$. In Figures 3.10 and 3.11 the spatial distributions of the significant wave height H_{m0}, mean wave period T_{m-10}, mean wave direction and directional spreading are shown for $\Delta\theta = 10°$ and $\Delta\theta = 2°$ (the latter is not fully converged; see the discussion below). In the present section only the differences between solutions obtained with different directional resolutions are considered. The mesh differences are denoted as $\Phi_{\Delta\theta} = \phi_{\Delta\theta_2} - \phi_{\Delta\theta_1}$, with ϕ denoting any of the four integral wave parameters mentioned above. In Figures 3.12 to 3.17 mesh differences are presented for the combinations of $\Delta\theta_1$ and $\Delta\theta_2$ listed in Table 3.5. Since the error behavior is analysed here, other combinations than the double resolution $\Delta\theta_2 = 2\Delta\theta_1$ have been considered as well. Latter combinations would have been sufficient to determine the order of the errors.

Figure	$\Delta\theta_2$ [°]	$\Delta\theta_1$ [°]
3.12	20	10
3.13	15	8
3.14	10	6
3.15	10	5
3.16	8	4
3.17	5	2.5

Table 3.5 Reference to figures in which mesh differences $\Phi_{\Delta\theta} = \phi_{\Delta\theta_2} - \phi_{\Delta\theta_1}$ are presented for combinations of directional resolutions $\Delta\theta_1$ and $\Delta\theta_2$.

The mesh differences decrease with decreasing values of $\Delta\theta$ down to 6° compare Figure 3.12, 3.13 and 3.14. The differences between the solution obtained with $\Delta\theta = 10°$ and $\Delta\theta = 6°$ are up to 0.1 m in significant wave height, up to 0.2 s in mean wave period, and more than 10° in mean wave direction (Figure 3.14) in the areas where the waves strongly refract. The differences in wave height and wave period are considered to be small, the differences in mean wave direction not. This implies that a directional resolution of 6° leads to more reliable solutions in areas with strong refraction.

Figures 3.15 shows some small isolated areas of increased mesh differences at the lee side of the islands, whereas they do not appear in Figure 3.14. This is probably due to the effect of scintillation. For decreasing values of $\Delta\theta$ the mesh differences at the lee side of the islands increase (see Figures 3.16 and 3.17). This means that the scintillation threshold can be put at $\Delta\theta = 6°$. Given that a decreasing value of $\Delta\theta$ leads, for values larger than the scintillation threshold, to more accuracy, we can conclude that, for the present test case, $\Delta\theta = 6°$ is optimal in the sense of accuracy.

It appears that the scintillation threshold coincides with the separation between convergence and bad convergence. In Figure 3.18 (see below) results of the convergence behaviour and the required CPU time are shown. The number of iterations for convergence, *n,conv*, is based on the curvature-based criterion (2.1), (2.3) with $\varepsilon_c = 0.001$. It appears that this number is approximately 30 for a directional resolution above the scintillation threshold, and much larger for values below it. The CPU time is measured on the Hydrax3-cluster at WL | Delft Hydraulics. The number of directional bins is equal to $360°/\Delta\theta$. The CPU time increases linearly with the number of directional bins. This is according to expectations. Now we turn to the simulations with a directional resolution of 2° and 2.5°. In these simulations, convergence is not attained after *n,max* = 80 iterations. Convergence is achieved in 98.30% ($\Delta\theta = 2°$) and 98.39% ($\Delta\theta = 2.5°$) of the wet grid points, where 99% is required to achieve convergence according the chosen criterion. This suggests that scintillation has a significant negative impact on the convergence behaviour. It appears that convergence is bad in the regions where the wave field has unrealistically large gradients. This has been verified by looking at the differences between the wave field after *n,max* and (*n,max* – 1) iterations, see Figure 3.19. This also proves that scintillation causes the unrealistic features in Figure 3.11, and that these features are not caused by lack of convergence, for example due to a ‘wiggly’ behaviour between solutions at subsequent iterates. Comparing Figure 3.11a with Figure 3.19 shows that the scintillation features are at least an order of magnitude larger than this presumed ‘wiggly’ behaviour. Therefore, there is

no reason to assume that the differences between the converged solution and the solution as shown in Figure 3.11 will be significantly larger than the differences shown in Figure 3.19. This has motivated us to include Figure 3.11 in the report, although the shown solution is not fully converged.

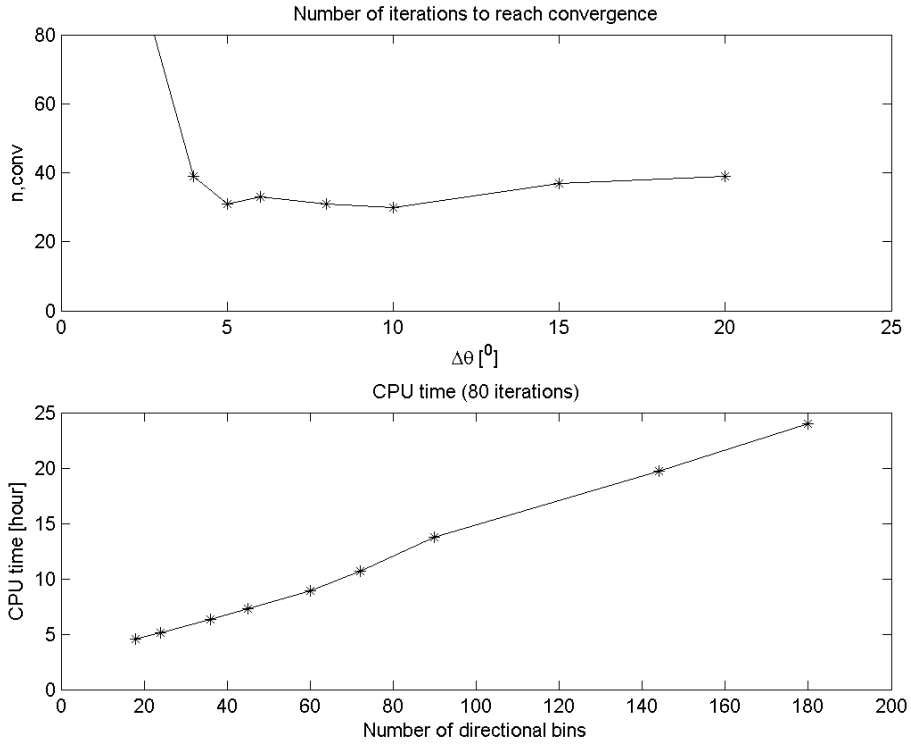

Figure 3.18. Convergence behaviour and required CPU time as a function of directional resolution.

3.3.5 Conclusions concerning spectral grid resolution

The spectral resolution concerns the discrete frequencies and the directions that have to be specified in SWAN. The frequency space is not investigated in the present study, because the use of the DIA as the default formulation for quadruplet interactions in SWAN restricts the choice of the frequency resolution. The geometric distribution with a relative change in frequency of 0.1 was part of the calibration of the DIA (Van Vledder et al., 2000).

According to the SWAN user manual (2006), the directional resolution should reflect the directional spreading of the incident wave condition. In the present study the sensitivity of the grid resolution for wind waves was investigated, with a focus on the Amelander Zeegat.

It turns out that there are two opposing requirements determining the choice for the directional resolution $\Delta\theta$. On the one hand, $\Delta\theta$ should be taken small enough to resolve the various wave directions accurately. On the other hand, it appears that $\Delta\theta$ cannot be chosen too small, since this leads to the occurrence of an undesired effect, namely scintillation, i.e. unrealistically large gradients in the computed wave field. Scintillation is a consequence of the fact that the SWAN model formulation does not include diffraction.

Unfortunately, there is no theory available (yet) that supports us in selecting an optimal value for $\Delta\theta$.

By close inspection of the differences in solutions obtained with different directional resolutions it was concluded that 6° is the smallest value for which scintillation effects are sufficiently small. The solution still changes, even significantly in mean wave direction, when the directional resolution is decreased below 6°, but errors due to scintillation become unacceptably large locally. Therefore we conclude that an optimal value for the directional resolution is 6^0.

Scintillation has a negative effects on the convergence behaviour of the SWAN computations. For the small directional resolutions 2° and 2.5° the computation did not meet the imposed (curvature-based) convergence criterion within 80 iterations.

We note that the conclusions concerning the optimal value of $\Delta\theta$ and the convergence behaviour in relation to scintillation are based on one test case only. It is recommended to investigate whether the conclusions are valid for other situations (e.g. other conditions, geographic grids, etc.).

4 Conclusions

4.1 Conclusions from the present study

Based on the results in the present study the following conclusions are drawn with respect to numerical aspects such as convergence behaviour and errors due to resolution in geographical space and spectral space:

Convergence behaviour

- For simulations of the Amelander Zeegat the original gradient-based convergence criterion yields solutions that are not sufficiently converged. By means of the curvature-based convergence criterion of Zijlema and Van der Westhuysen (2005), more accurate, converged wave parameters are obtained.
- The default settings of the curvature-based convergence criterion appear to be not strict enough for some isolated regions, in which the relative errors in the wave height and wave period are up to 10%. These large errors occur in regions with strong depth-induced breaking and triad interaction, such as the North Sea coast of the barrier islands and the ebb tidal delta, as well as in the regions immediately downwind of the barrier islands, where young wind sea is generated (also concluded in WL, 2007).

Geographical grid resolution

- Doubling the grid size roughly yields doubled global errors, which implies the order of accuracy with respect to the grid resolution to be of the order 1.
- The largest errors are found on the ebb-tidal delta and in between the islands. For the largest area with mesh size of 100 m, the errors in the wave height H_{m0}, wave period $T_{m-1,0}$, mean wave direction θ and directional spreading σ are in the order of 10 – 20 cm, 0.2 – 0.3 s, 5 – 10° and 5 – 10° respectively. For the smallest area with mesh size of h = 20m, the largest difference in H_{m0}, $T_{m-1,0}$, θ and σ are in order of 2 – 5 cm, 0.1 – 0.2 s, 5 – 10° and 2 – 5°, respectively.
- The errors due to simplification of the physical processes by means of parameterisation used in SWAN are 5-10 cm for the significant wave height and 1-2 s for the mean wave period. In this respect the 100 m resolution would yield grid discretisation errors that are larger than physical representation errors. The discretisation errors based on the 20 m grid resolution are smaller than the physical representation errors. With respect to the hindcasts of the Amelander Zeegat, grids with a resolution of the order 20 m are preferred over those of the order 100 m.
- Activation of the quadruplets by means of the DIA has hardly an effect on the geographic grid discretisation error. Therefore, the original idea that the DIA hinders the geographic grid convergence, is unfounded.

Directional resolution

- The geometric distribution with a relative change in frequency of 0.1 was part of the calibration of the DIA (Van Vledder et al., 2000). Changing the frequency resolution would yield unexpected and undesired results. Unless a new calibration of the DIA is

carried out or an alternative formulation for quadruplet interactions is applied, investigating the frequency resolution is useless.

- In the presently used test case of the Amelander Zeegat, directional resolutions smaller than 6° led to unrealistically large gradients in the computed wave field. This process is called scintillation and is a consequence of the absence of diffraction in the SWAN model.
- Especially the mean wave direction changes significantly in regions with strong refraction, as the directional resolution is decreased. For values smaller than 6° the scintillation strongly affects the accuracy, mainly at the lee side of the islands. Based on the single test case we conclude that an optimal value for the directional resolution is 6^0.
- Due to the scintillation effects the convergence behaviour of the SWAN computations is bad. For the small directional resolutions 2° and 2.5° the computation did not meet the imposed (curvature-based) convergence criterion within 80 iterations.

4.2 Comparison with WL / RIKZ / Alkyon / NRL (2007)

The present study aims at resolving the major issues from the discussion between the executor and the external reviewer of the report by WL / RIKZ / Alkyon / NRL (2007). In this section the results from WL / RIKZ / Alkyon / NRL (2007) and the present study are compared with respect to the three issues mentioned in Section 1.2.

1. Effect of the physical accuracy of source terms on the numerical accuracy
The errors due to geographical grid resolution are larger in the presence of source terms than without. Comparing the errors in Tables 2.1 and 2.2 in WL / RIKZ / Alkyon / NRL (2007) with the errors in Tables 3.1 and 3.3 of the present study shows that the difference is approximately a factor 5-10. However, there is no systematic behaviour in the errors. For locations AZB41 and AZB42 errors of 30-40 cm in significant wave height were observed in WL / RIKZ / Alkyon / NRL (2007). In the present study the spatial distribution of the errors shows much less variation.

Including the source terms in the SWAN computations has a significant effect on the errors due to geographical resolution. Including the source terms in the analysis is also of more practical relevance. Insight is obtained in the effect of choosing a different geographical resolution, also in comparison to physical representation errors.

2. Sensitivity of directional resolution
In the present study a sensitivity study has been carried out to gain insight in the effect of applying a variety of values for the directional resolution. Too large values yield significant inaccuracies because variations in the wave direction cannot be resolved. Too small values yield unrealistic gradients in the wave field (scintillation) due to the absence of diffraction in SWAN. An optimal value of 6° was determined for the Amelander Zeegat, based on one test case. Following the approach in WL / RIKZ / Alkyon / NRL (2007), conclusions about the optimal value for the directional resolution could not be obtained.

3. The choice of maximum number of iterations for benchmark solution
The main conclusions stated in Section 4.1 were also made in WL / RIKZ / Alkyon / NRL (2007). The question was however whether the solution obtained after 30 iterations could be

taken as a converged solution, at least at the buoy locations. Figures 2.2c, 2.3c and 2.4c show that the relative change in both significant wave height and mean wave period is sufficiently small after approximately 25 iterations. Therefore, the choice of taking the solution after 30 iterations as a benchmark, is valid.

5 References

Holthuijsen, L.H. and N. Booij (1994). Bottom induced scintillation of long- and short-crested waves. In *Proc of International Symposium: Waves – Physical and Numerical Modelling*, Canada, p. 604 – 613. August 1994.

Royal Haskoning (2003). Betrouwbaarheid SWAN in de Westerschelde. Vergelijk golfberekeningen en metingen. Rapport Royal Haskoning 9M5697/1246, Juni 2003 (in Dutch).

SWAN user manual (2006). SWAN User Manual, version 40.51. Delft University of Technology. (http://vlm089.citg.tudelft.nl/swan/index.htm)

Van Vledder, G. Ph. , T.H.C. Herbers, R.J. Jensen, D.T. Resio and B. Tracy (2000). Modelling of non-linear quadruplet wave-wave interactions in operational wave models. In *Proc. of Int. Conf. of Coastal Eng.*, Sydney, p. 797-811.

WL / Alkyon (2003). Reliability of SWAN at the Petten sea defence. Report WL | Delft Hydraulics / Alkyon H4197/A1138, November 2003.

WL (2006). Storm hindcasts Norderneyer Seegat and Amelander Zeegat.Report WL | Delft Hydraulics H4803.11, August 2006.

WL / RIKZ / Alkyon / Naval Research Laboratory (2007). Sensitivity analysis of numerical aspects of SWAN. Activity 3.1 of SBW project Waddensea. Report WL | Delft Hydraulics / RIKZ / Alkyon / Naval Research Laboratory H4803.60, May 2007.

WL (2007). Reducing the computational time of SWAN by dynamic deactivation of grid points. Report WL | Delft Hydraulics H4918.37, August 2007.

WL / Alkyon (2007). Storm hindcasts for Wadden Sea. Hindcasts in inlet systems of Ameland and Norderney and Lunenburg Bay. Report WL | Delft Hydraulics H4918.20, September 2007.

A Summary of review previous report

Attached is the summary of the discussion (in Dutch) about the review of the report of WL/RIKZ/Alkyon/NRL (2007).

Memo

Ministerie van Verkeer en Waterstaat
Rijkswaterstaat

Aan
Andries Roelfzema

Van
Martin Verlaan
Doorkiesnummer
06 22 20 30 44
Datum
25 april 2007
Bijlage(n)
-
Onderwerp
Samenvatting van de bespreking over de review van het SBW-rapport “Sensitivity analysis of numerical aspects”

Beste Andries,

Hierbij ontvang je een terugmelding over de akties die zijn uitgevoerd naar aanleiding van jouw vraag om de review van Mart Borsboom op het deel van het rapport “Sensitivity analysis of numerical aspects”, dat door Marcel Zijlema is gescheven, met Mart en Marcel te bespreken. Ik ben gestart met het lezen van de documenten die je mij had gegeven:

1. Het rapport
2. De review van Mart
3. De reaktie van Marcel
4. De aangepaste versie van het rapport waarin 2 en 3 zijn verwerkt.
5. Een versie van 4 met daarin nieuwe opmerkingen van Mart

Afgelopen dinsdag 17 april hebben we deze stukken met elkaar besproken en gediscussieerd over de resterende verschillen van inzicht en mogelijke oplossingen. Hieronder wil ik de belangrijkste gesprekspunten even kort samenvatten:

1. Bij het uitvoeren van een studie naar numerieke convergentie met een complex model moet men altijd een afweging maken tussen een reductie van de complexiteit om het probleem beter te kunnen bestuderen en duidelijker conclusies te trekken m.b.t. het experiment en aan de andere kant het beperken van de vereenvoudigingen om te zorgen dat de conclusies die je over het experiment kan trekken ook nog iets zeggen over het werkelijke vraagstuk. Een lastig probleem hierbij is dat SWAN discrete-interactietermen (DIA) voor quadruplets bevat, waarvan op voorhand bekend is dat de numerieke nauwkeurigheid als niet of weinig afneemt met een toenemende ruimtelijke resolutie. Marcel heeft in zijn rapport daarom het probleem verder

RWS Rijksinstituut voor Kust en Zee Den Haag
Postadres Postbus 20907, 2500 EX Den Haag
Bezoekadres Kortenaerkade 1
Telefoon +31(0)70 3114311
Fax +31(0)70 3114 321

vereenvoudigd zodat er duidelijker conclusies over de numerieke nauwkeurigheid als functie van de geografische roosterresolutie konden worden getrokken. Anderzijds is het resultaat door deze grote aanpassing weinig bruikbaar om iets te zeggen over de benodigde ruimtelijke resolutie van de modellen binnen SBW, omdat de brontermen hierin een belangrijke rol spelen. Marcel en Mart zijn het er niet over eens of de fysische nauwkeurigheid van de brontermen invloed heeft op de numerieke nauwkeurigheid, maar toch kon er wel overeenstemming worden bereikt over de vervolgstappen.
Na enige discussie zijn Marcel en Mart het er nl. over eens dat het zeer nuttig zou zijn om de experimenten te herhalen met alle brontermen aan en nog een keer met alleen de DIA termen uit, omdat deze mogelijk voor de grootste problemen zorgen zowel qua nauwkeurigheid als convergentie. Van een convergentie in de ruimte in de wiskundige zin is dan mogelijk geen sprake, maar de verschillen zijn waarschijnlijk wel indicatief voor de orde van grootte van de ruimtelijke discretisatiefouten. Marcel geeft wel aan dat hij hiervoor binnen de huidige opdrachten geen tijd heeft, want het rapport is gebaseerd op resultaten uit de periode dat Marcel bij RIKZ werkzaam was terwijl hij tegenwoordig voor de TU Delft werkt. Anderzijds geeft Mart aan dat hij de huidige versie niet acceptabel vindt.

2. In het onderdeel “Accuracy of spectral grid resolution” wordt een poging gedaan om de huidige keuze voor de spectrale resolutie te onderbouwen. Helaas blijkt na enige discussie dat de afleiding mogelijk een fout bevat, waardoor deze doelstelling niet kan worden bereikt. De spectrale resolutie is dus mogelijk niet voldoende, maar wordt op dit moment beperkt door de DIA, die niet goed werkt voor een hogere resolutie in het spectrale domein. Deze paragraaf kan echter wel worden omgeschreven om te onderbouwen dat bij de huidige spectrale resolutie een verdere verhoging van de ruimtelijke resolutie geen zin heeft. Dit ondervangt dan tevens het feit dat op basis van de hierboven voorgestelde aanpassingen m.b.t. de ruimtelijke resolutie mogelijk geen harde conclusies kunnen worden getrokken over het al dan niet voldoende zijn van de huidige ruimtelijke resolutie. Dat het verhogen van de spectrale resolutie zin heeft voor deining heeft Gerbrant van Vledder in het vervolg van het rapport al laten zien. Het verhogen van de spectrale resolutie kan echter niet worden doorgevoerd zolang er geen verbeteringen worden aangebracht aan de DIA. Dit onderwerp wordt daarmee een duidelijk aandachtspunt voor het vervolg. Anderzijds kan het model mogelijk wel zinvol worden ingezet in zijn huidige vorm, mits de resultaten goed worden gevalideerd met metingen en er zeer voorzichtig wordt omgesprongen met numerieke aanpassingen als ruimtelijke resolutie, (spectrale) roosters, etc. Deze tekstuele aanpassingen zijn van beperkte omvang en zowel Mart als Marcel kunnen zich hierin vinden.
3. In het onderdeel “Convergence behaviour” wordt gekeken naar het convergentie van het iteratieproces. Mart vraagt zich af of het iteratieproces wel helemaal is geconvergeerd na 30 iteraties. Dit is een aanname in dit hoofdstuk, die achteraf door Marcel is getoetst maar niet gerapporteerd. Marcel zegt dit wel te kunnen en willen aanpassen, maar heeft hier binnen de huidige opdracht

geen tijd voor. Marcel geeft aan geen ander resultaat van deze aktie te voorzien, maar Mart wil graag dat de lezer dit zelf kan beoordelen.

4. De overige, kleinere opmerkingen van Mart op de laatste versie van het rapport kunnen Marcel en Mart prima rechtstreeks oplossen.

Samengevat kan worden gesteld dat de verschillen van inzicht kunnen worden overbrugd door een aantal aanpassingen door Marcel, waarvoor hij extra experimenten moet uitvoeren. Marcel geeft aan hiervoor extra tijd nodig te hebben. Indien door SBW aan deze randvoorwaarde kan worden voldaan is het mogelijk het rapport langs de geschetste lijnen af te ronden. Indien deze aanzienlijke aanpassingen worden doorgevoerd is het wenselijk de nieuwe resultaten opnieuw te laten reviewen.

Met vriendelijke groet,

Martin Verlaan

Figures

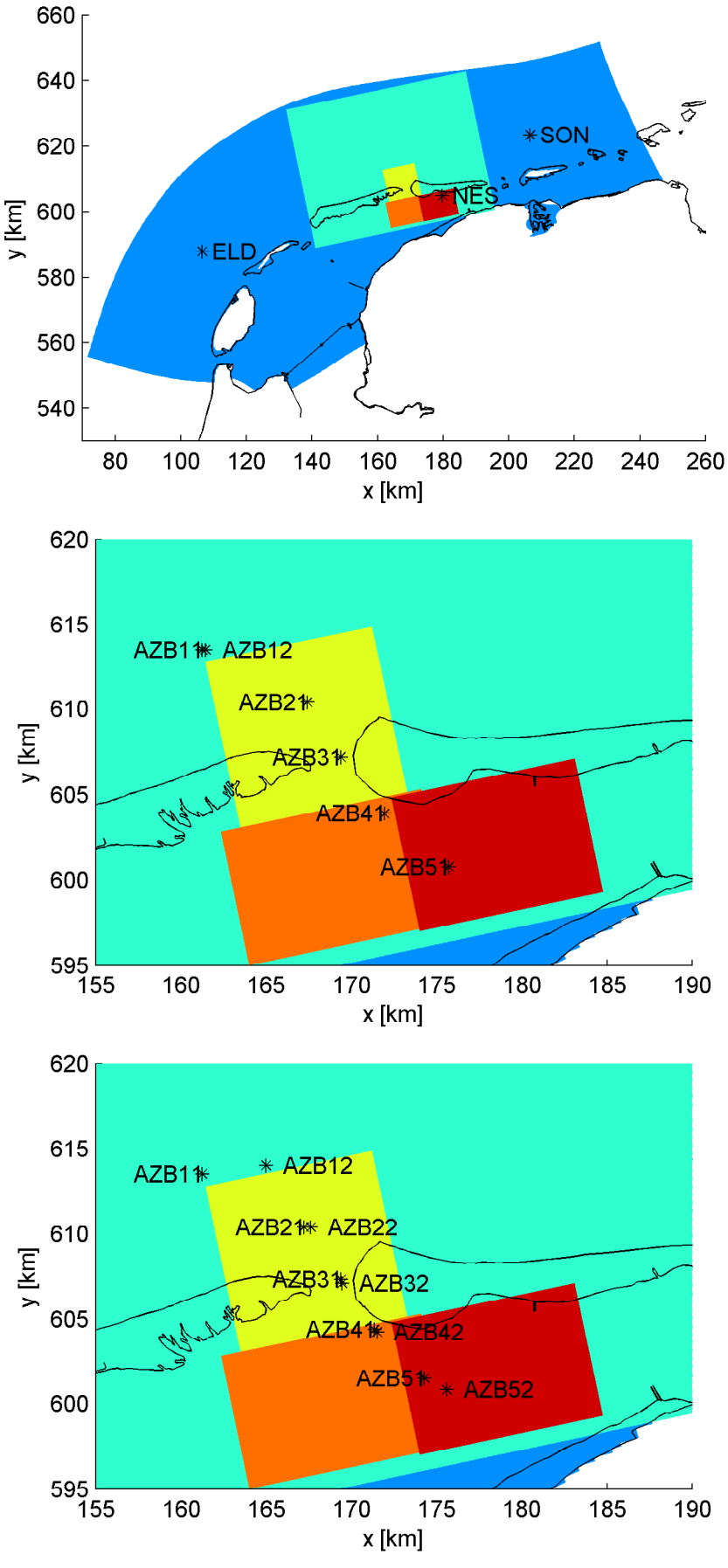

Curvi-linear grid, area1 (light-blue), area2 (yellow), area3 (orange) and area4 (red) with offshore buoy locations (upper), buoys locations in Ameland inlet in 2003/04 (middle) and in 2004/05 (lower panel)

WL | DELFT HYDRAULICS	H4918.39	Fig. 2.1

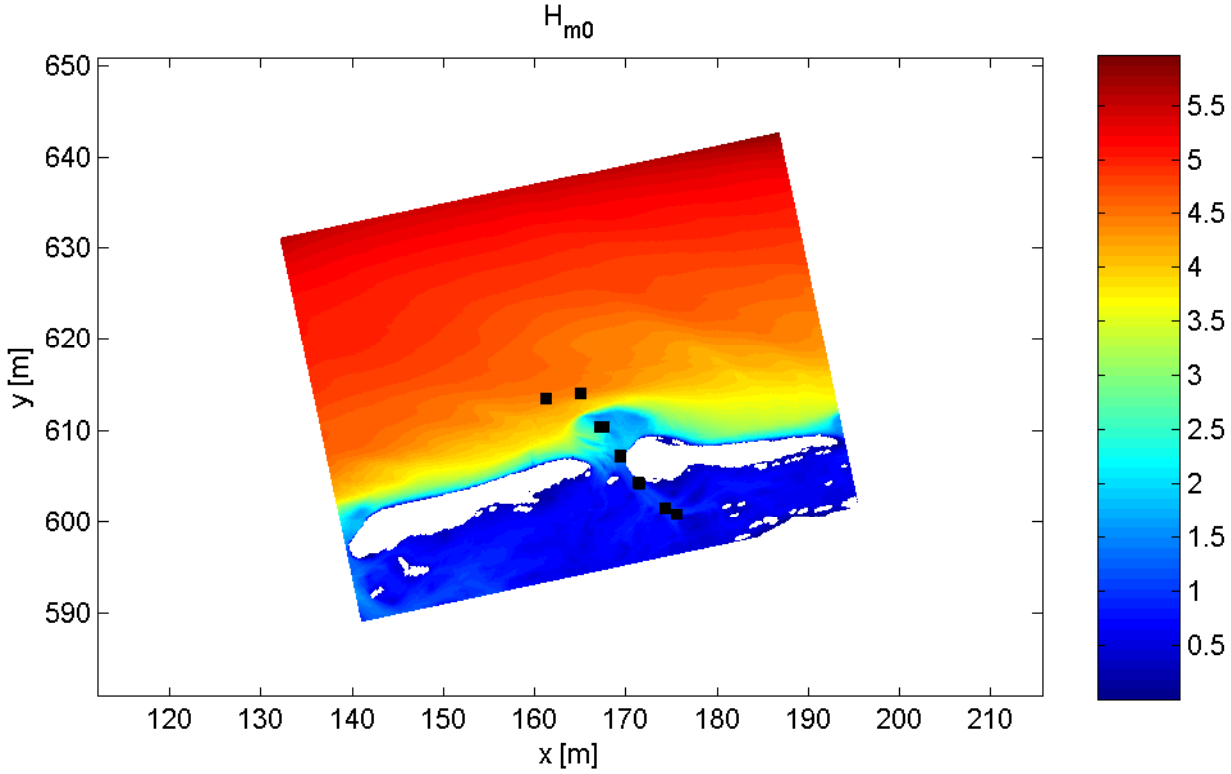

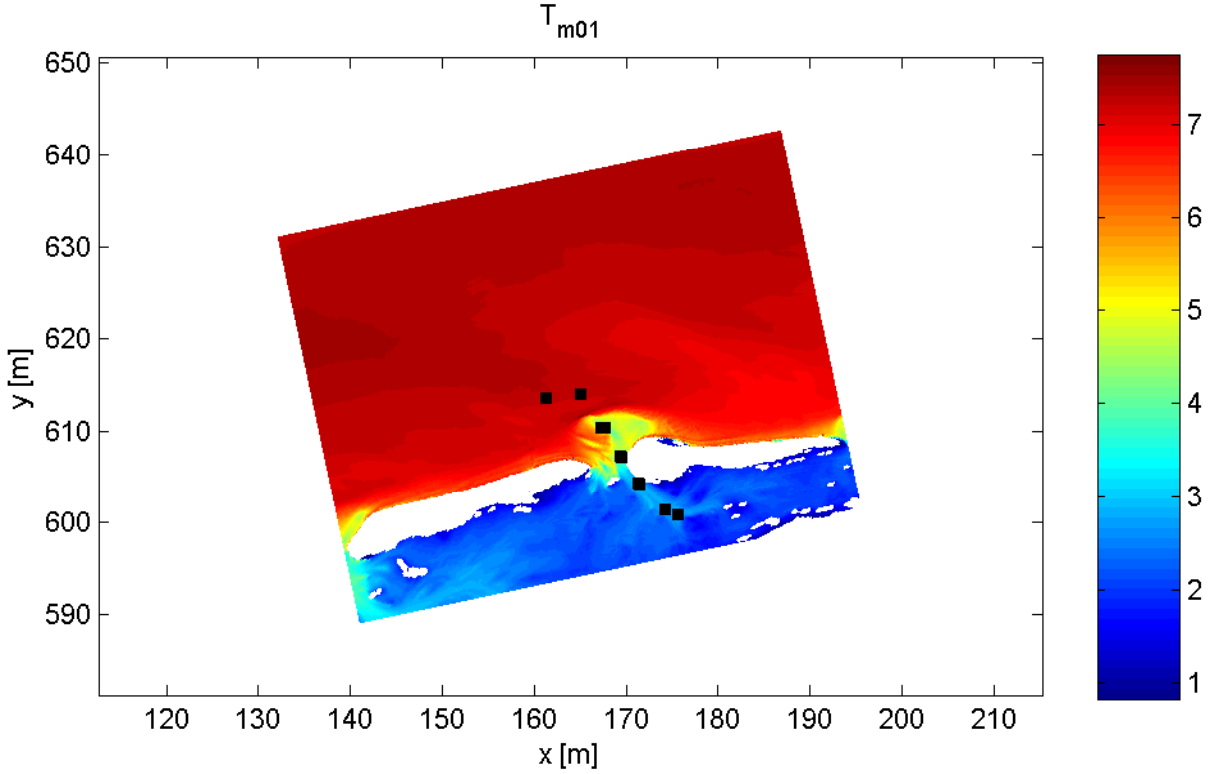

Solution of H_{m0} and T_{m01} in Amelander Zeegat after n,max iterations	grid 1 (100m)	
WL | DELFT HYDRAULICS	H4918.39	Fig. 2.2a

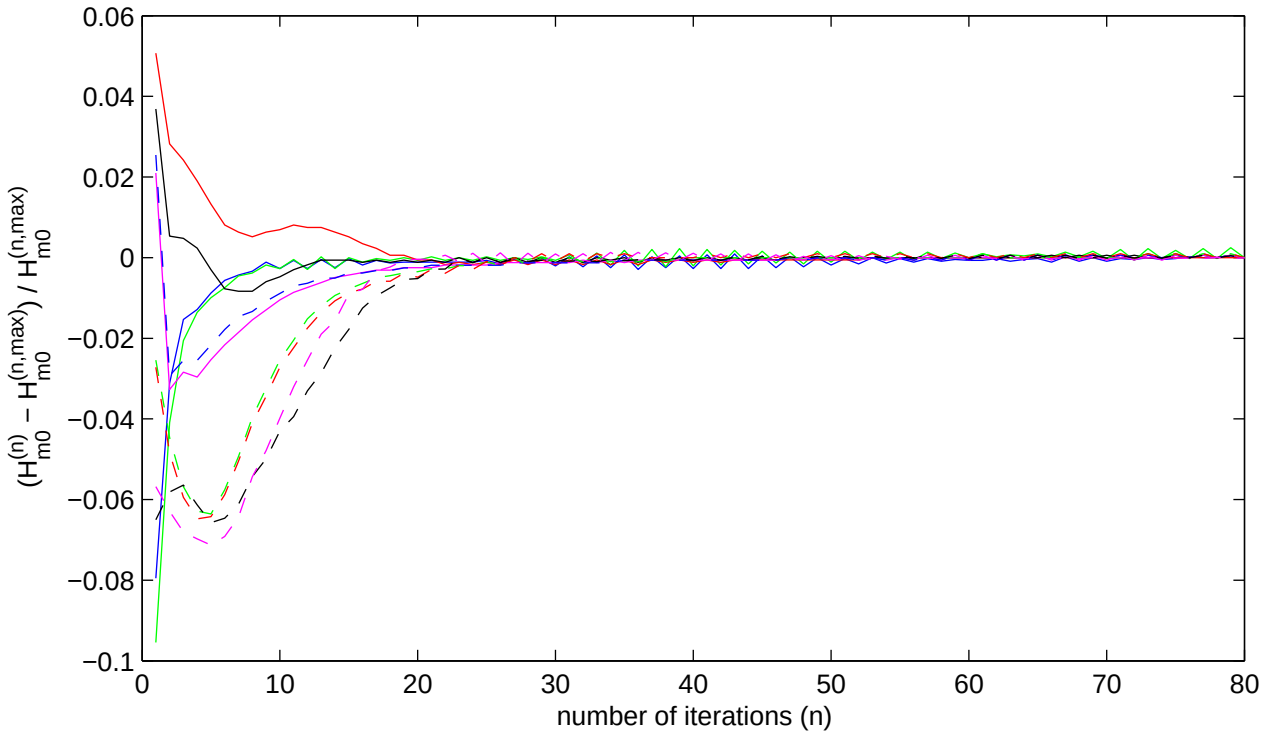

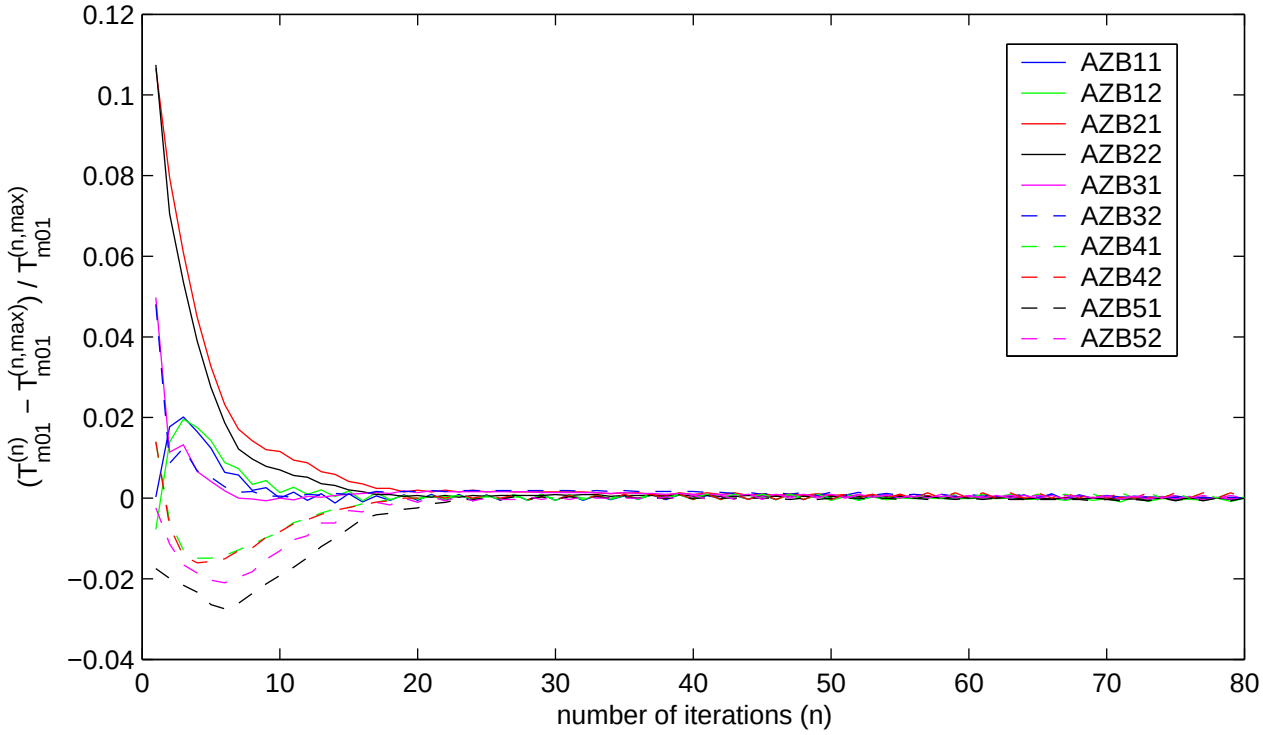

Convergence behaviour of H_{m0} and T_{m01} at Amelander Zeegat buoys Error relative to solution after n,max=80 iterations	grid 1 (100m)	
WL | DELFT HYDRAULICS	H4918.39	Fig. 2.2b

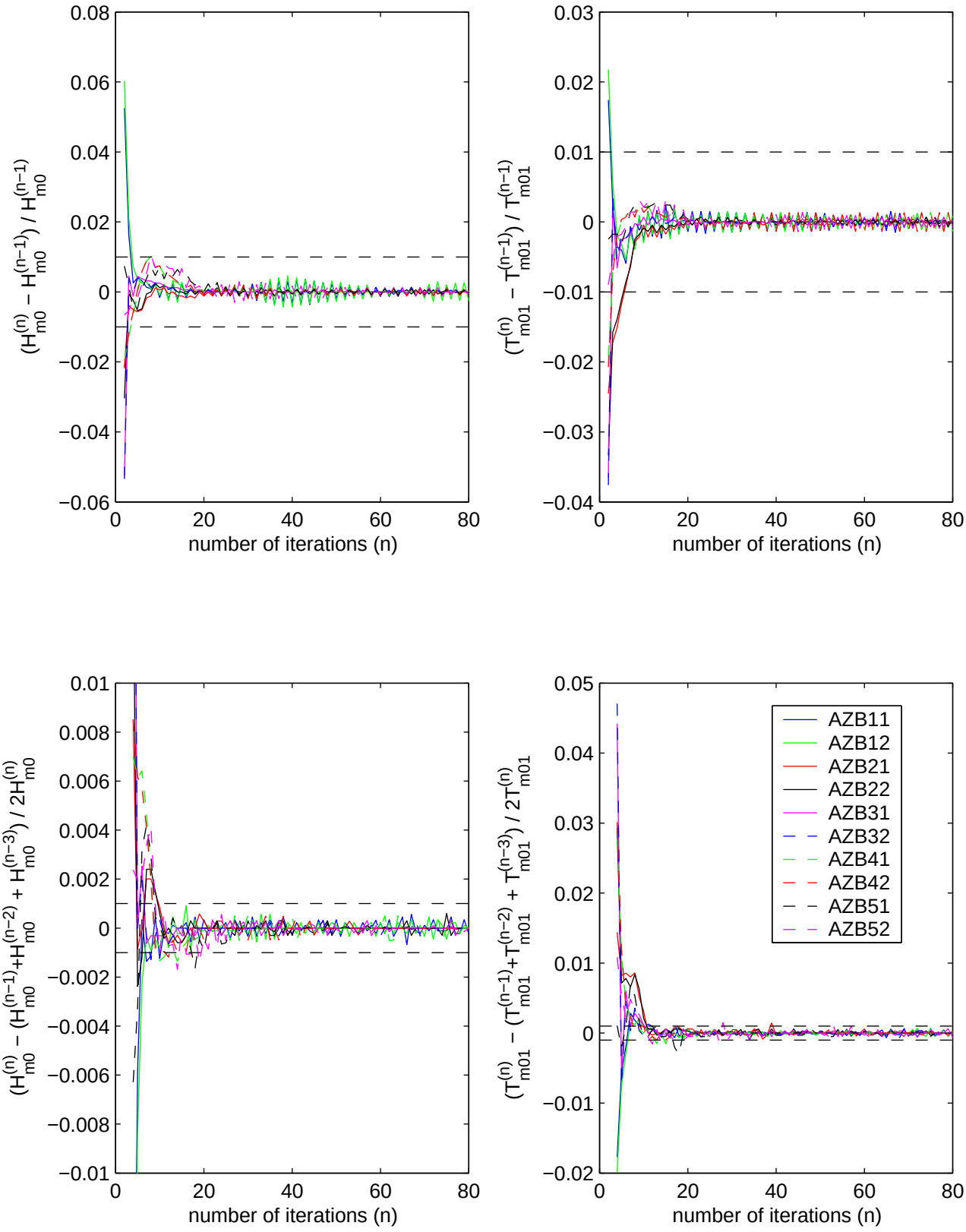

Convergence behaviour of H_{m0} and T_{m01} at Amelander Zeegat buoys Gradient−based and curvature−based	grid 1 (100m)	
WL | DELFT HYDRAULICS	H4918.39	Fig. 2.2c

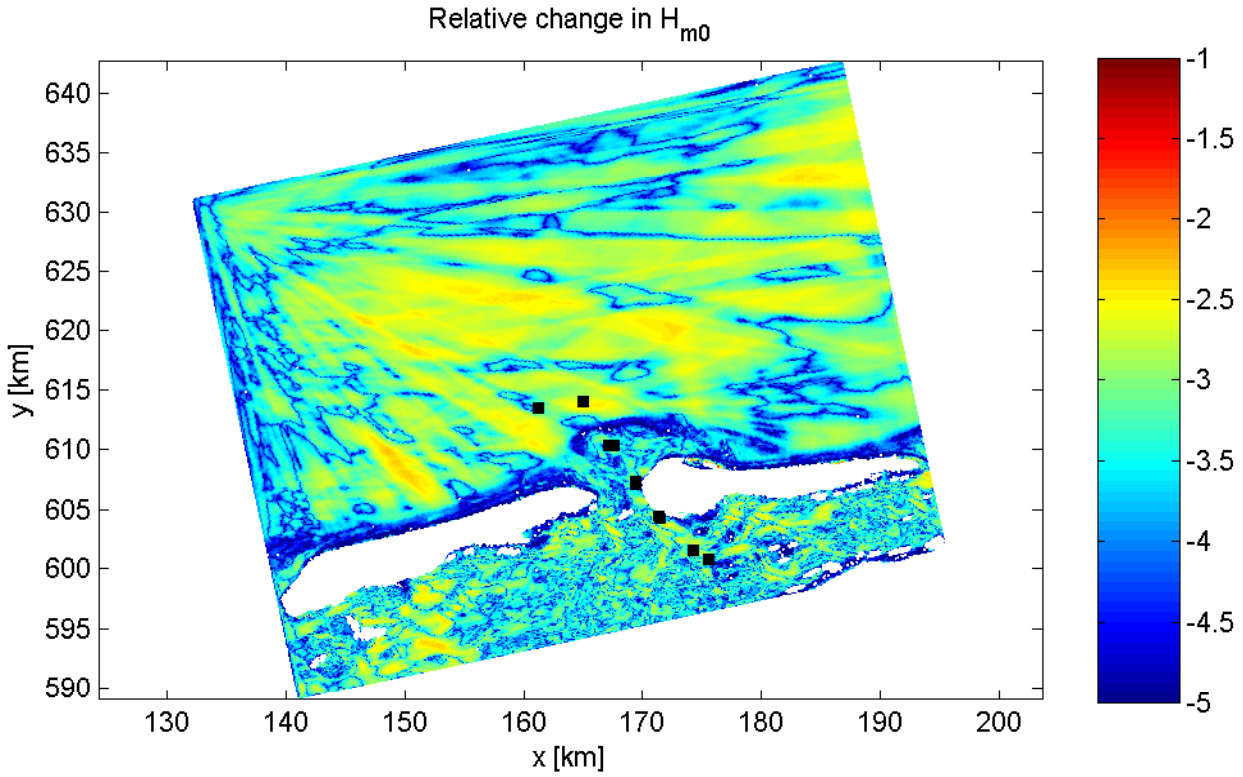

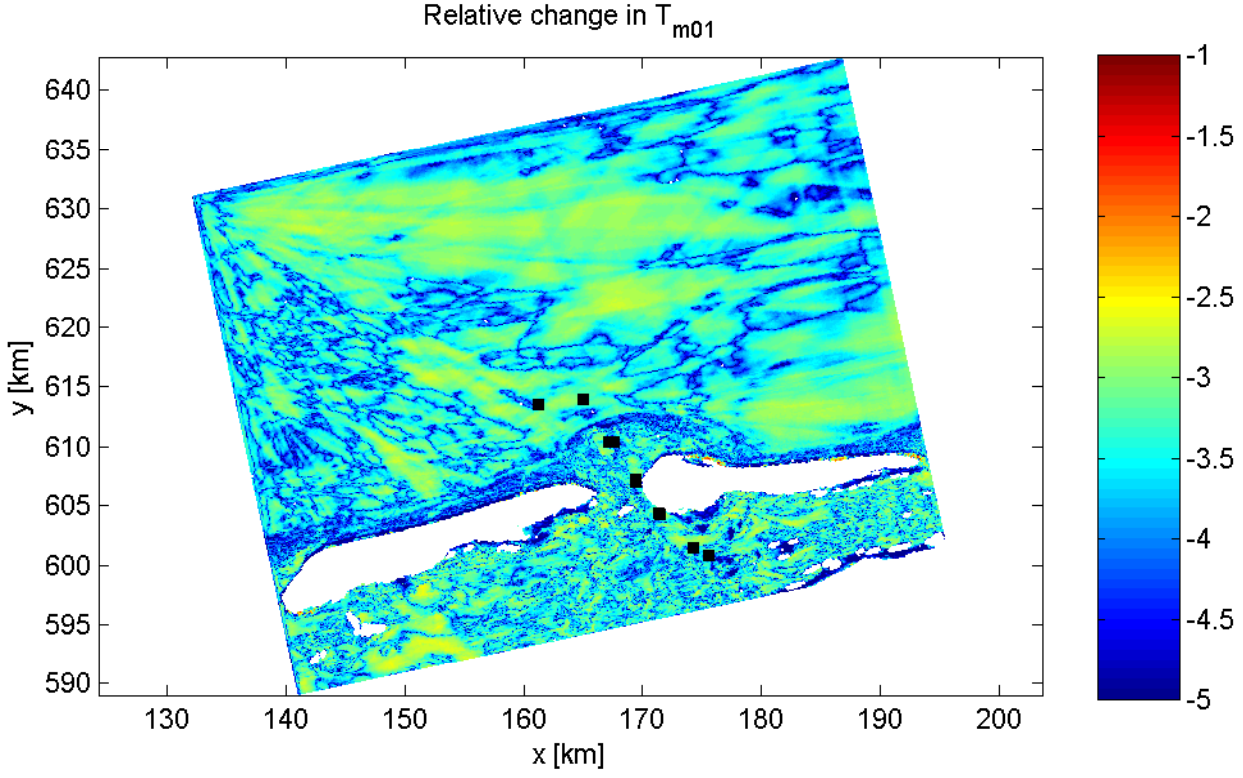

Convergence behaviour of H_{m0} and T_{m01} in Amelander Zeegat Relative change in final iteration: $^{10}\text{Log}(\lvert\phi^{(n,max)} - \phi^{(n,max-1)}\rvert / \phi^{(n,max)})$	grid 1 (100m)	
WL | DELFT HYDRAULICS	H4918.39	Fig. 2.2d

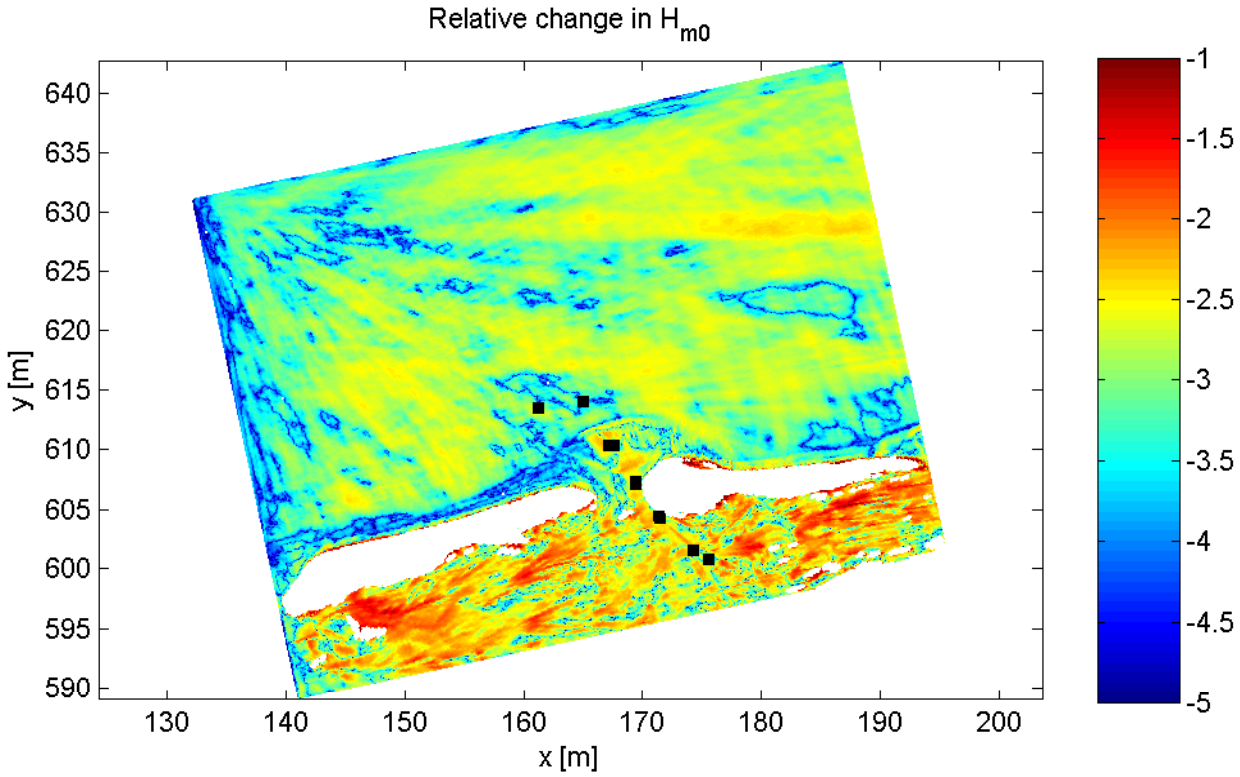

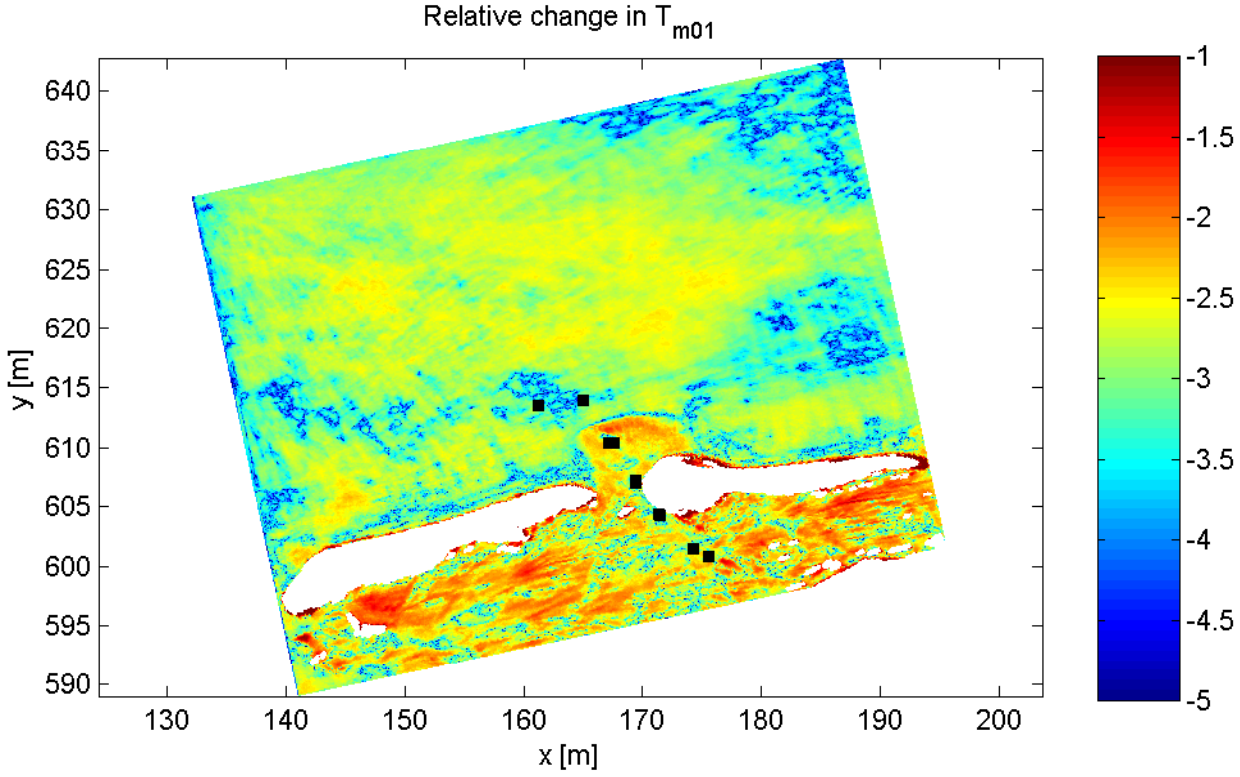

Convergence behaviour of H_{m0} and T_{m01} in Amelander Zeegat Relative change after convergence: $^{10}\mathrm{Log}(\lvert\phi^{(n,max)} - \phi^{(n,conv)}\rvert / \phi^{(n,max)})$	grid 1 (100m)	
WL | DELFT HYDRAULICS	H4918.39	Fig. 2.2e

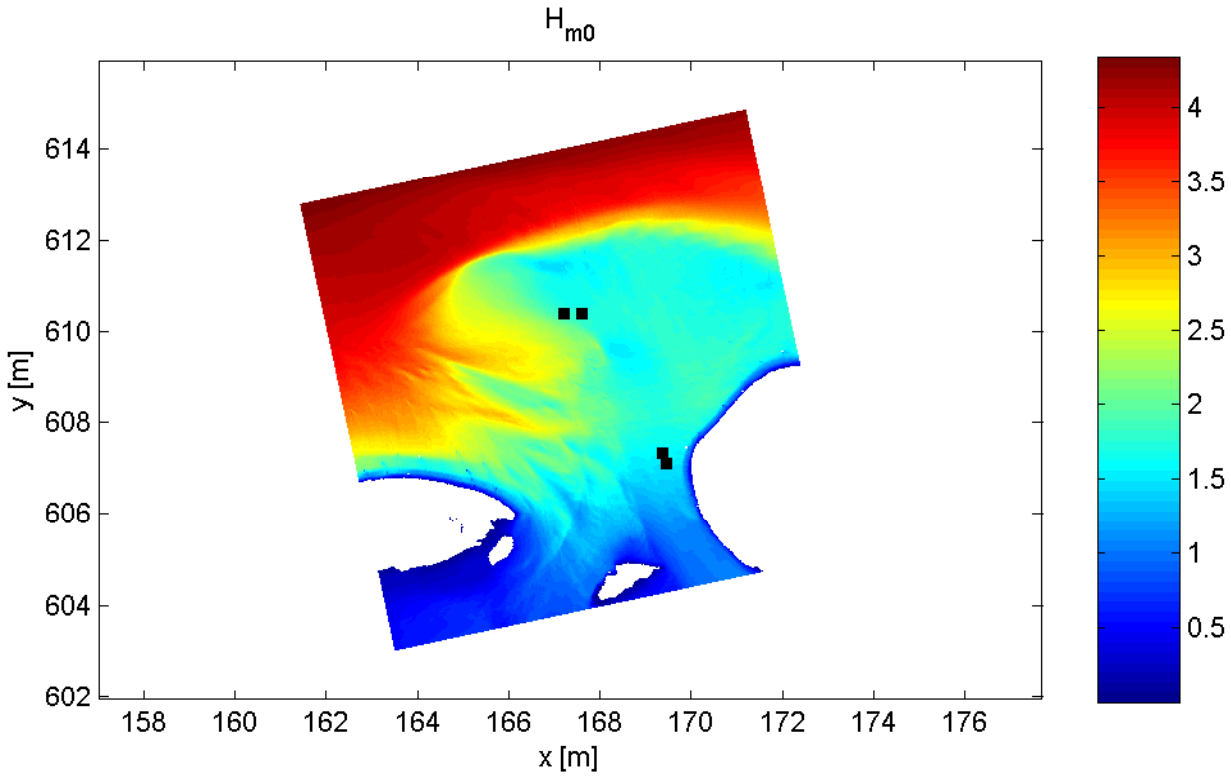

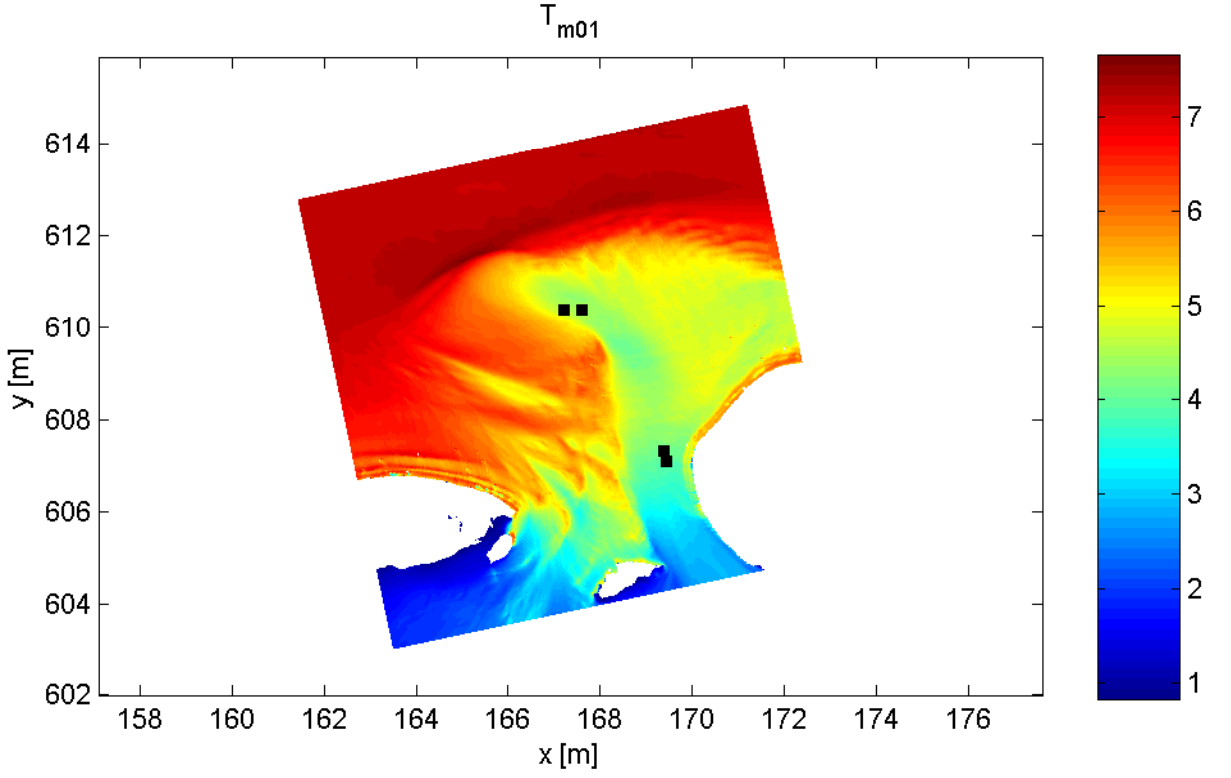

Solution of H_{m0} and T_{m01} in Amelander Zeegat after n,max iterations	grid 2 (20m)	
	uniform water level / no current	
WL | DELFT HYDRAULICS	H4918.39	Fig. 2.3a

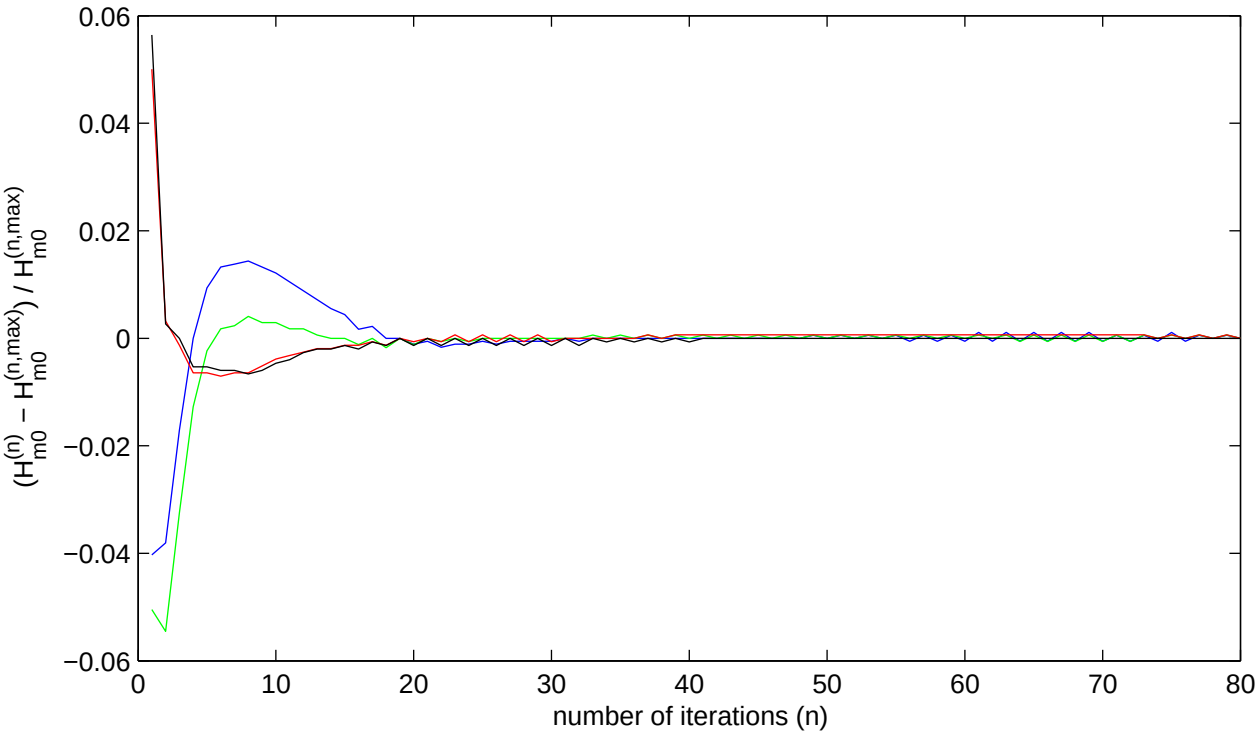

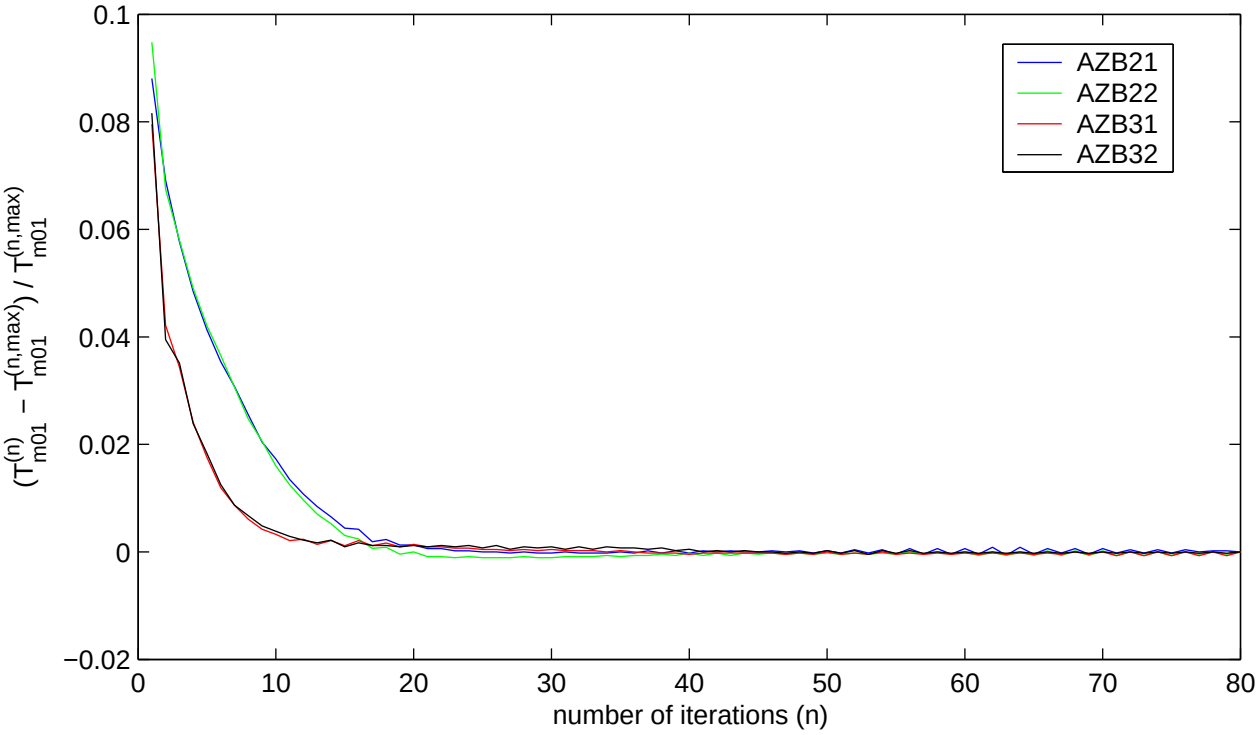

Convergence behaviour of H_{m0} and T_{m01} at Amelander Zeegat buoys Error relative to solution after n,max=80 iterations	grid 2 (20m)	
	uniform water level / no current	
WL | DELFT HYDRAULICS	H4918.39	Fig. 2.3b

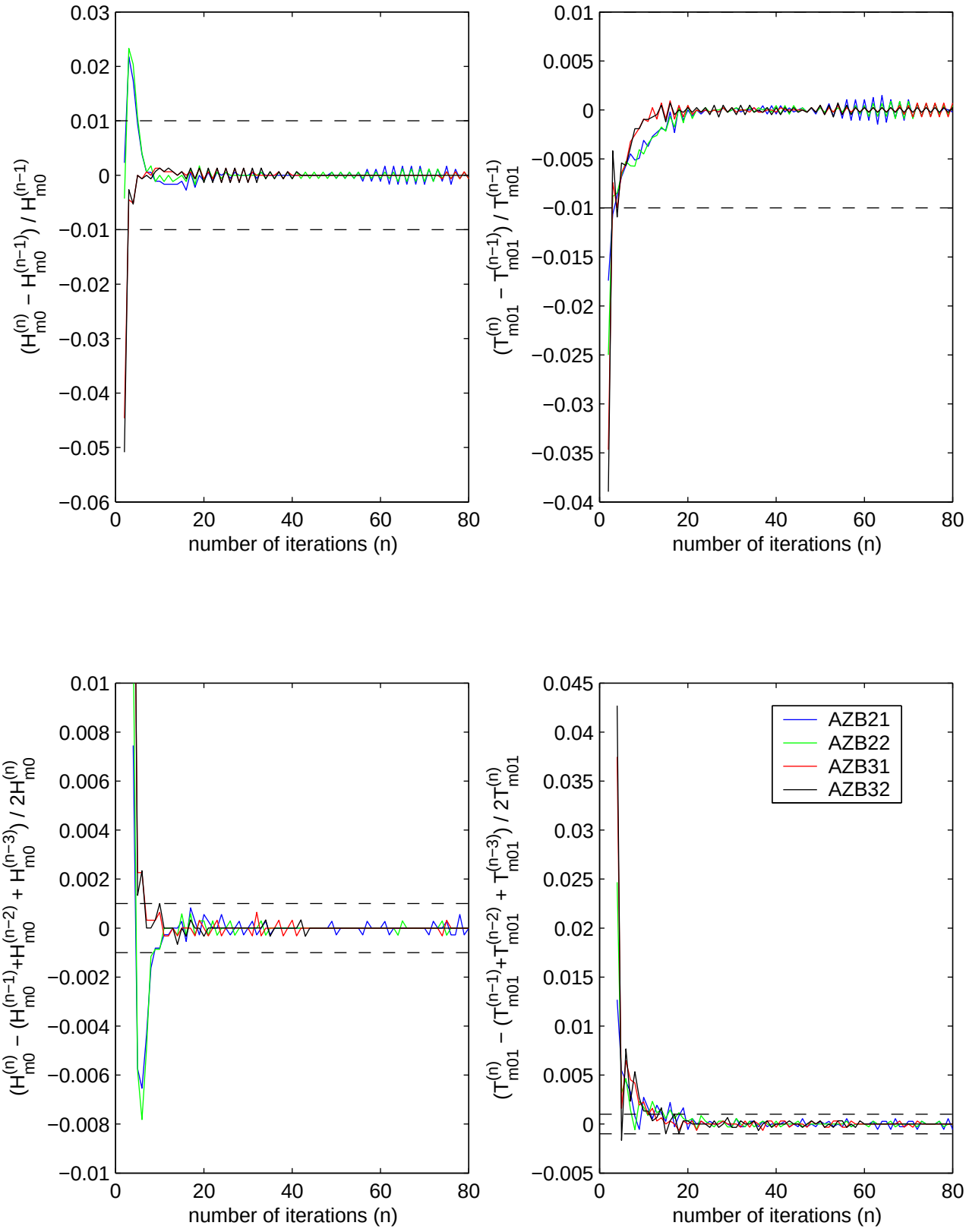

Convergence behaviour of H_{m0} and T_{m01} at Amelander Zeegat buoys Gradient−based and curvature−based	grid 2 (20m)	
	uniform water level / no current	
WL | DELFT HYDRAULICS	H4918.39	Fig. 2.3c

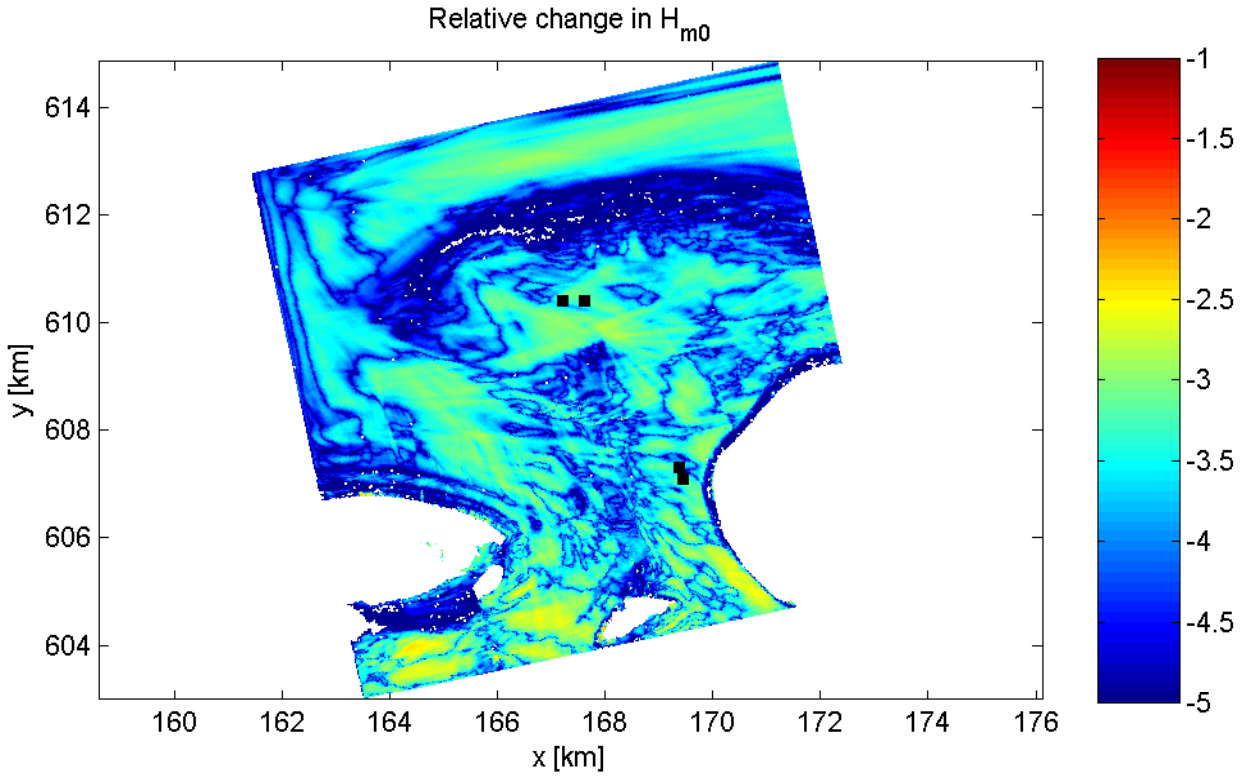

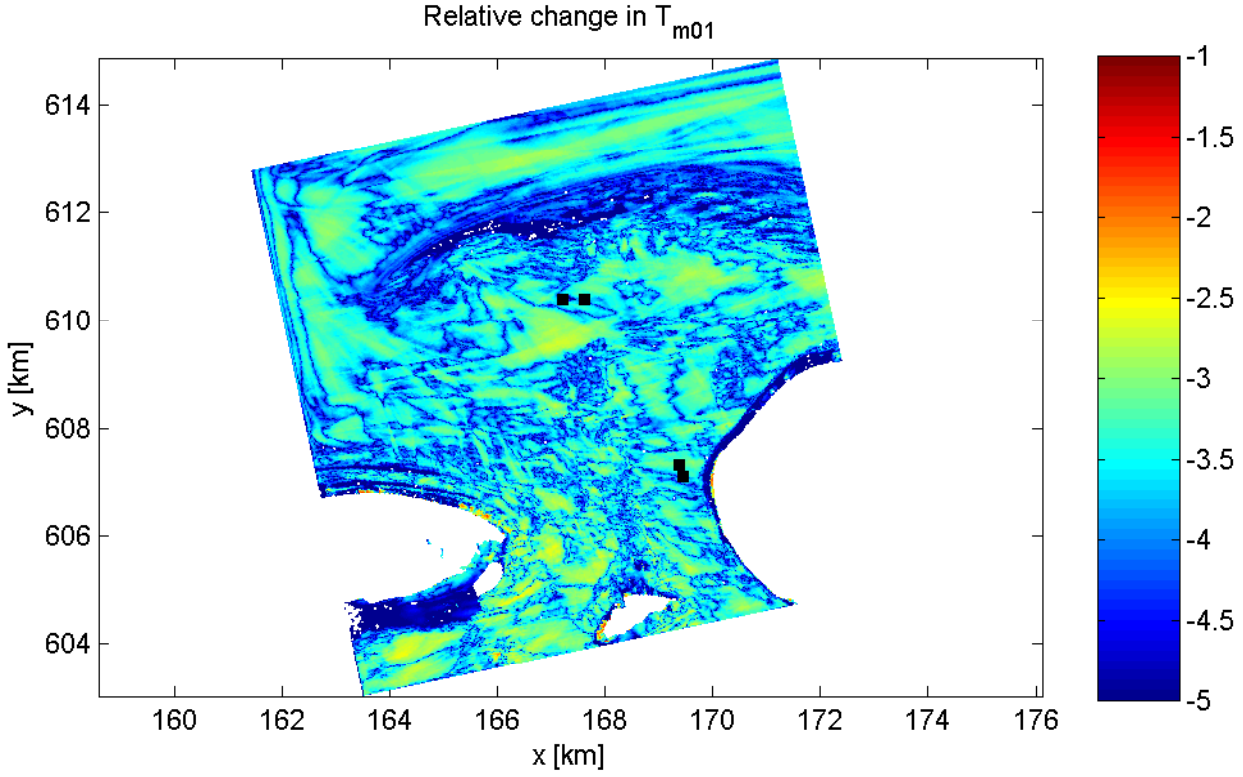

Convergence behaviour of H_{m0} and T_{m01} in Amelander Zeegat Relative change in final iteration: $^{10}\text{Log}(\lvert\phi^{(n,max)} - \phi^{(n,max-1)}\rvert / \phi^{(n,max)})$	grid 2 (20m)	
	uniform water level / no current	
WL | DELFT HYDRAULICS	H4918.39	Fig. 2.3d

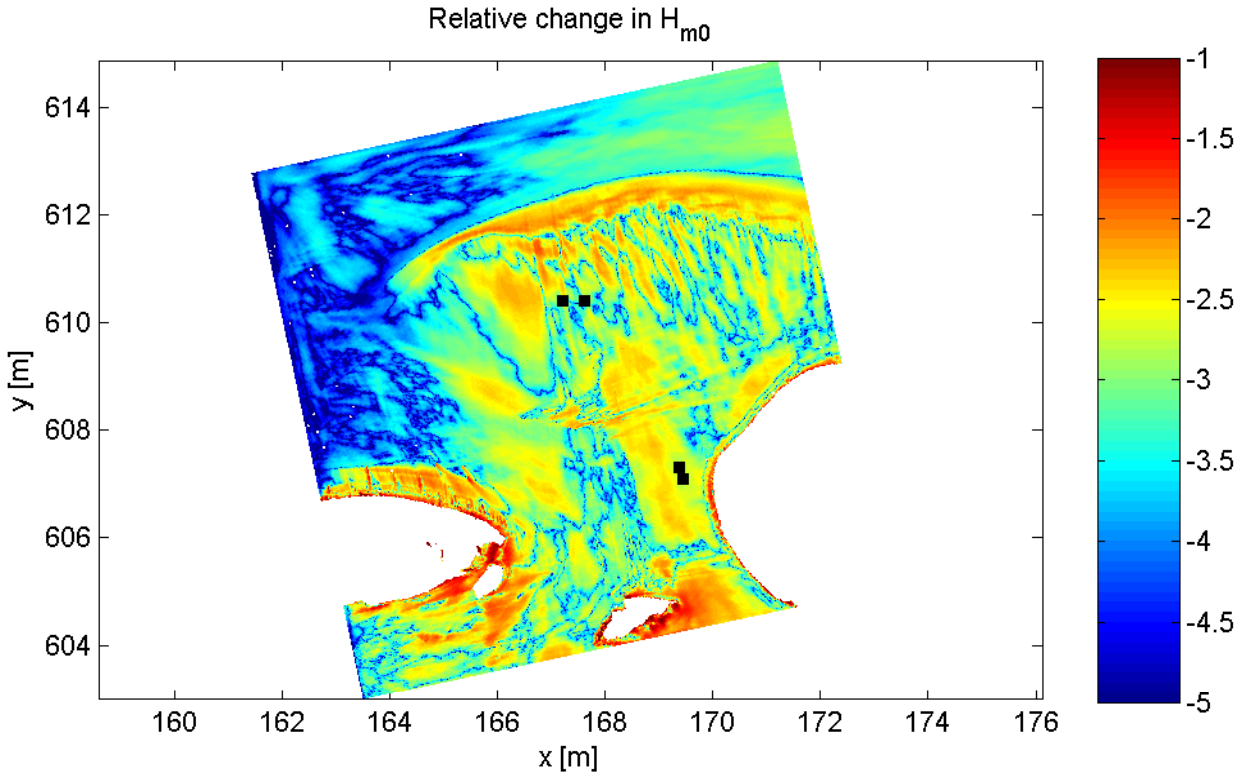

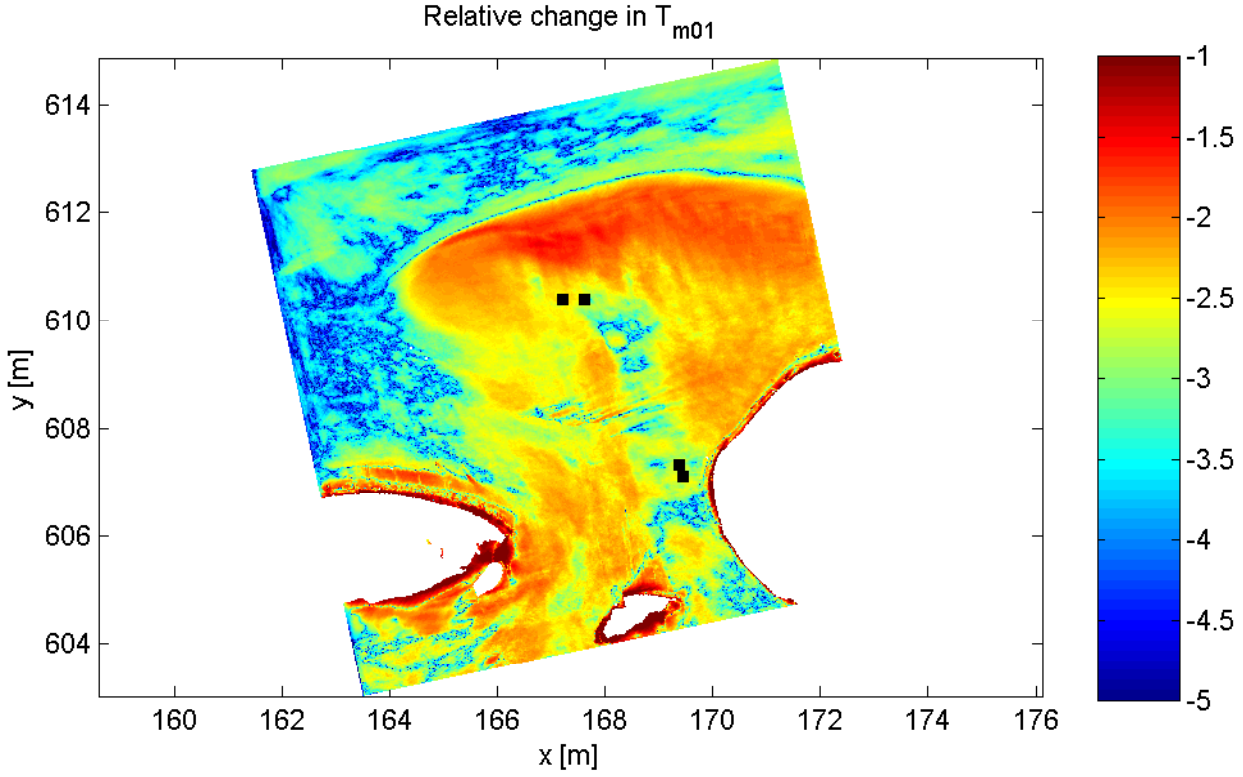

Convergence behaviour of H_{m0} and T_{m01} in Amelander Zeegat Relative change after convergence: $^{10}\text{Log}(\lvert\phi^{(n,max)} - \phi^{(n,conv)}\rvert / \phi^{(n,max)})$	grid 2 (20m)	
	uniform water level / no current	
WL | DELFT HYDRAULICS	H4918.39	Fig. 2.3e

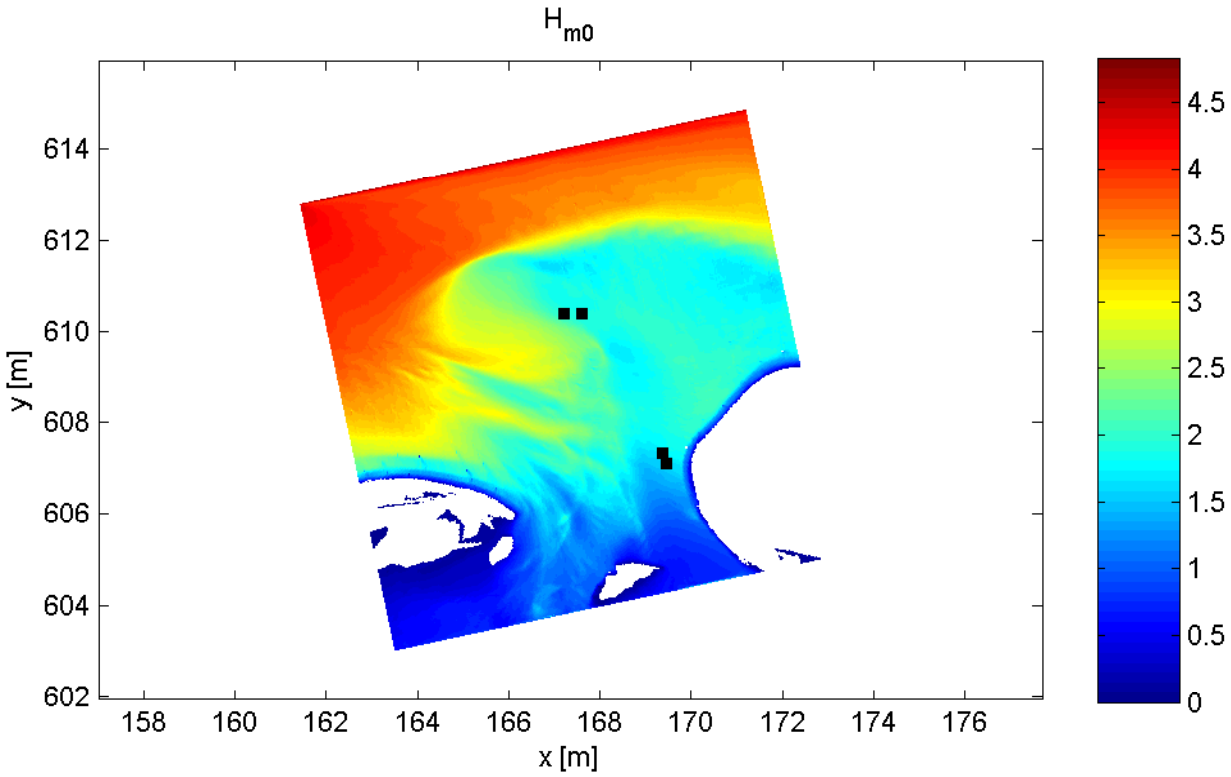

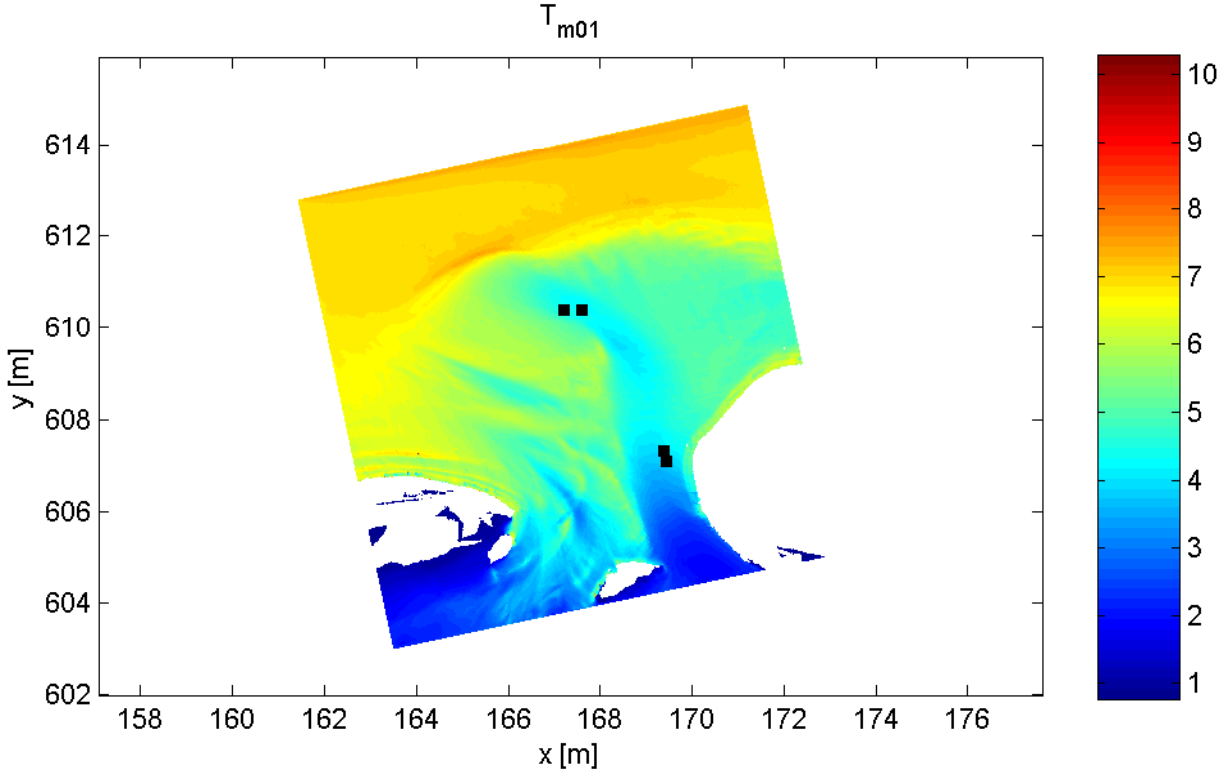

Solution of H_{m0} and T_{m01} in Amelander Zeegat after n,max iterations	grid 2 (20m)	
	spatially varying water level / current	
WL | DELFT HYDRAULICS	H4918.39	Fig. 2.4a

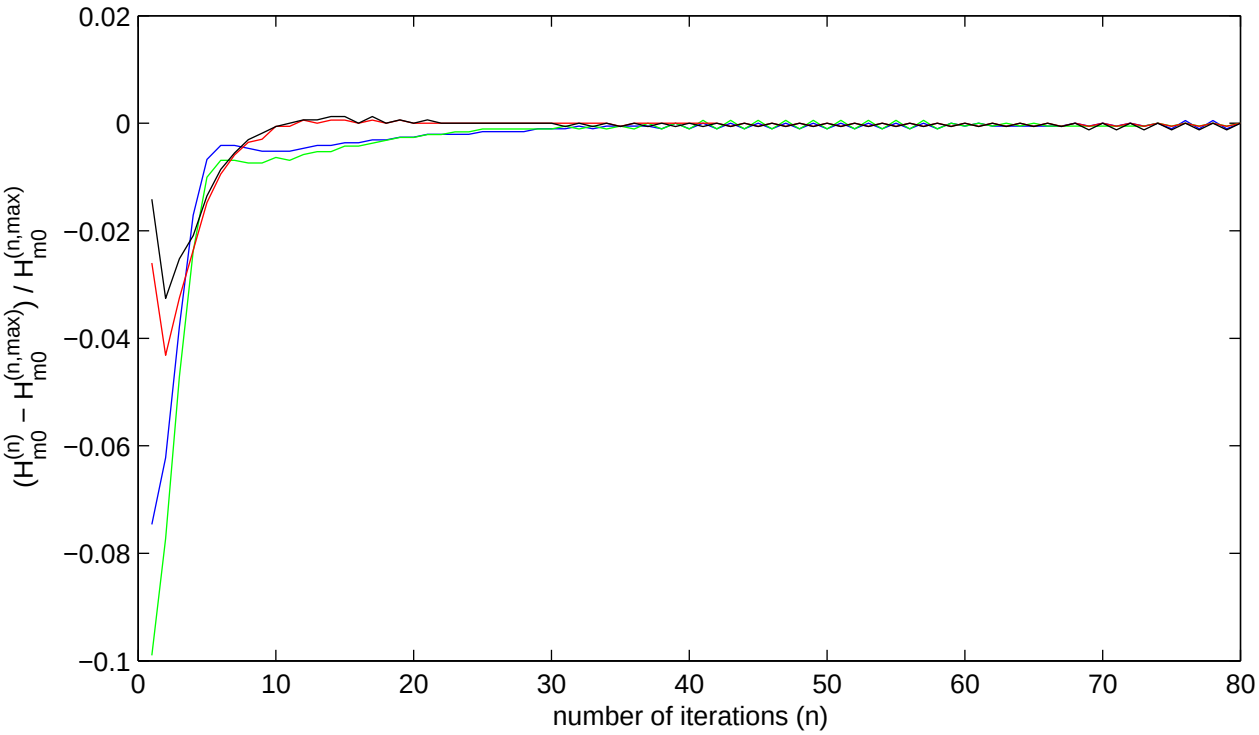

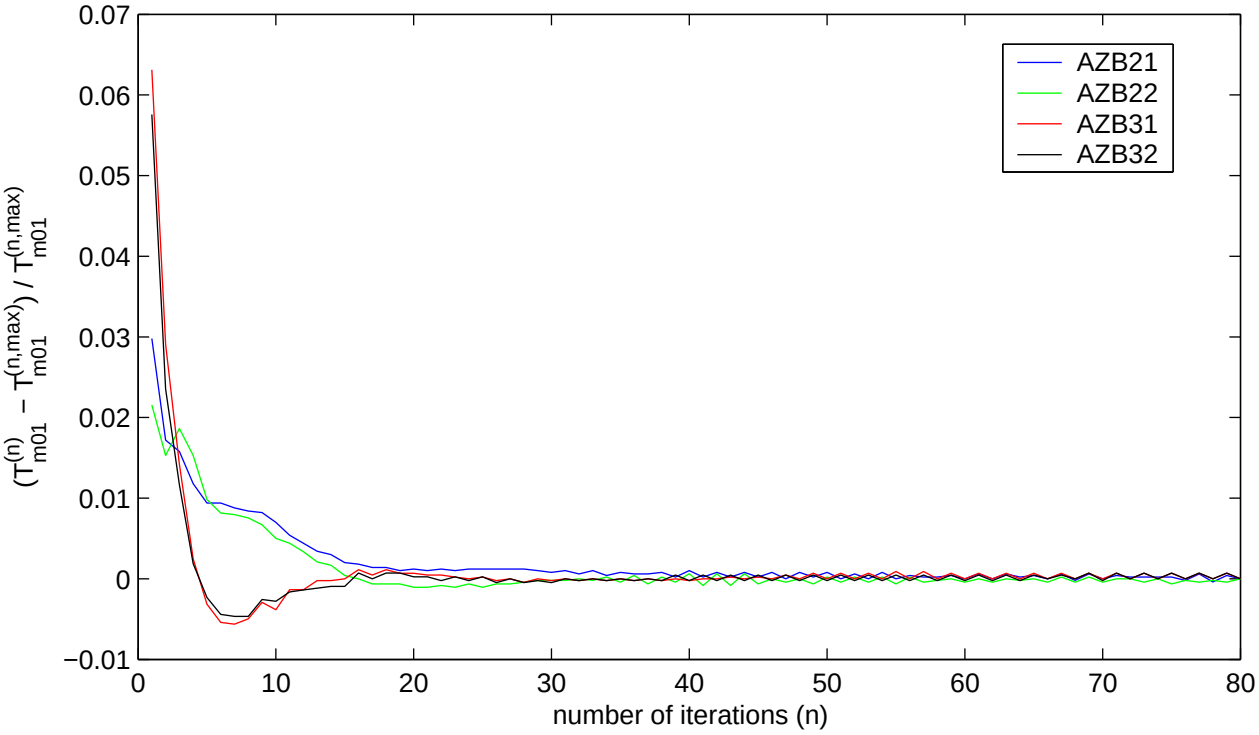

Convergence behaviour of H_{m0} and T_{m01} at Amelander Zeegat buoys Error relative to solution after n,max=80 iterations	grid 2 (20m)	
	spatially varying water level / current	
WL | DELFT HYDRAULICS	H4918.39	Fig. 2.4b

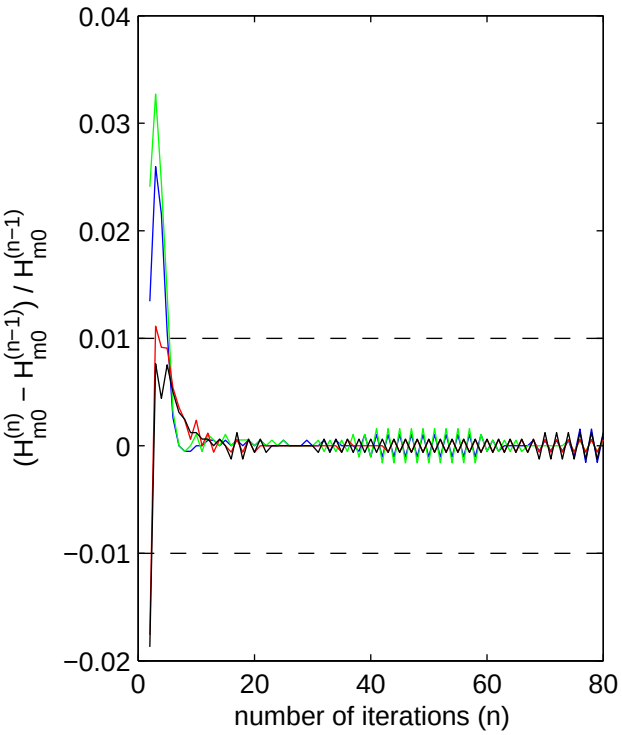

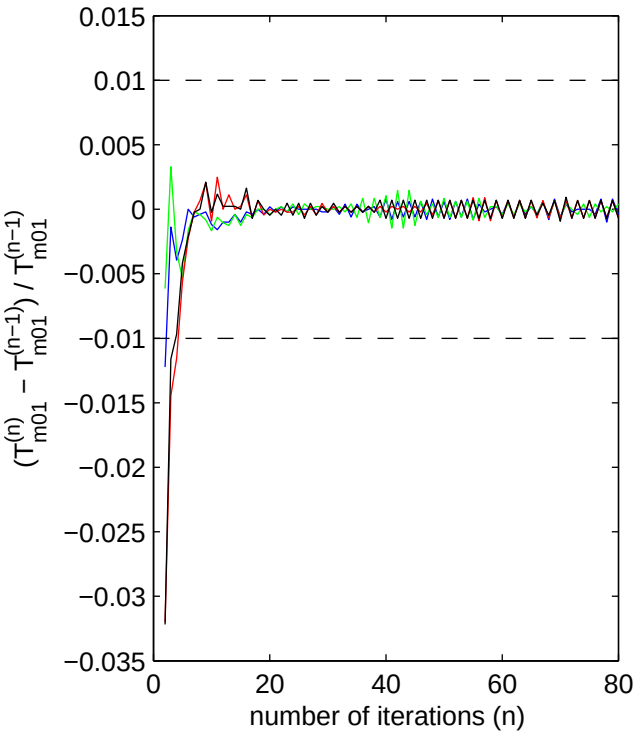

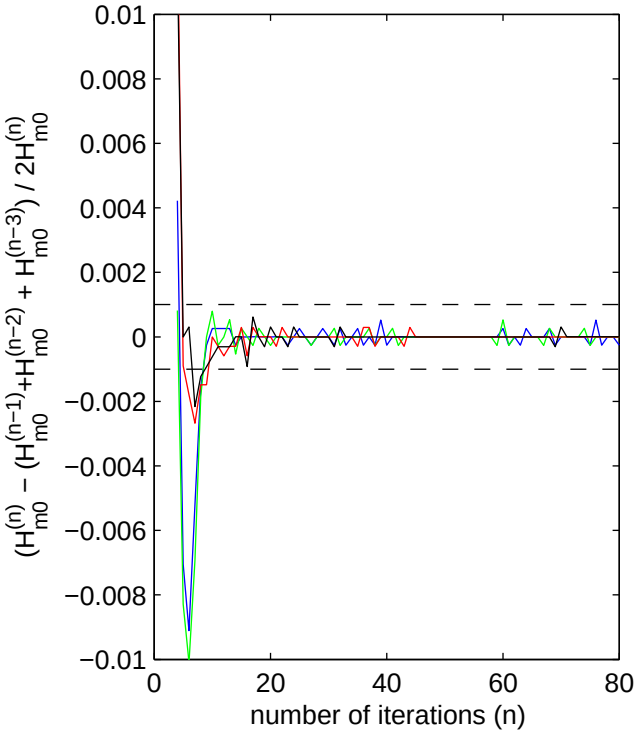

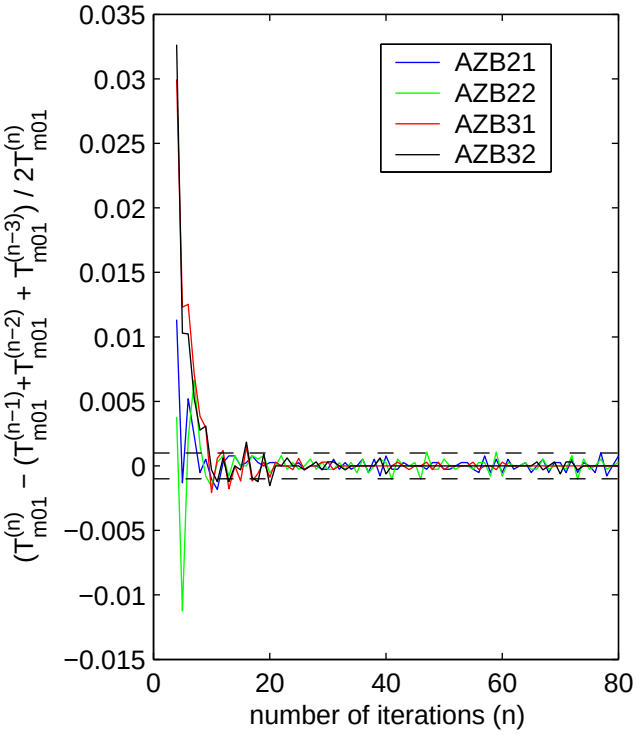

Convergence behaviour of H_{m0} and T_{m01} at Amelander Zeegat buoys Gradient−based and curvature−based	grid 2 (20m)	
	spatially varying water level / current	
WL | DELFT HYDRAULICS	H4918.39	Fig. 2.4c

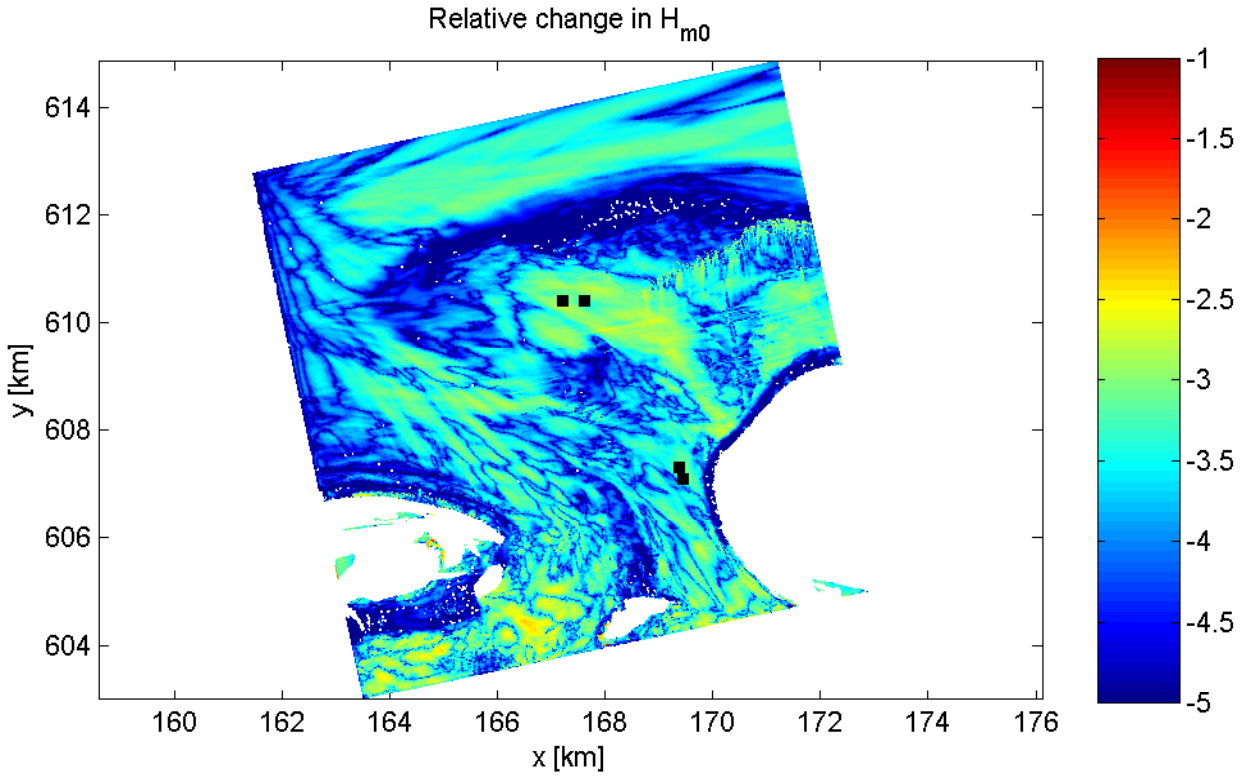

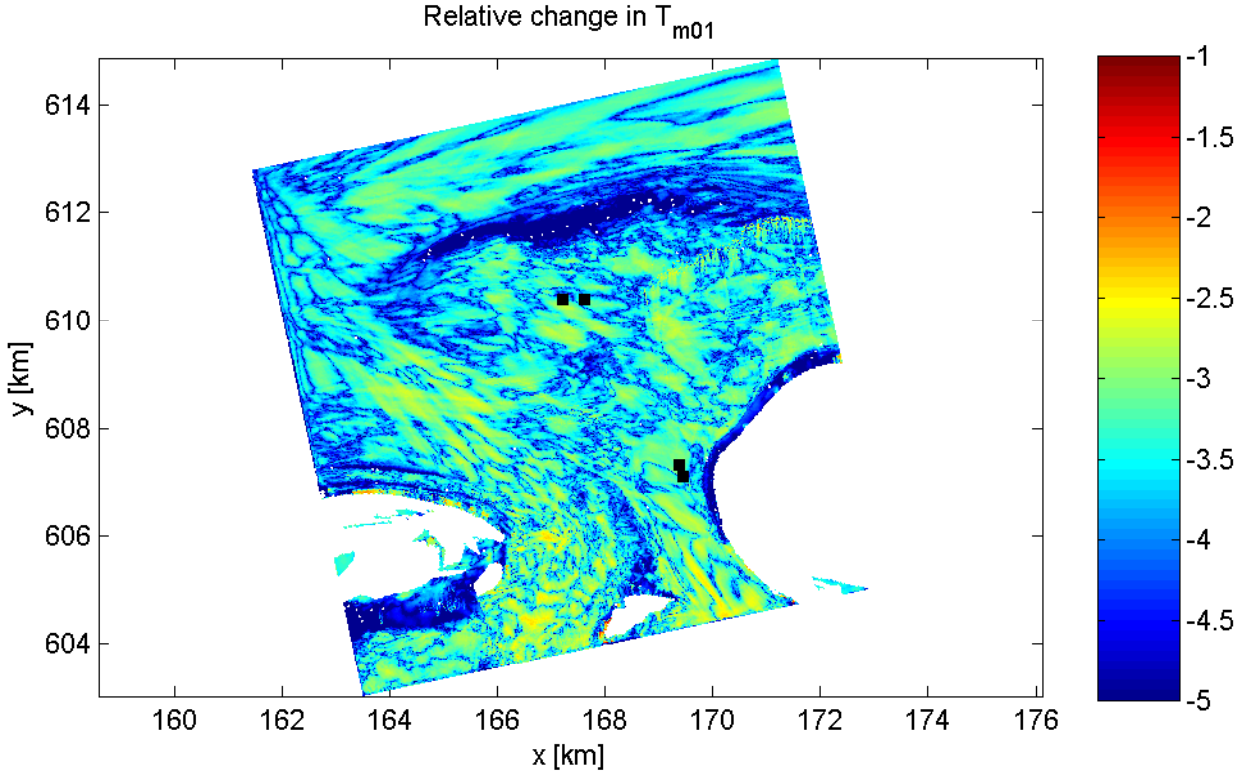

Convergence behaviour of H_{m0} and T_{m01} in Amelander Zeegat Relative change in final iteration: $^{10}\text{Log}(\lvert\phi^{(n,max)} - \phi^{(n,max-1)}\rvert / \phi^{(n,max)})$	grid 2 (20m)	
	spatially varying water level / current	
WL | DELFT HYDRAULICS	H4918.39	Fig. 2.4d

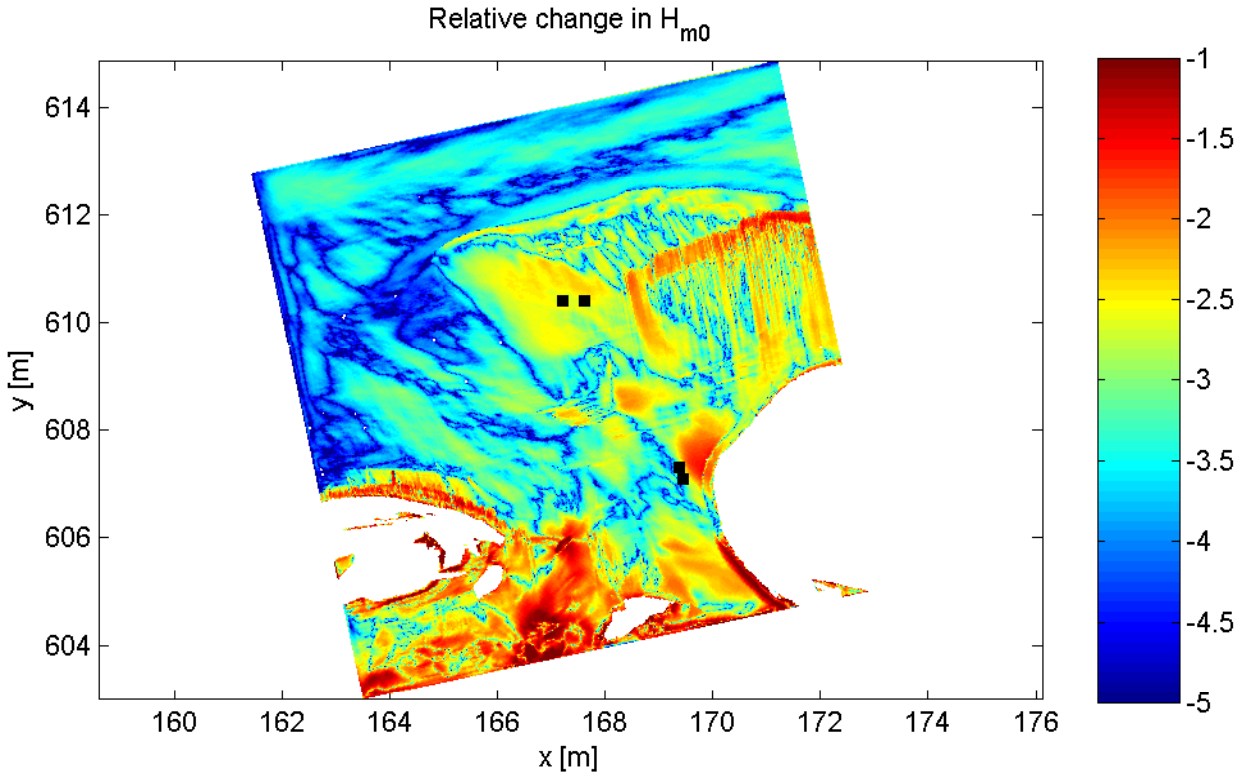

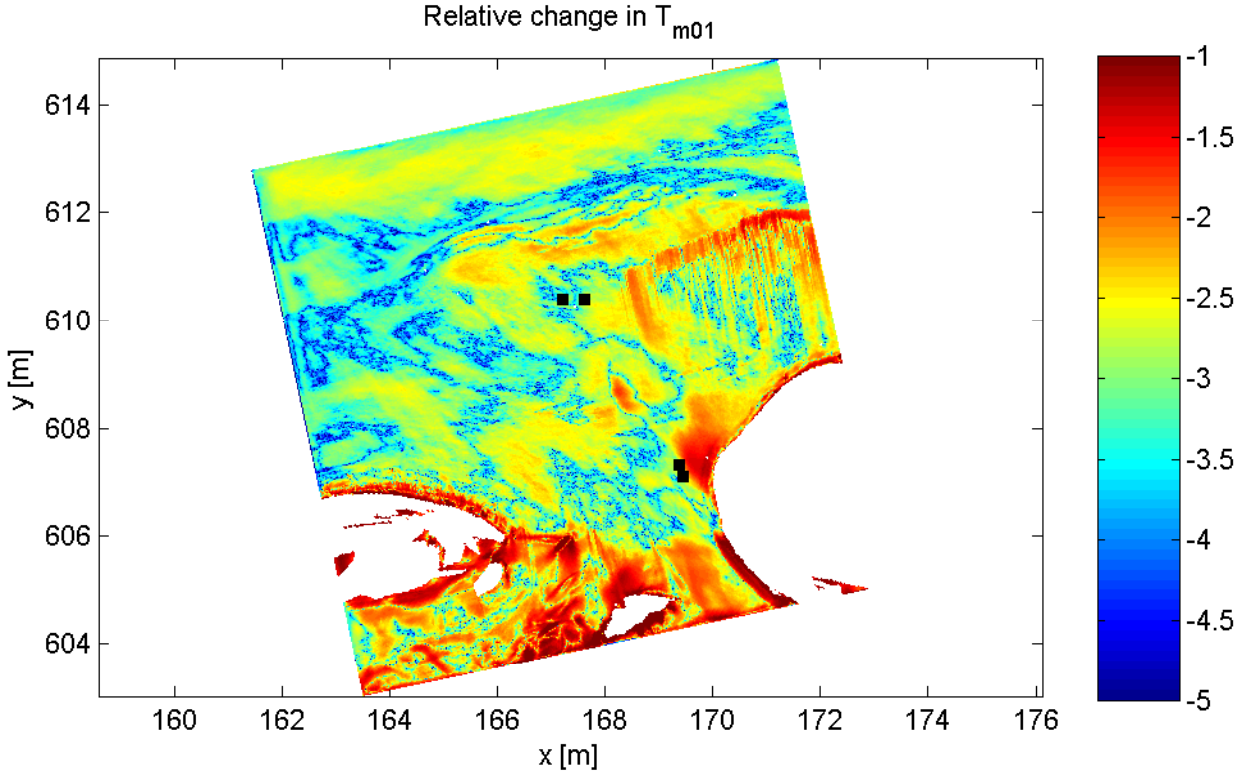

Convergence behaviour of H_{m0} and T_{m01} in Amelander Zeegat Relative change after convergence: $^{10}\text{Log}(\lvert\phi^{(n,max)} - \phi^{(n,conv)}\rvert / \phi^{(n,max)})$	grid 2 (20m)	
	spatially varying water level / current	
WL | DELFT HYDRAULICS	H4918.39	Fig. 2.4e

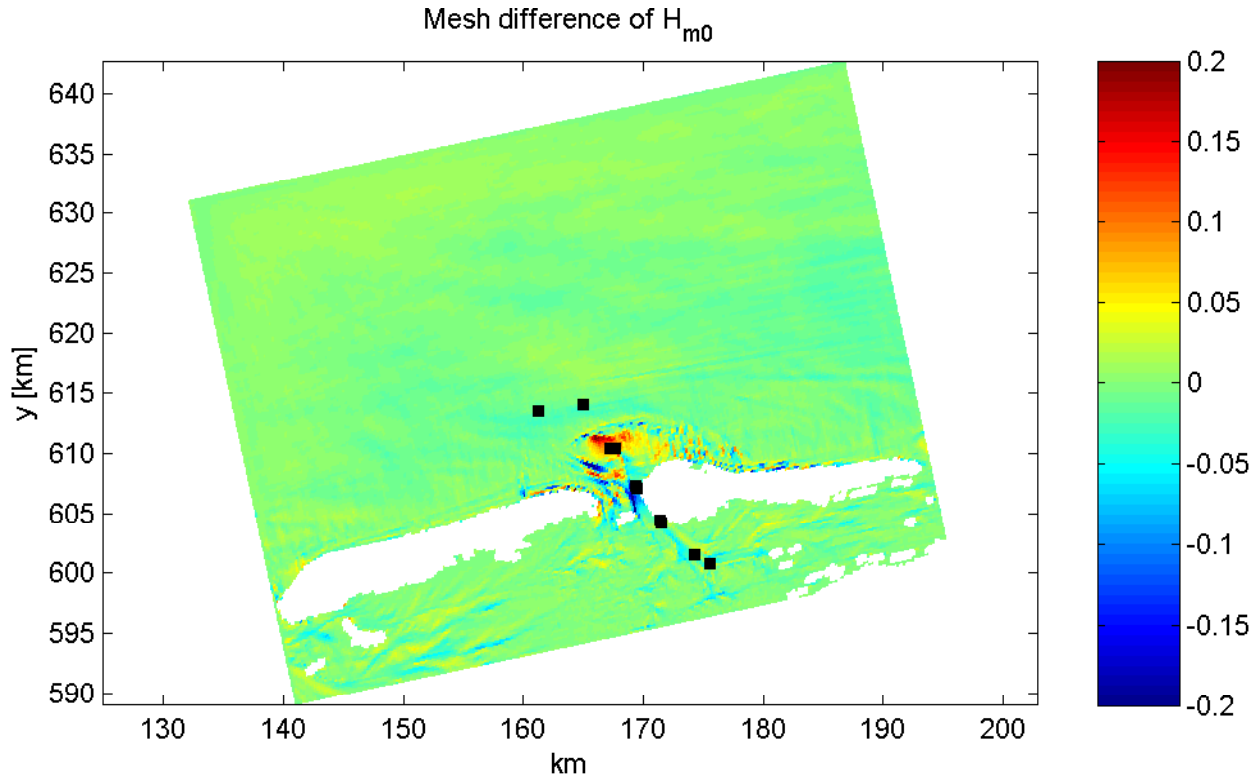

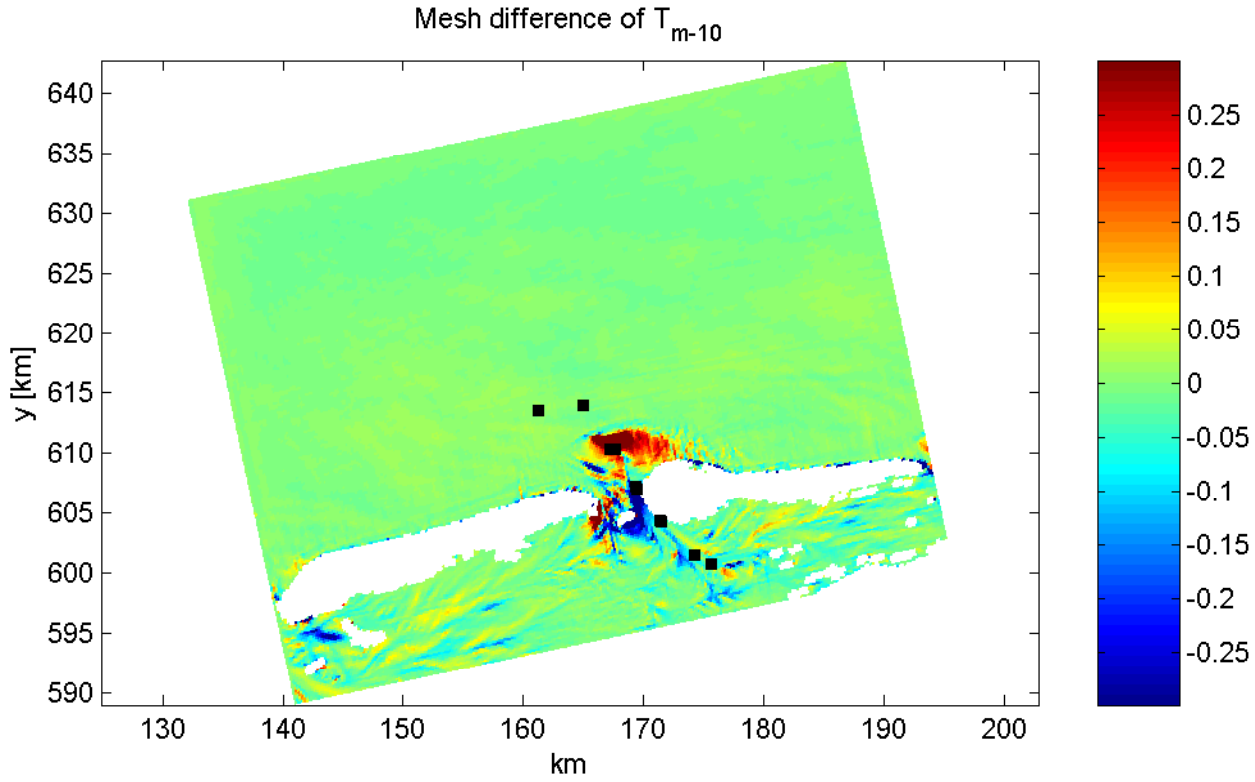

Mesh differences of wave parameters on grid 1 of Amelander Zeegat with h=100m (computations with quadruplets)

WL | DELFT HYDRAULICS | H4918.39 | Fig. 3.1a

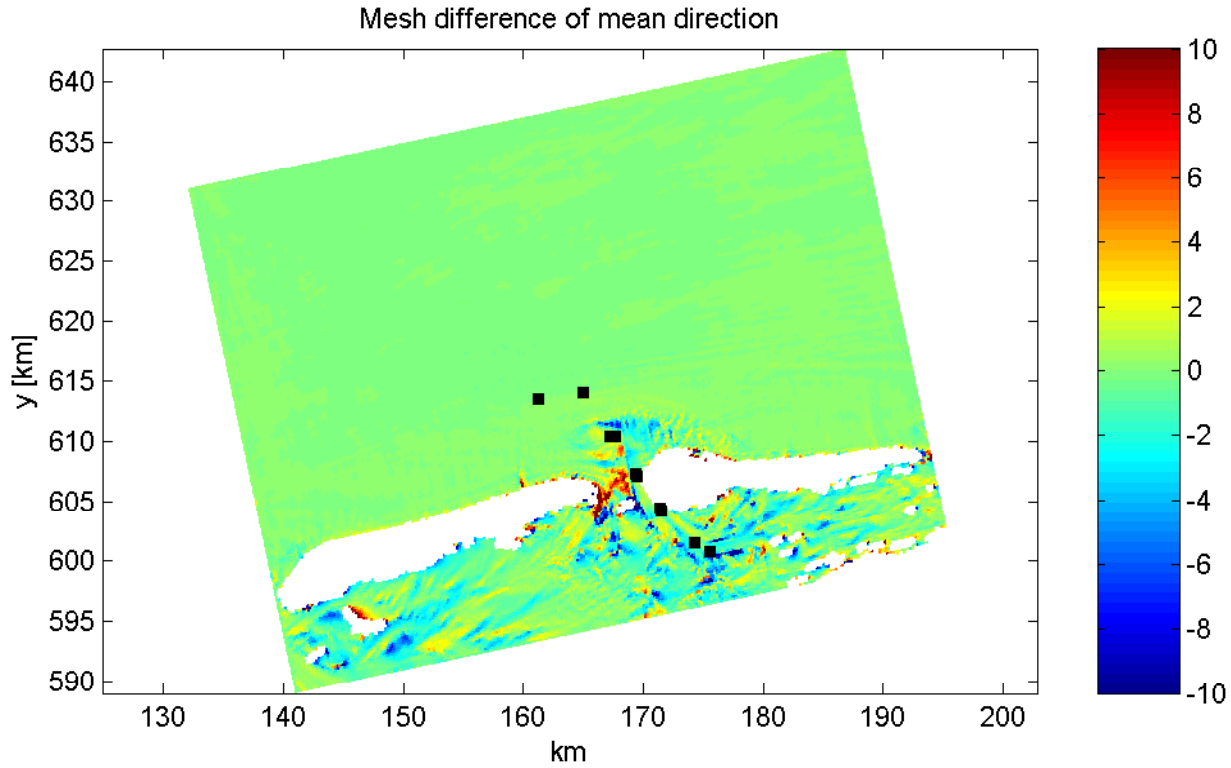

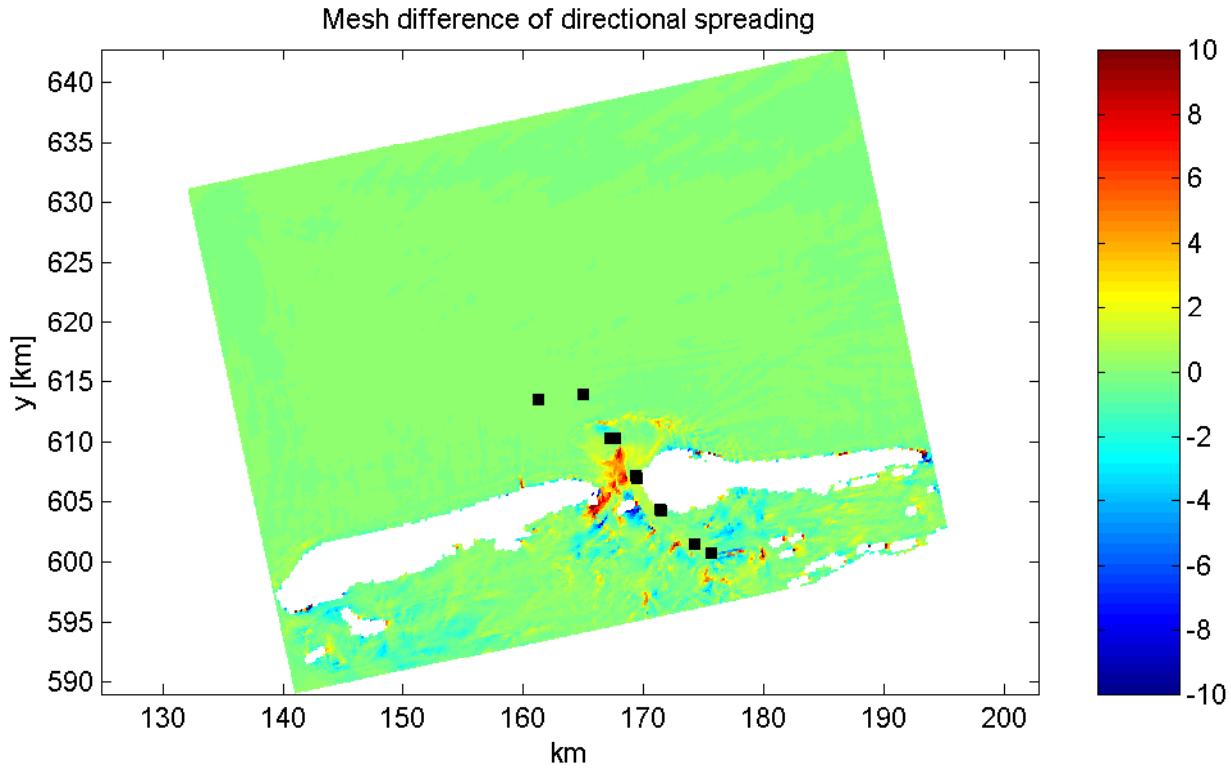

Mesh differences of wave parameters on grid 1 of Amelander Zeegat with h=100m (computations with quadruplets)

WL | DELFT HYDRAULICS

H4918.39

Fig. 3.1b

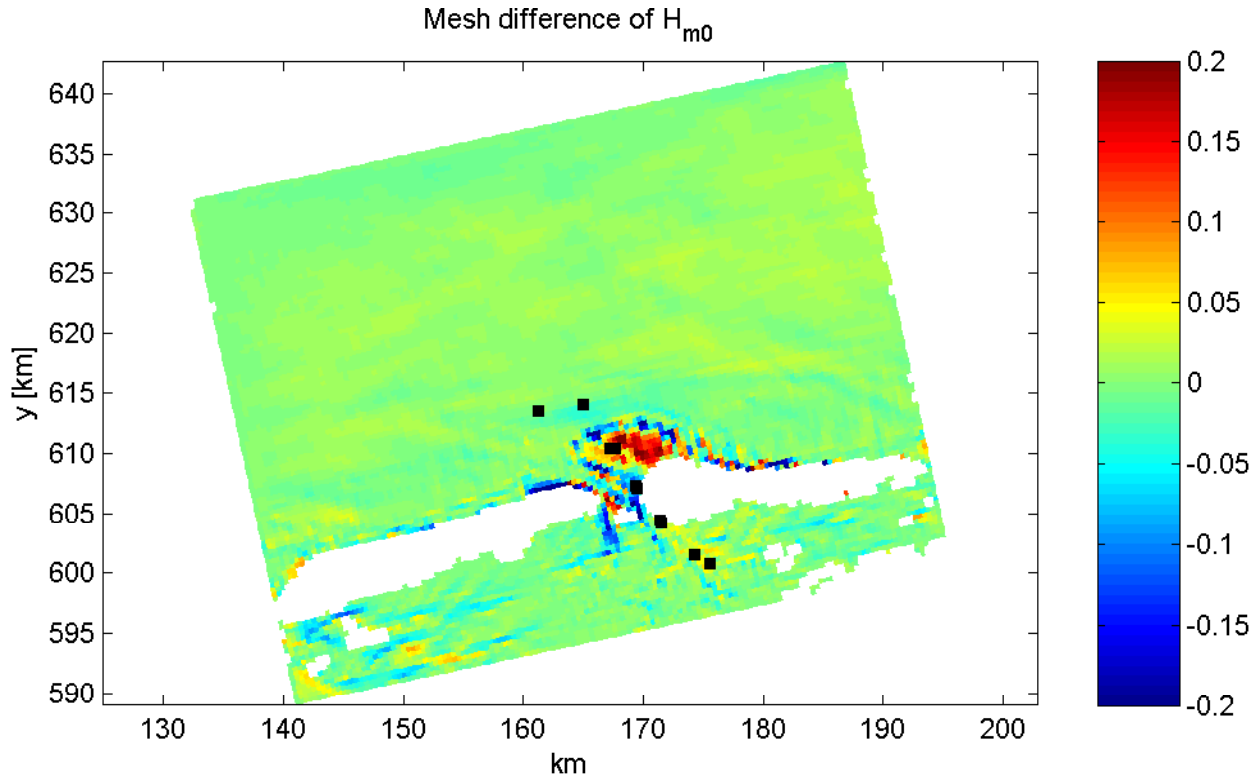

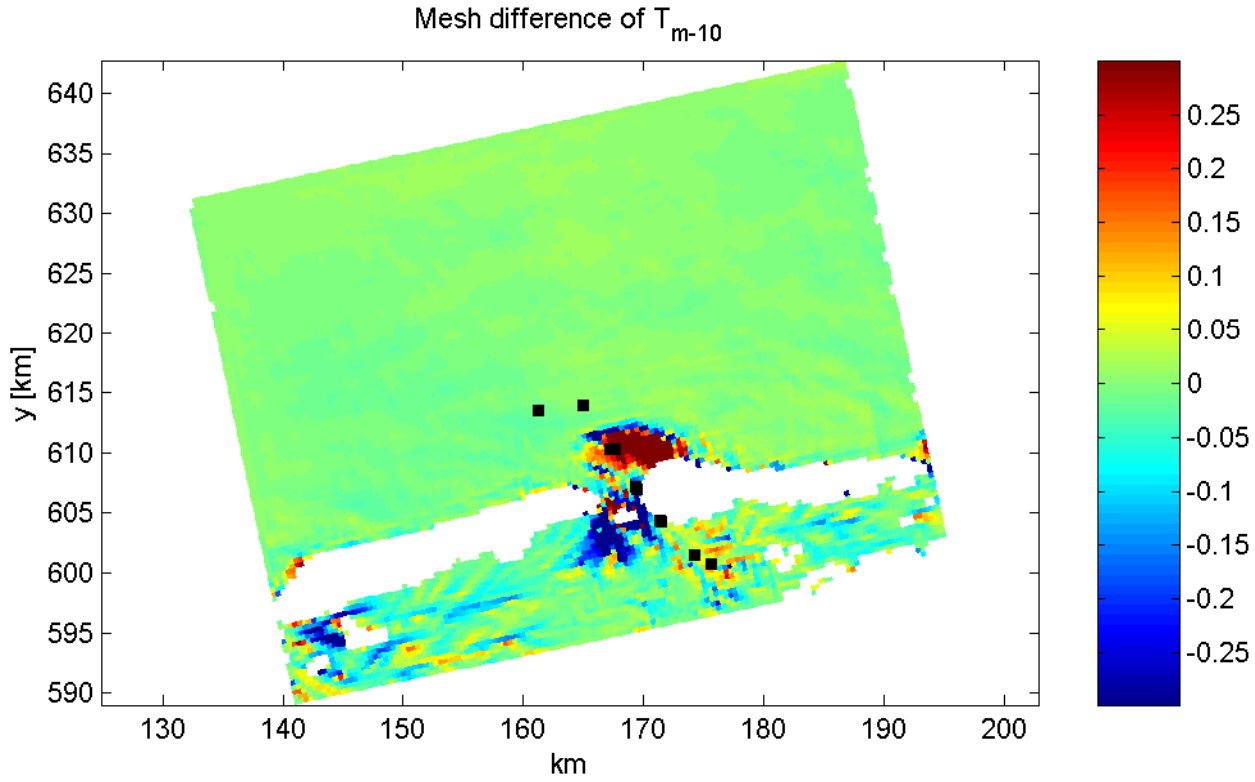

Mesh differences of wave parameters on grid 1 of Amelander Zeegat with h=200m (computations with quadruplets)

WL | DELFT HYDRAULICS

H4918.39

Fig. 3.2a

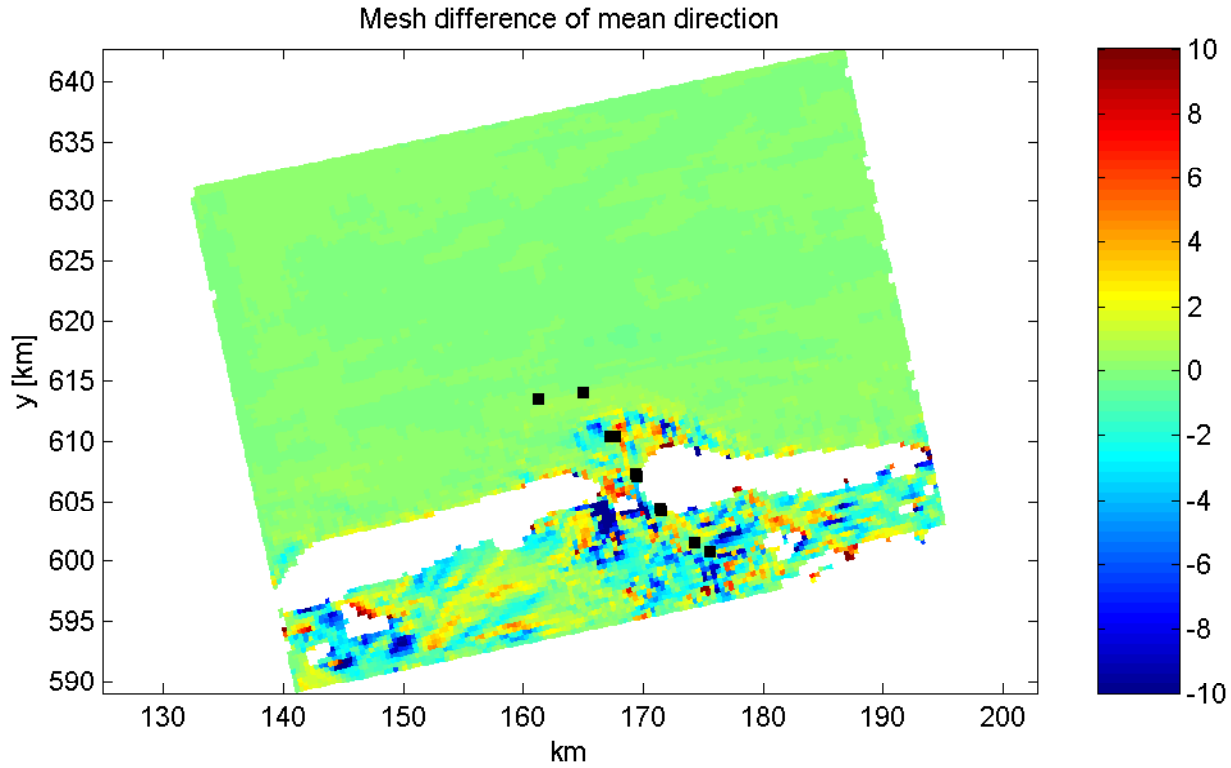

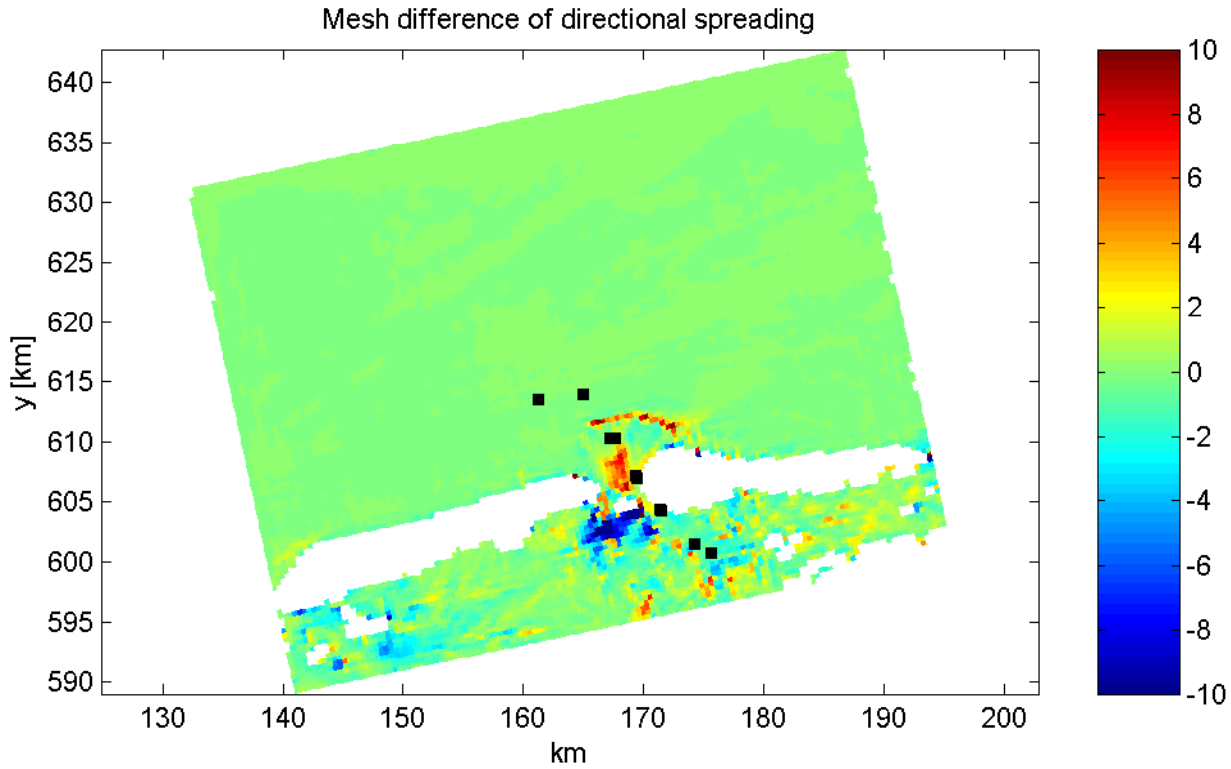

Mesh differences of wave parameters on grid 1 of Amelander Zeegat with h=200m (computations with quadruplets)

WL | DELFT HYDRAULICS

H4918.39

Fig. 3.2b

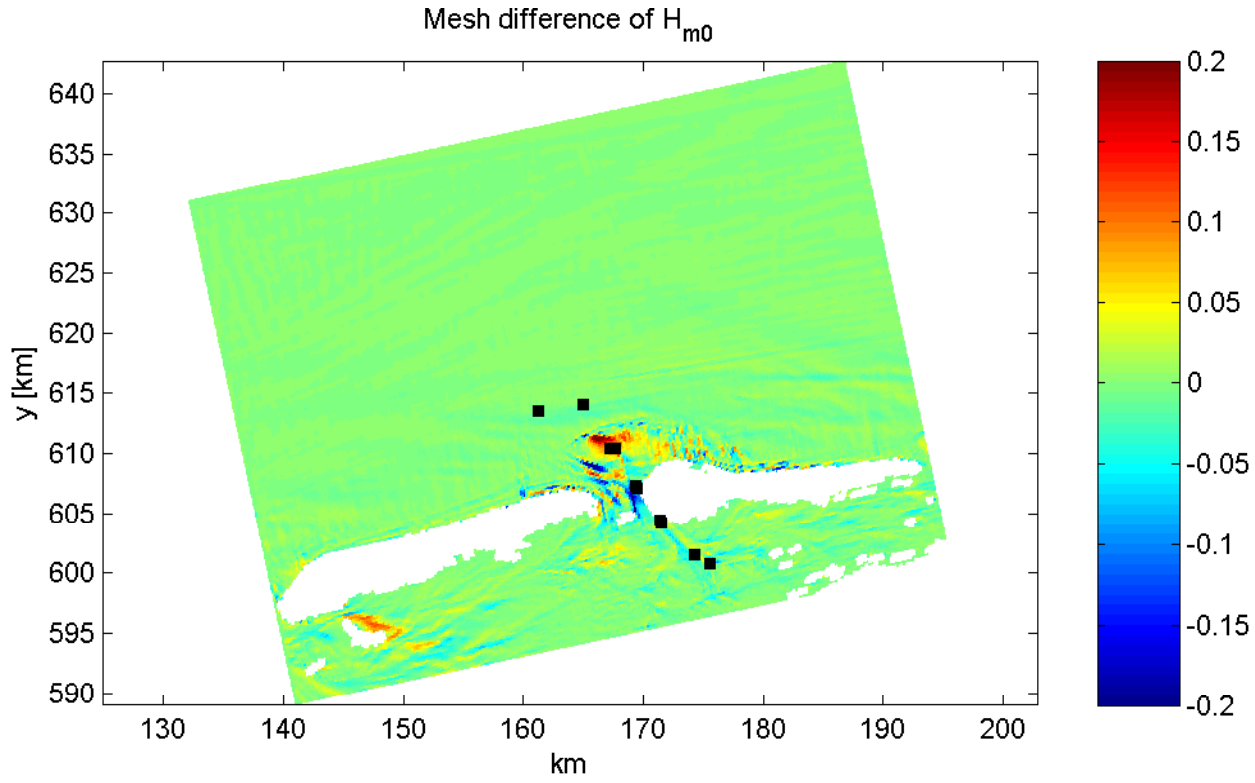

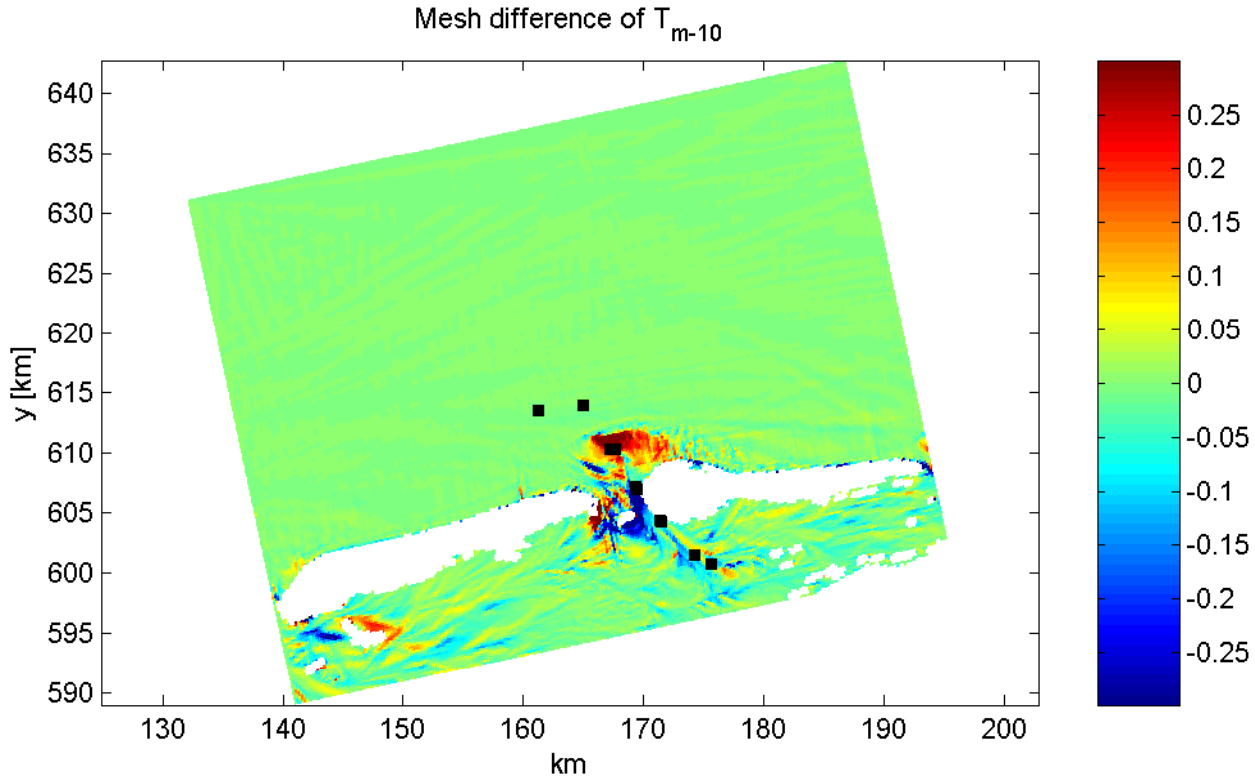

Mesh differences of wave parameters on grid 1 of Amelander Zeegat with h=100m (computations without quadruplets)

WL | DELFT HYDRAULICS

H4918.39

Fig. 3.3a

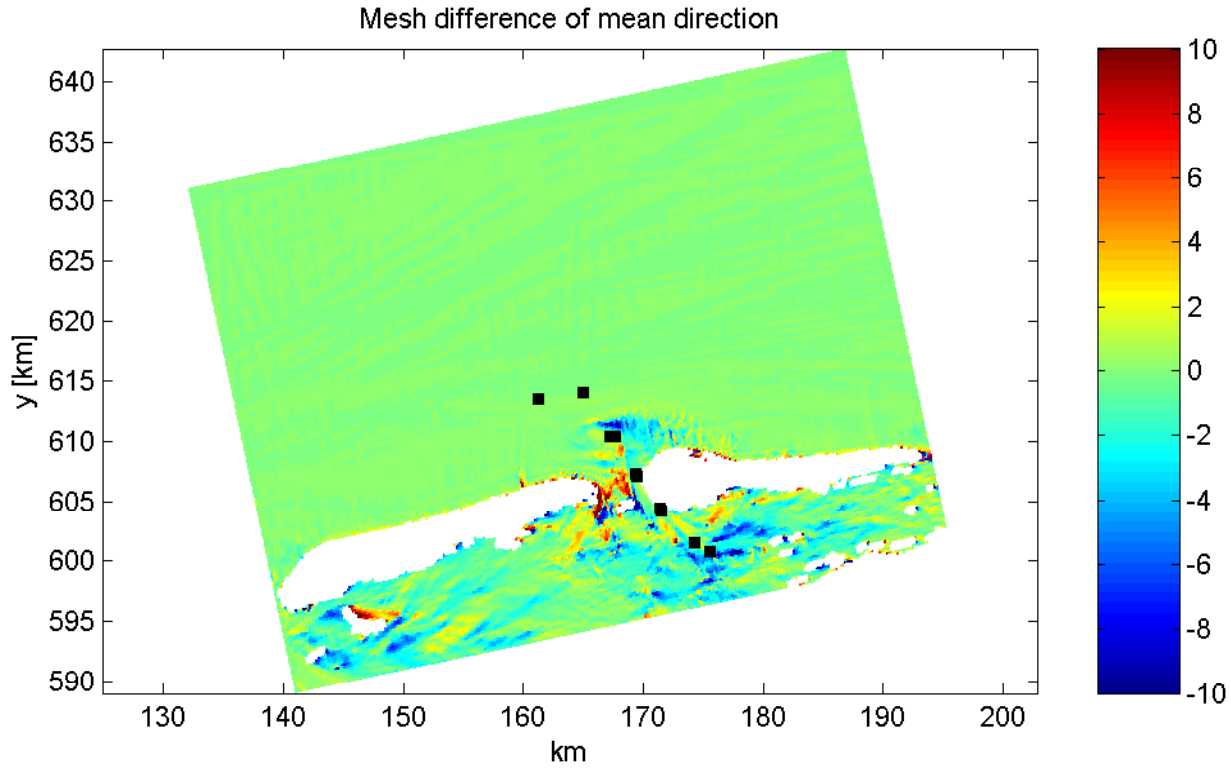

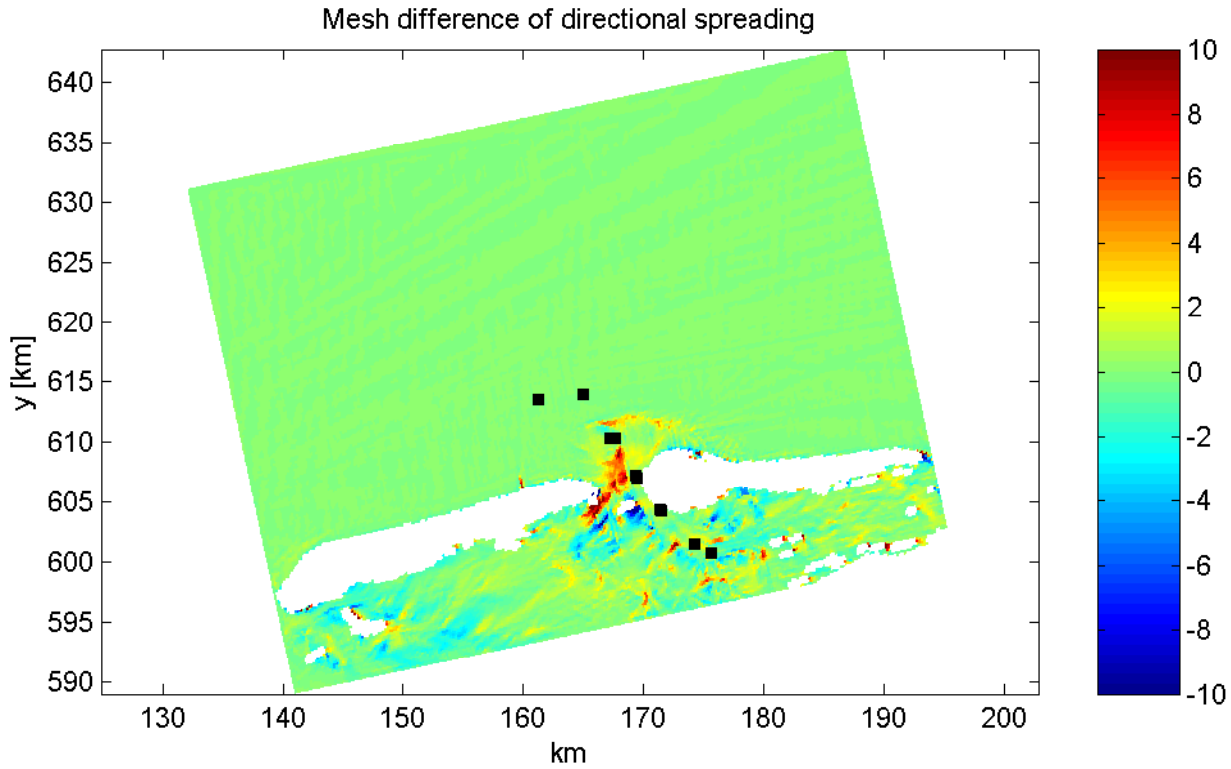

Mesh differences of wave parameters on grid 1 of Amelander Zeegat with h=100m (computations without quadruplets)

WL | DELFT HYDRAULICS | H4918.39 | Fig. 3.3b

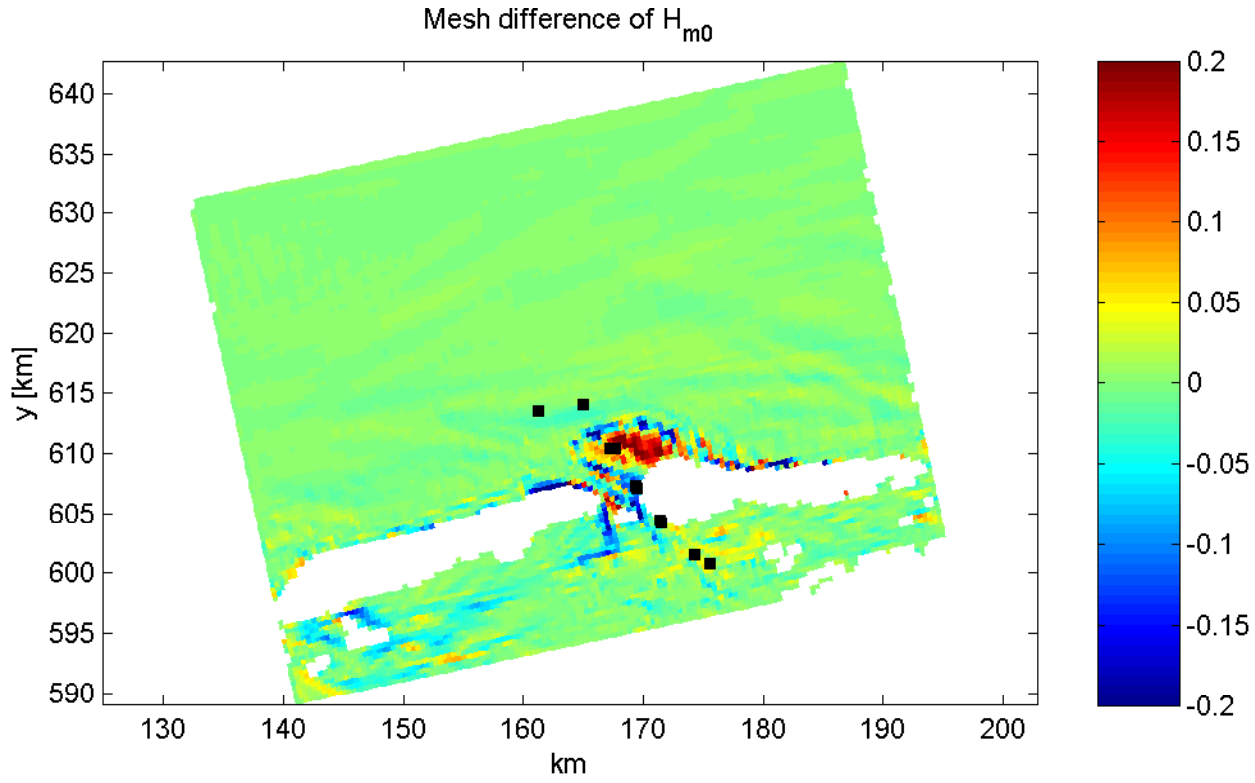

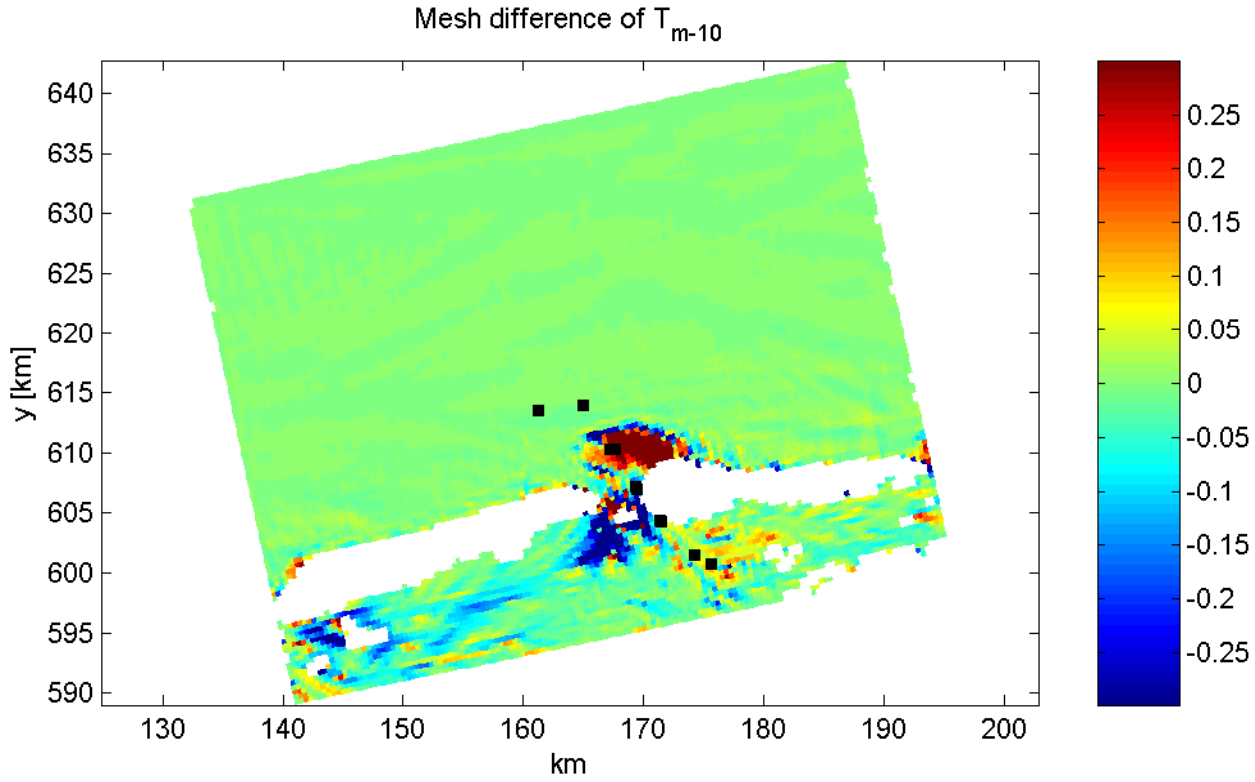

Mesh differences of wave parameters on grid 1 of Amelander Zeegat with h=200m (computations without quadruplets)

WL | DELFT HYDRAULICS	H4918.39	Fig. 3.4a

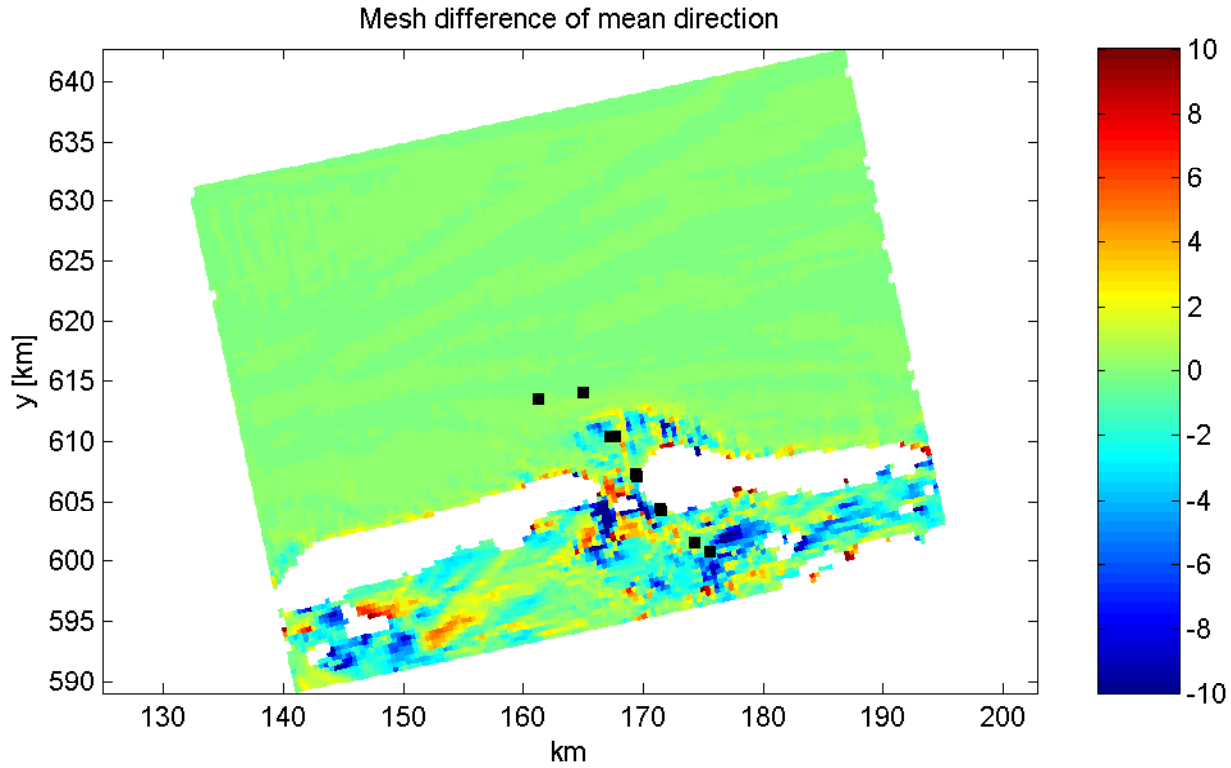

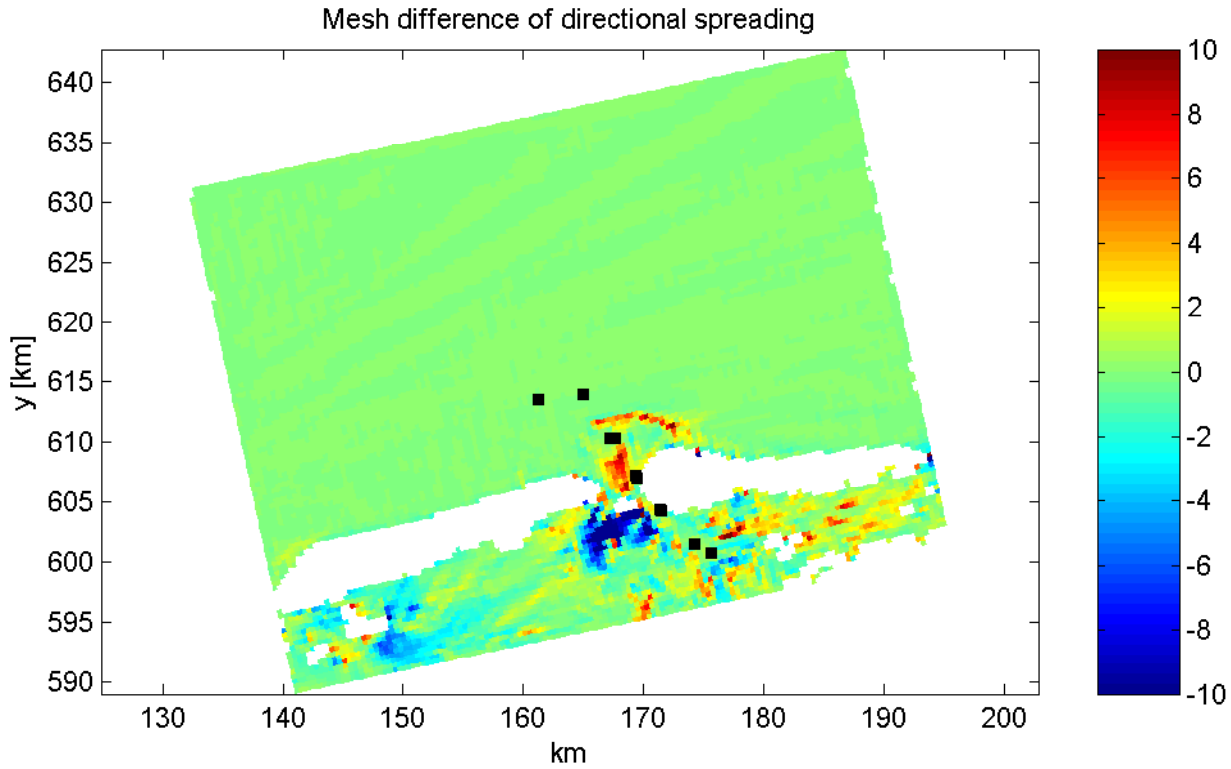

Mesh differences of wave parameters on grid 1 of Amelander Zeegat with h=200m (computations without quadruplets)

WL | DELFT HYDRAULICS	H4918.39	Fig. 3.4b

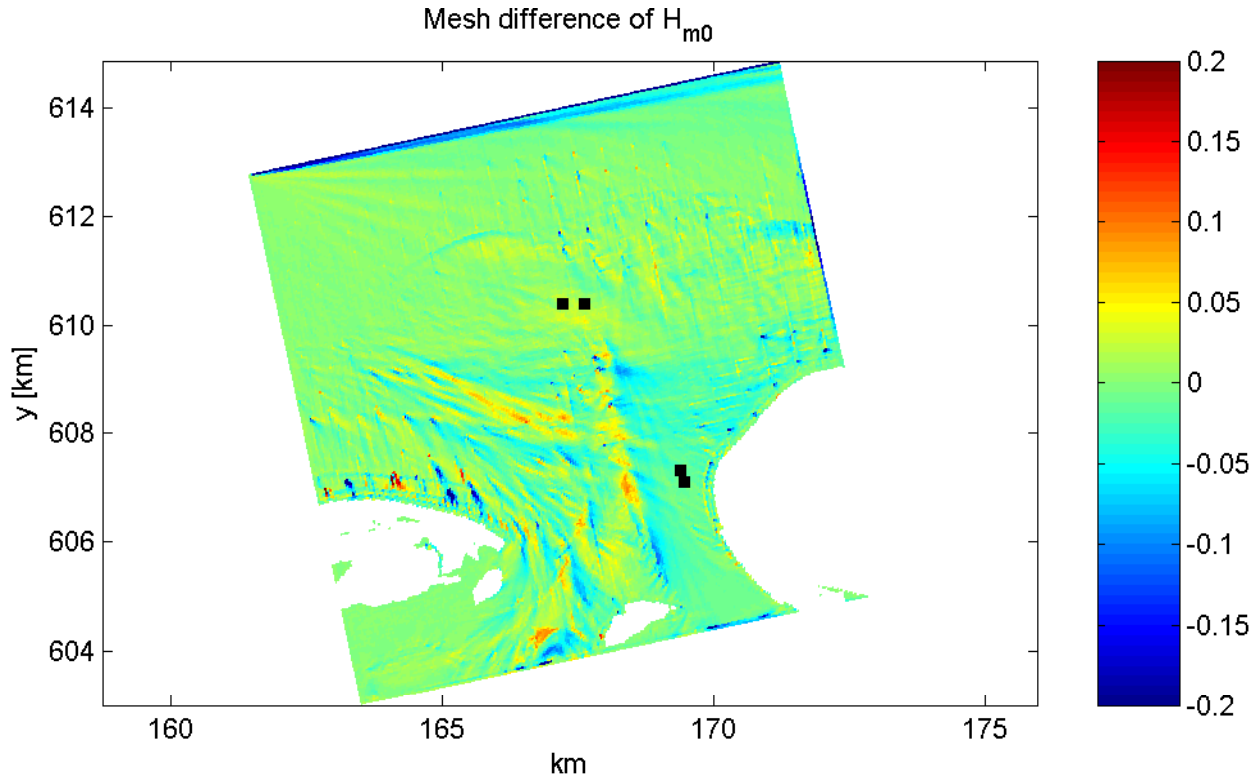

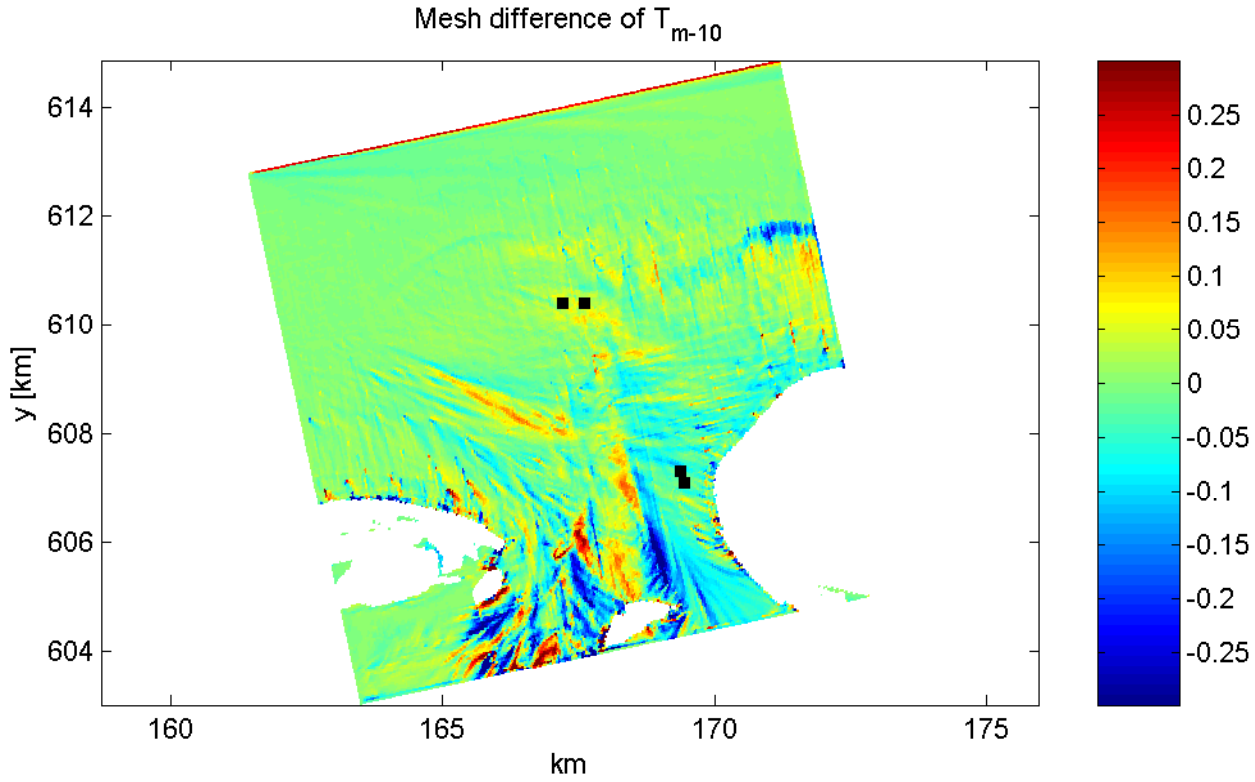

Mesh differences of wave parameters on grid 2 of Amelander Zeegat with h=20m (computations with quadruplets)

WL | DELFT HYDRAULICS	H4918.39	Fig. 3.5a

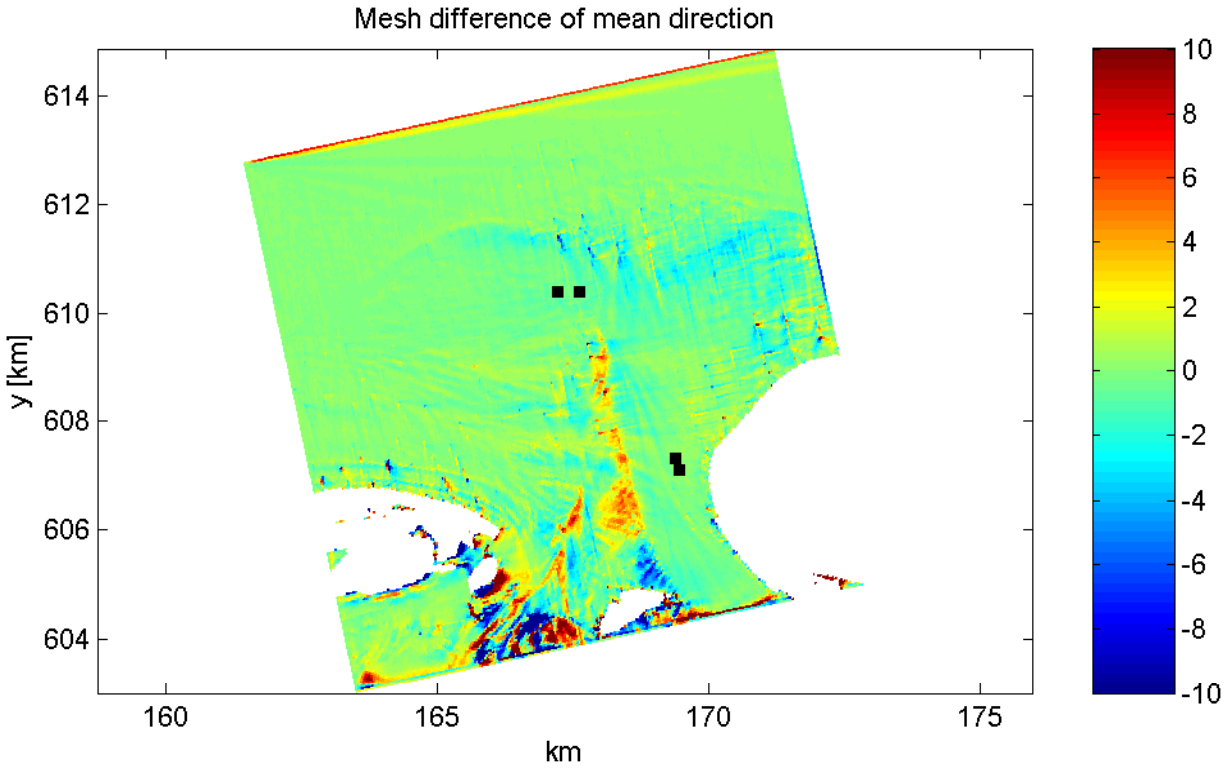

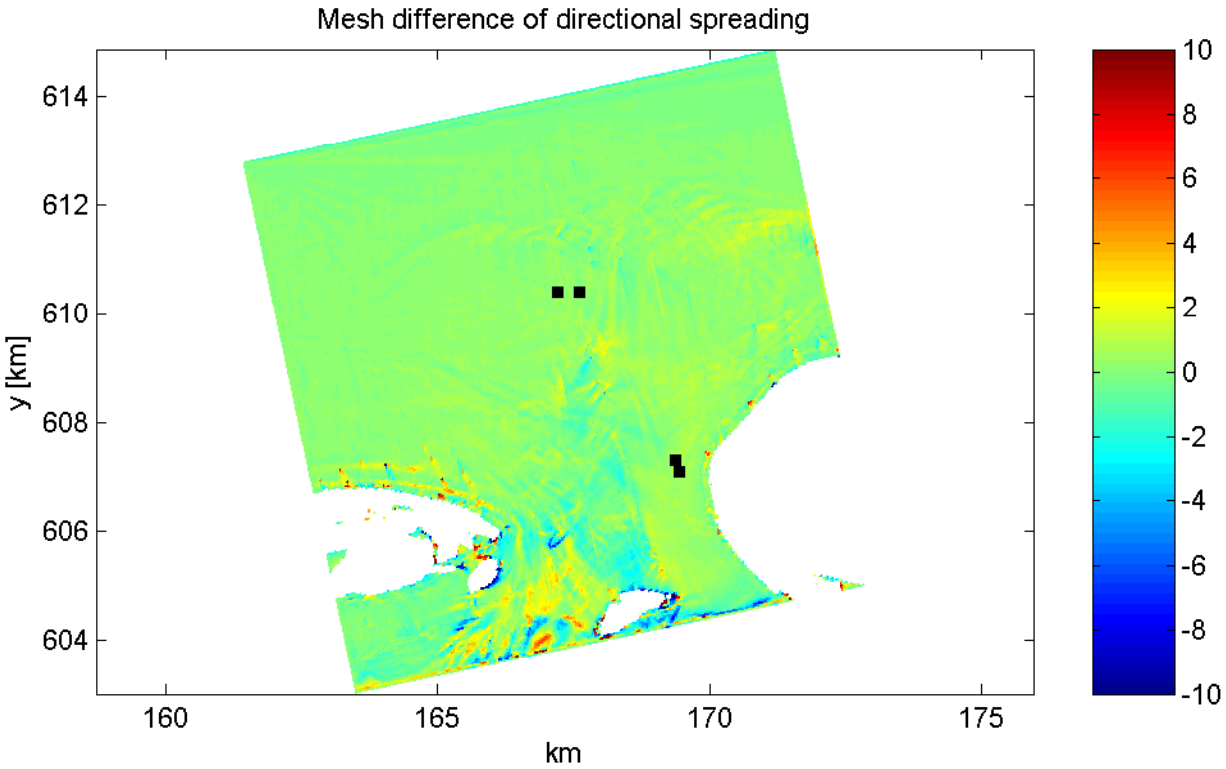

Mesh differences of wave parameters on grid 2 of Amelander Zeegat with h=20m (computations with quadruplets)

WL | DELFT HYDRAULICS | H4918.39 | Fig. 3.5b

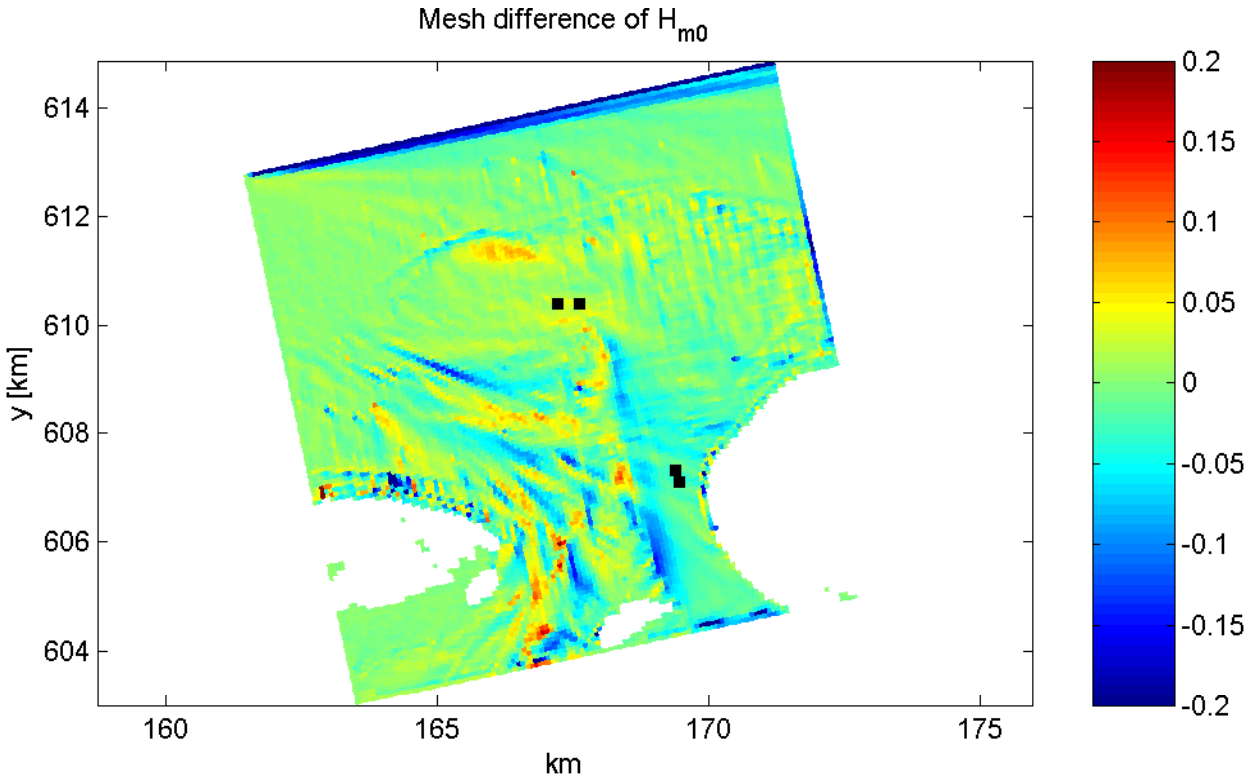

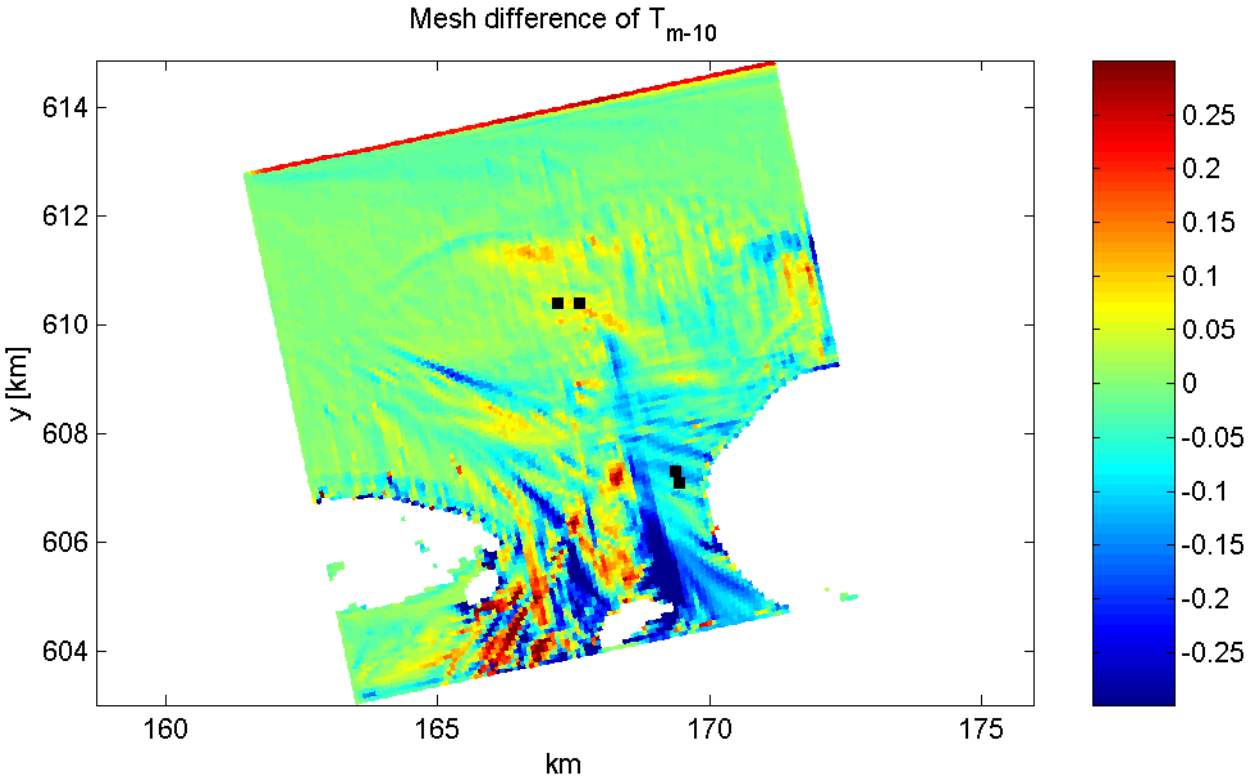

Mesh differences of wave parameters on grid 2 of Amelander Zeegat with h=40m (computations with quadruplets)

WL | DELFT HYDRAULICS | H4918.39 | Fig. 3.6a

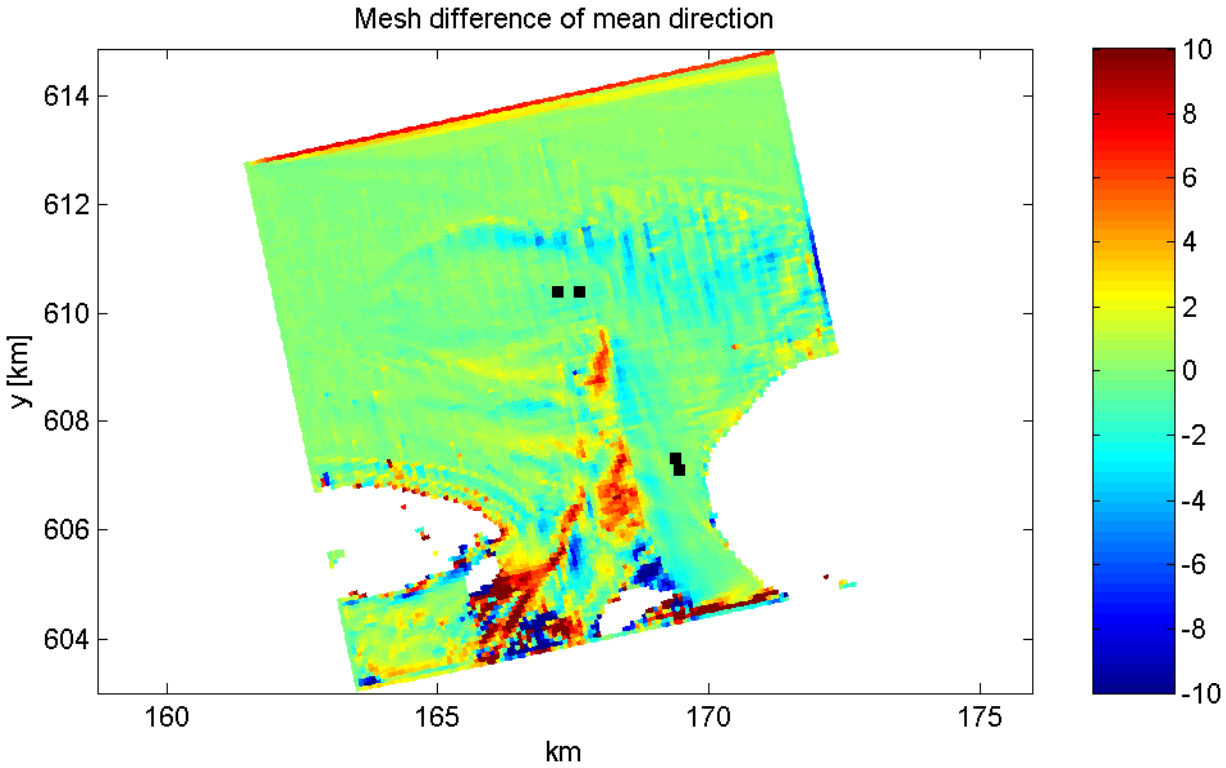

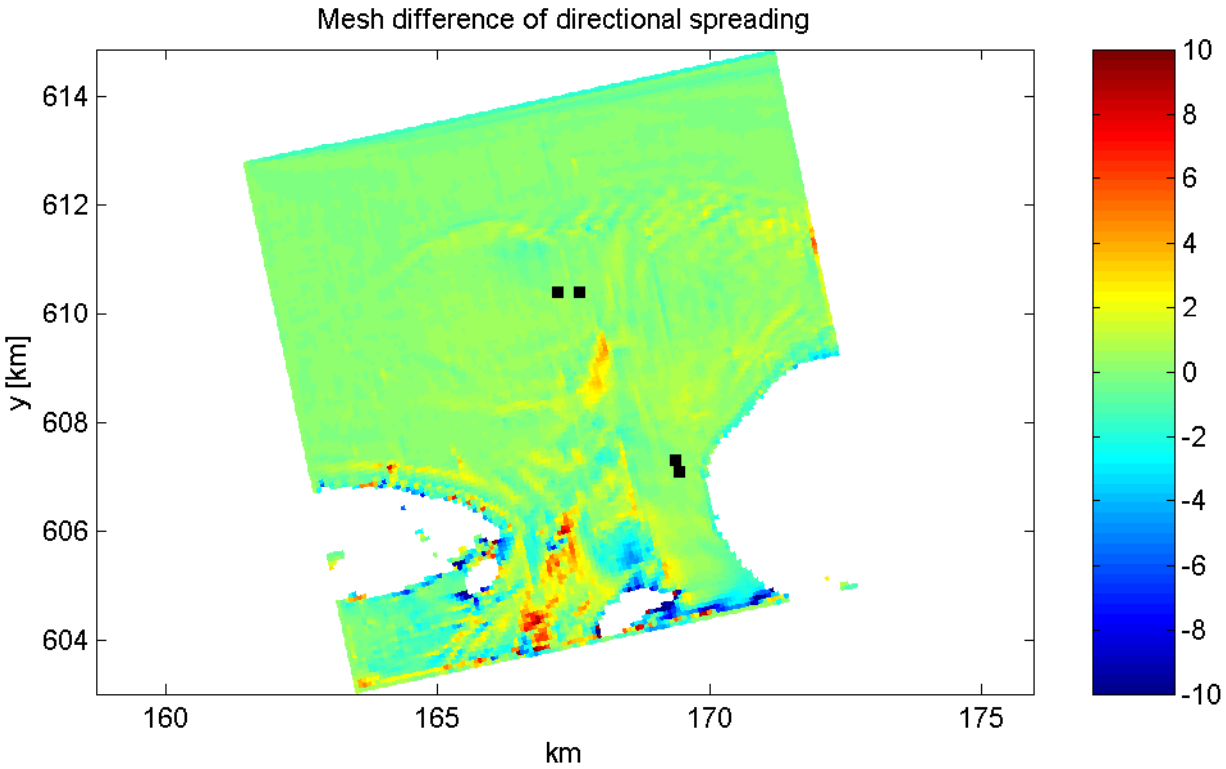

Mesh differences of wave parameters on grid 2 of Amelander Zeegat with h=40m (computations with quadruplets)

WL | DELFT HYDRAULICS	H4918.39	Fig. 3.6b

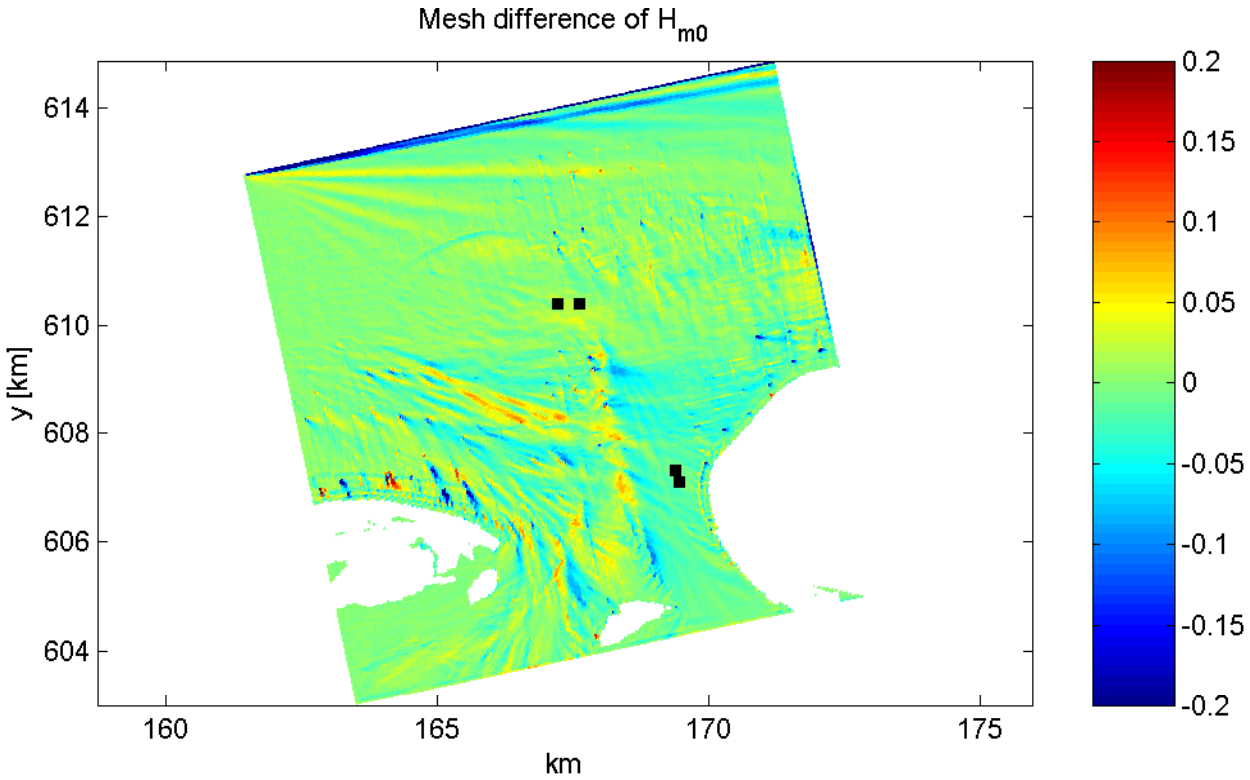

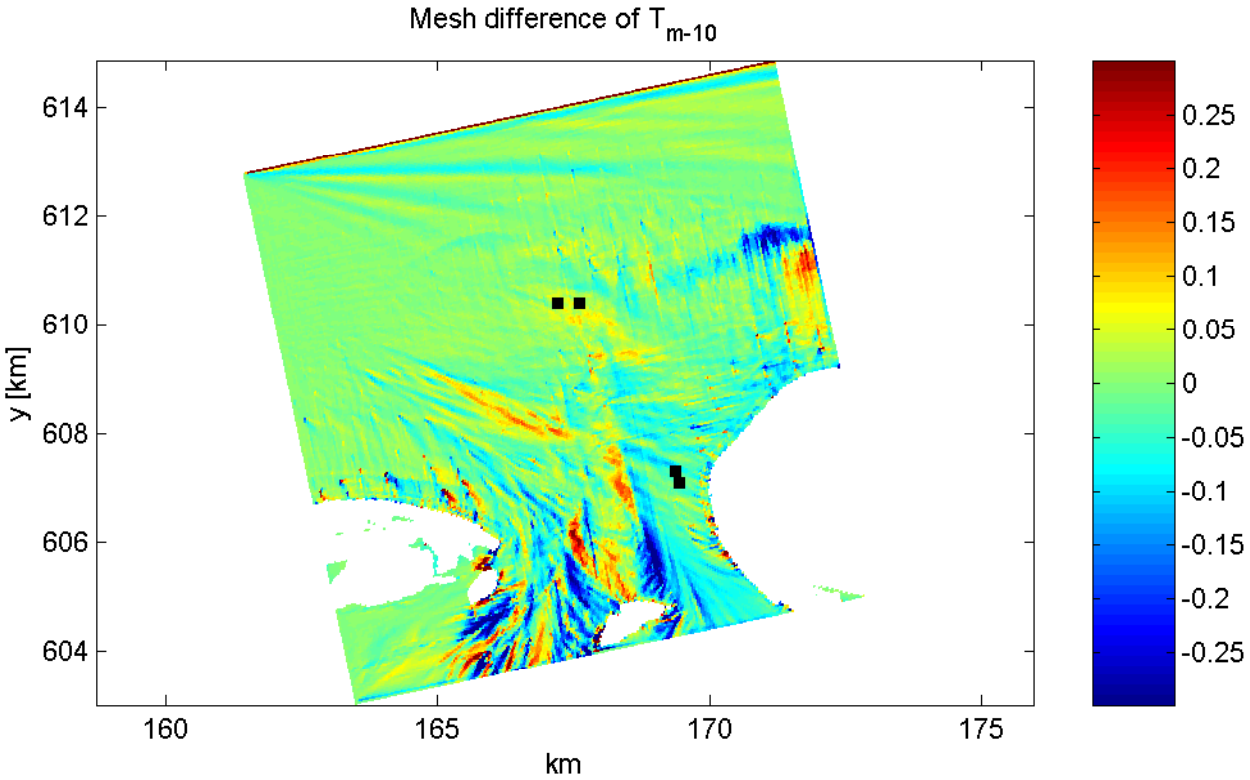

Mesh differences of wave parameters on grid 2 of Amelander Zeegat with h=20m (computations without quadruplets)

WL | DELFT HYDRAULICS	H4918.39	Fig. 3.7a

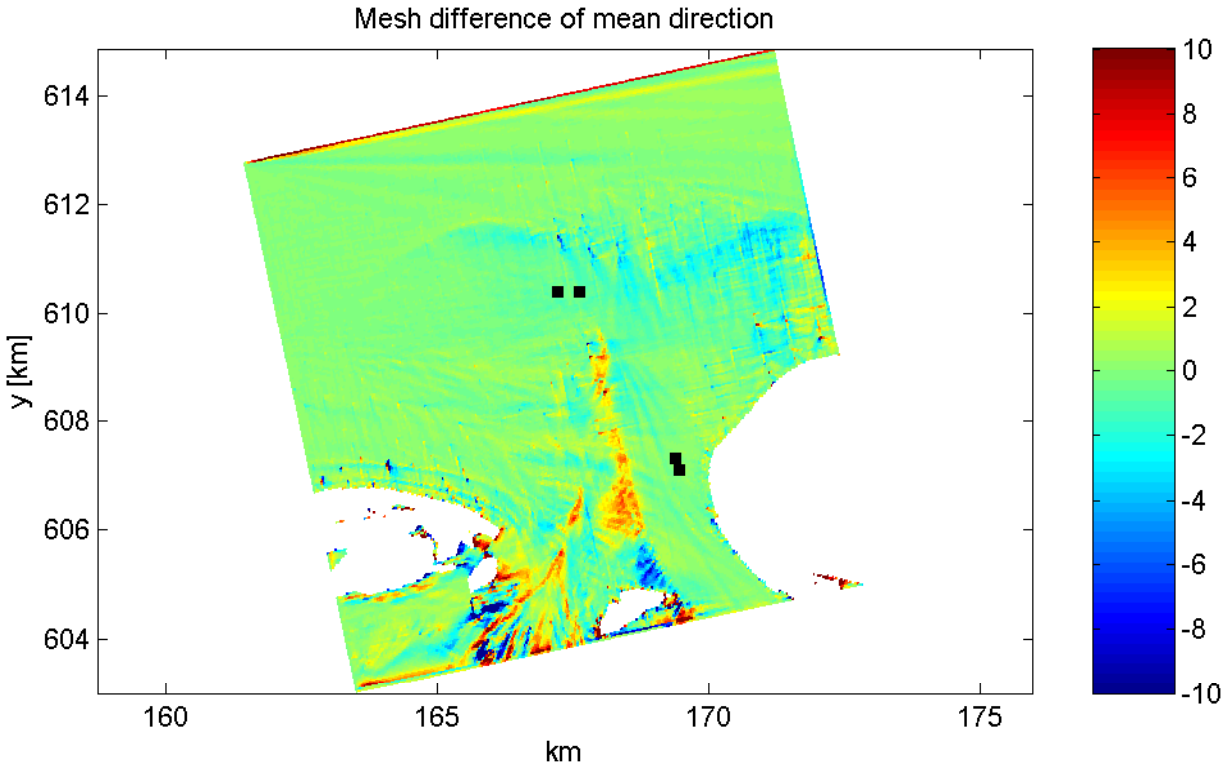

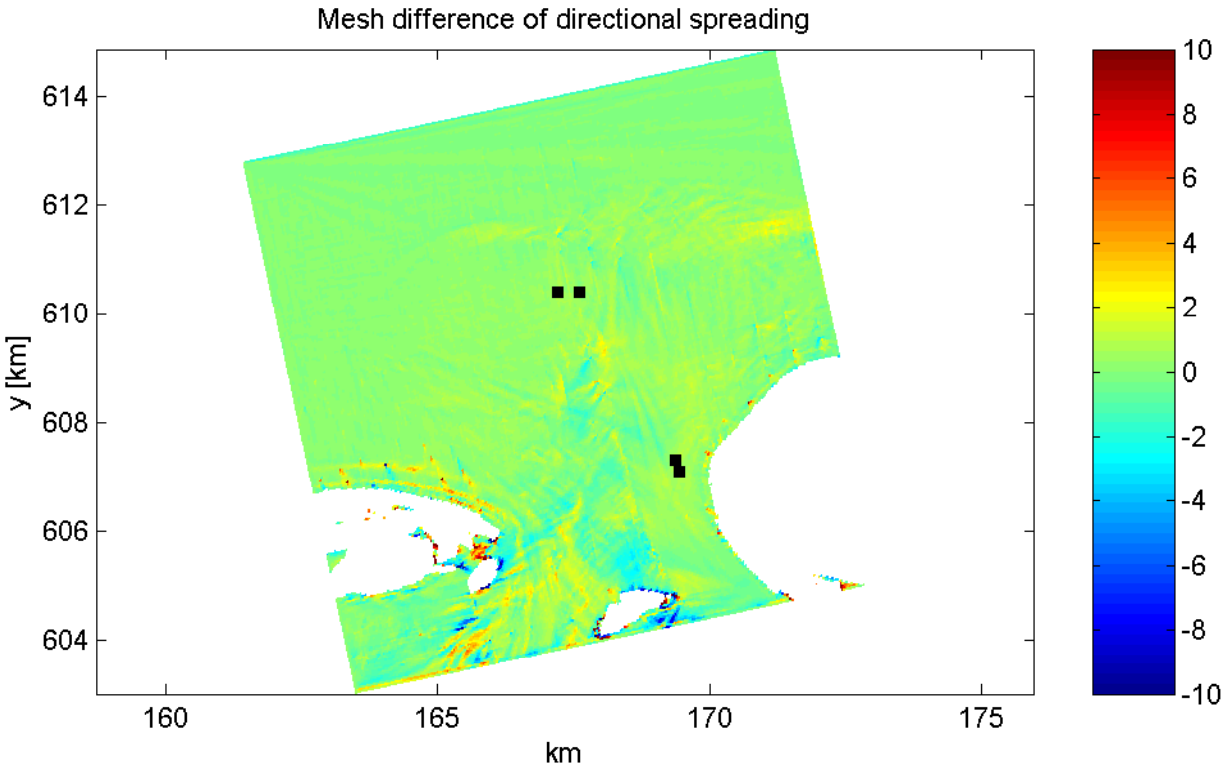

Mesh differences of wave parameters on grid 2 of Amelander Zeegat with h=20m (computations without quadruplets)

WL | DELFT HYDRAULICS	H4918.39	Fig. 3.7b

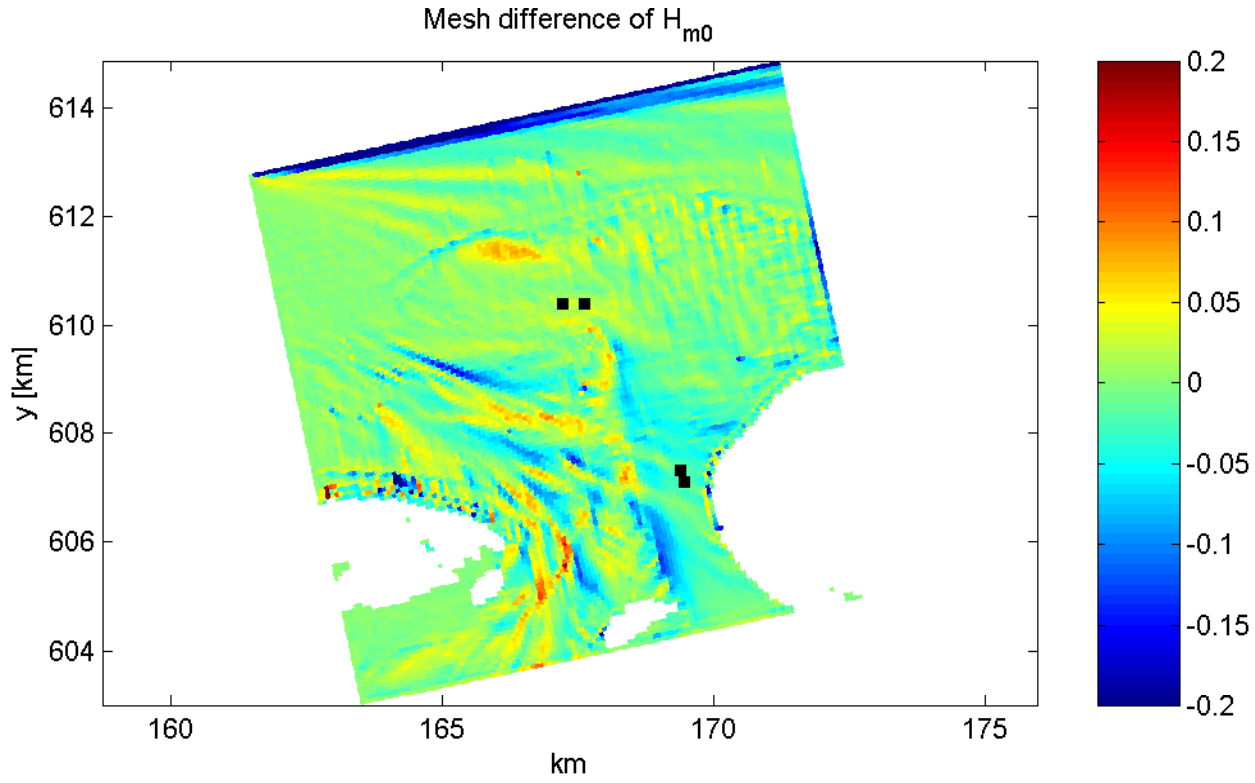

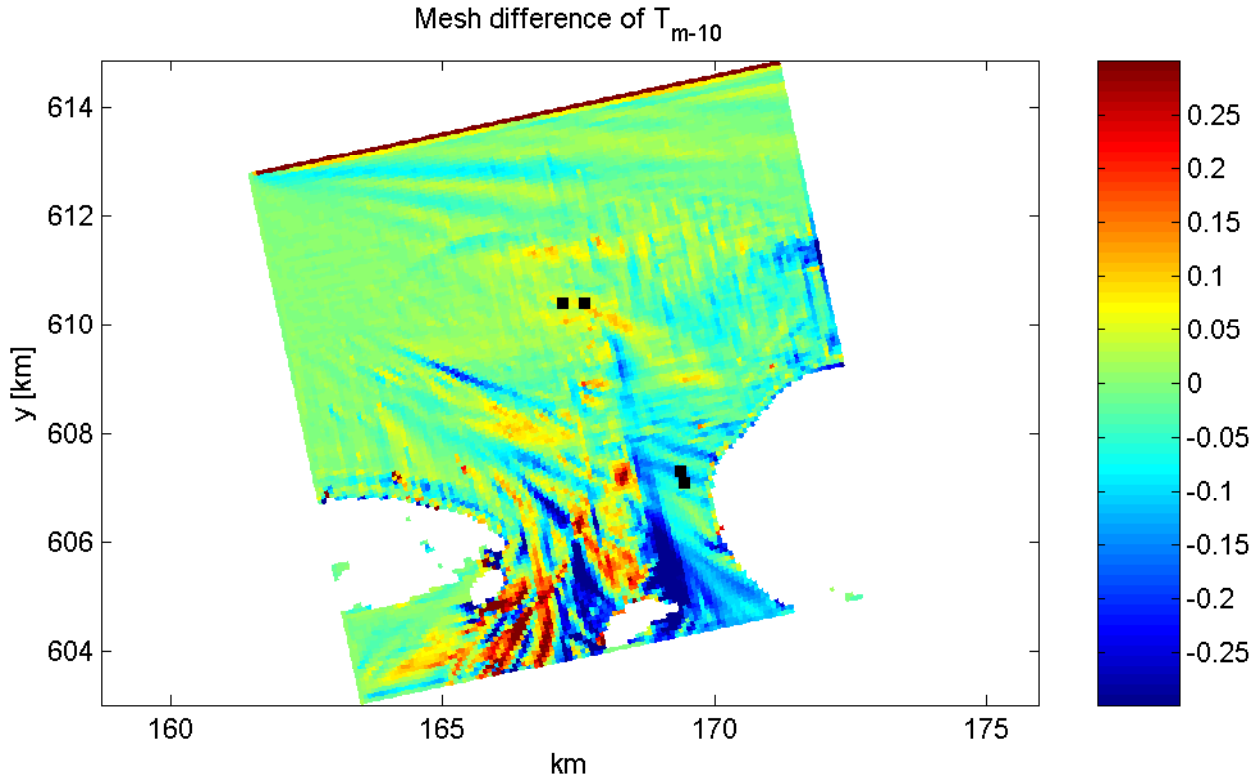

Mesh differences of wave parameters on grid 2 of Amelander Zeegat with h=40m (computations without quadruplets)

WL | DELFT HYDRAULICS	H4918.39	Fig. 3.8a

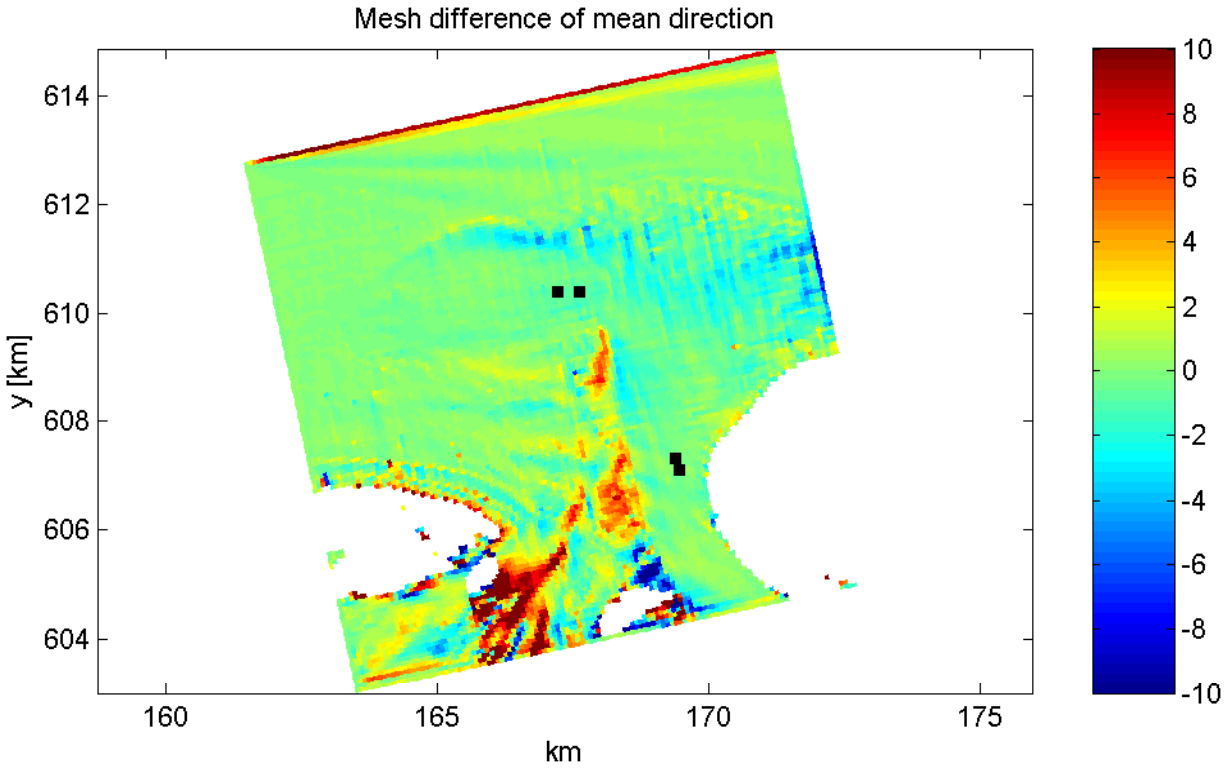

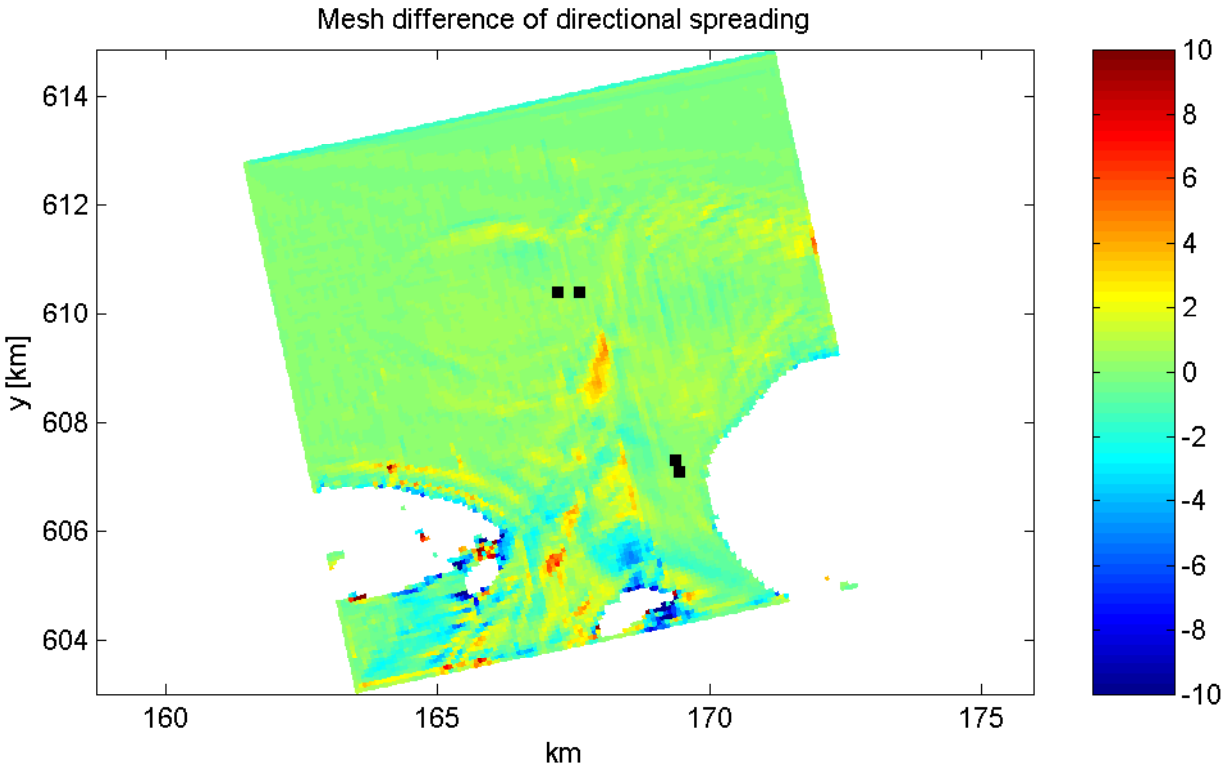

Mesh differences of wave parameters on grid 2 of Amelander Zeegat with h=40m (computations without quadruplets)

WL | DELFT HYDRAULICS

H4918.39

Fig. 3.8b

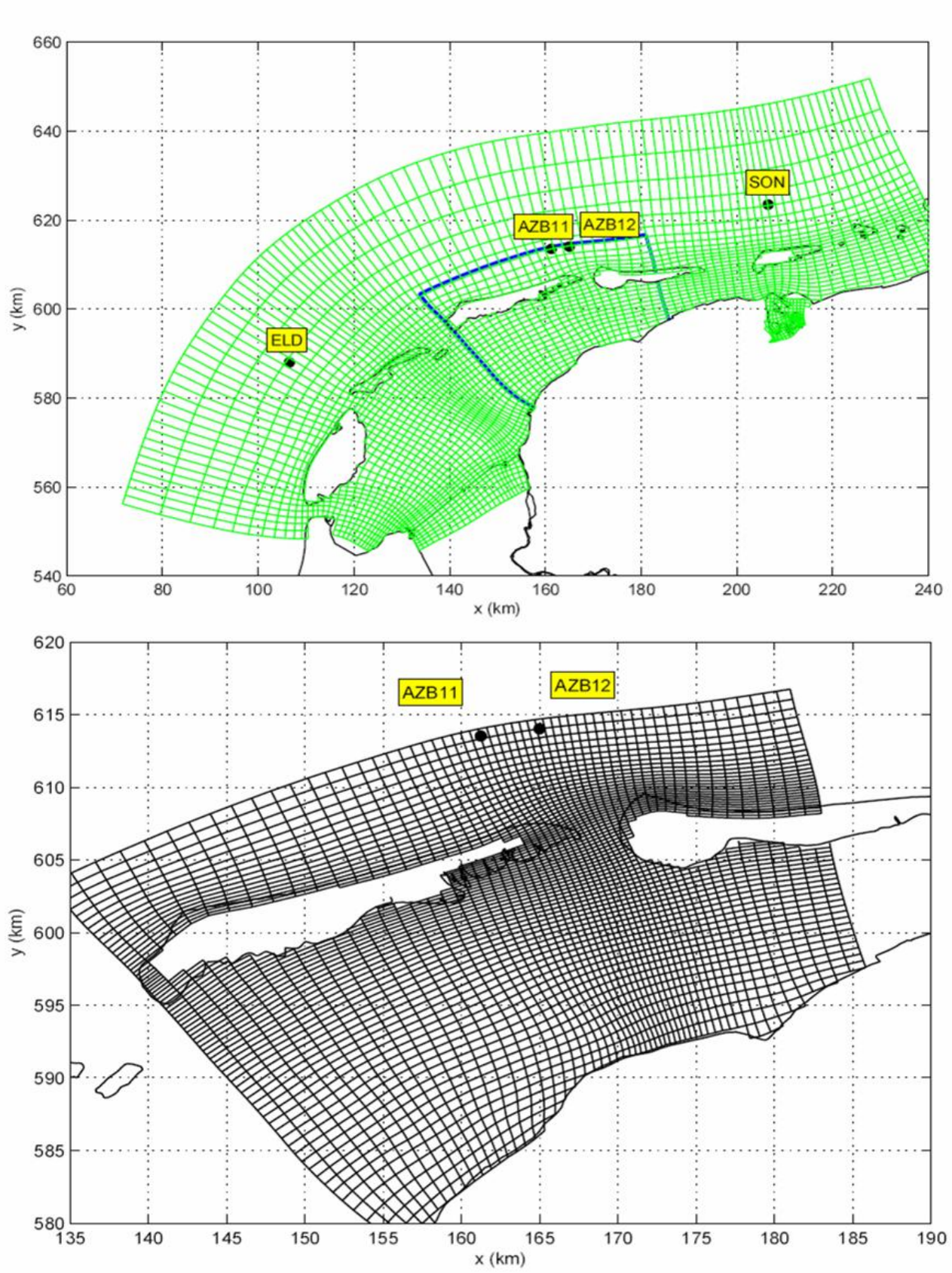

Grid lines of curvi-linear grid of Kuststrook model (upper panel) and of detaield grid AZG3A (lower panel). Every fourth grid line is shown. Location of wave buoys SON, ELD, AZB11 and AZB12.

WL | DELFT HYDRAULICS	H4918.39	Fig. 3.9

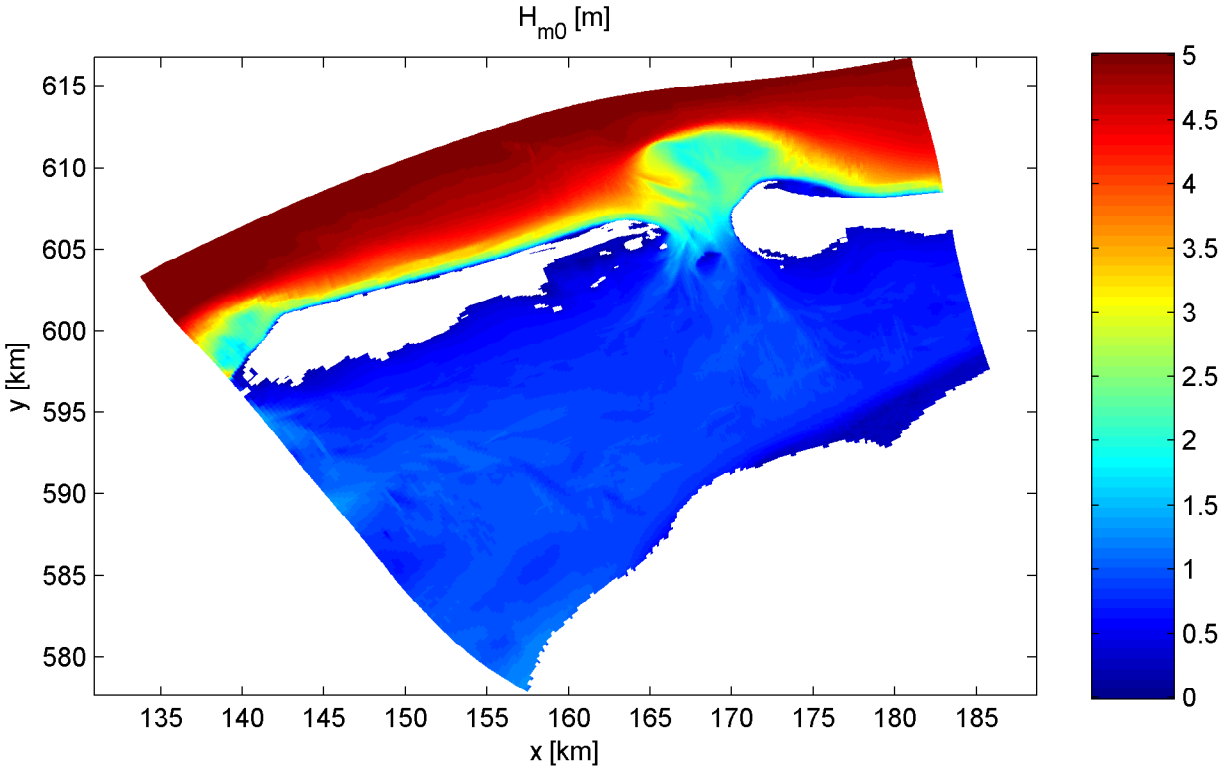

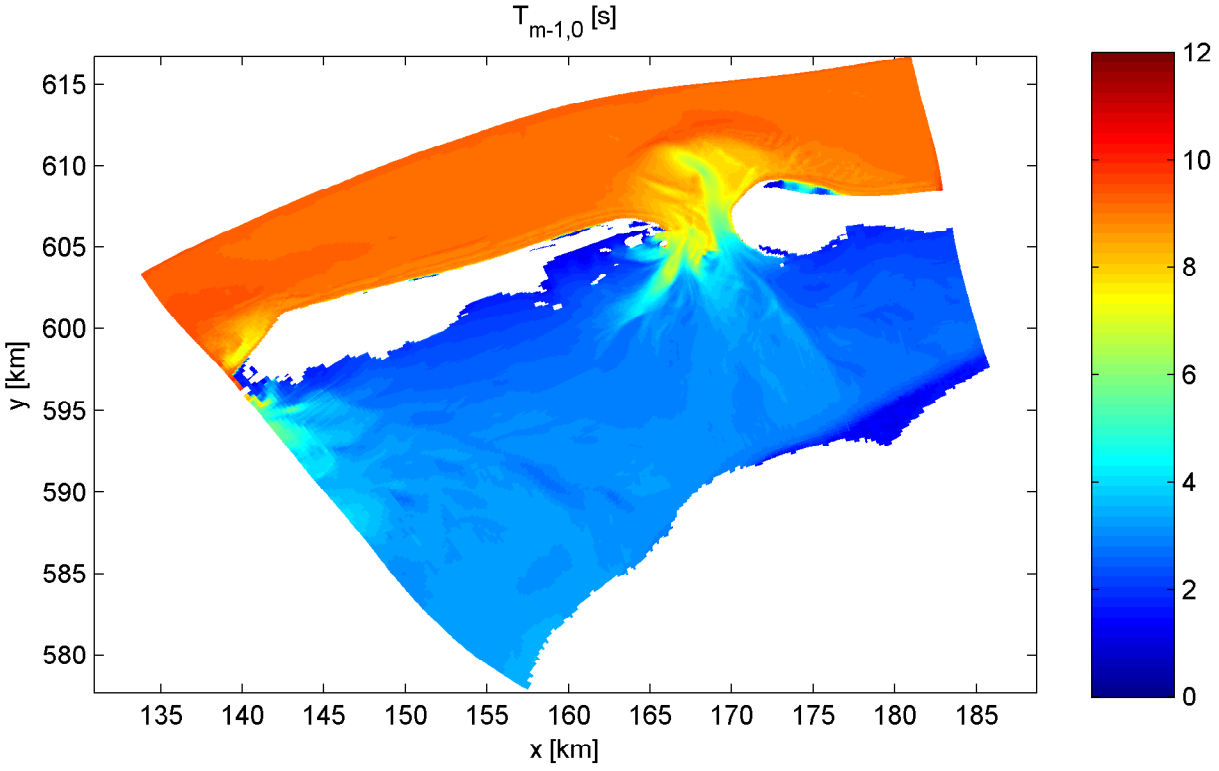

Solution in Amelander Zeegat
with $\Delta\theta$ = 10 deg

WL | DELFT HYDRAULICS

H4918.39

Fig. 3.10a

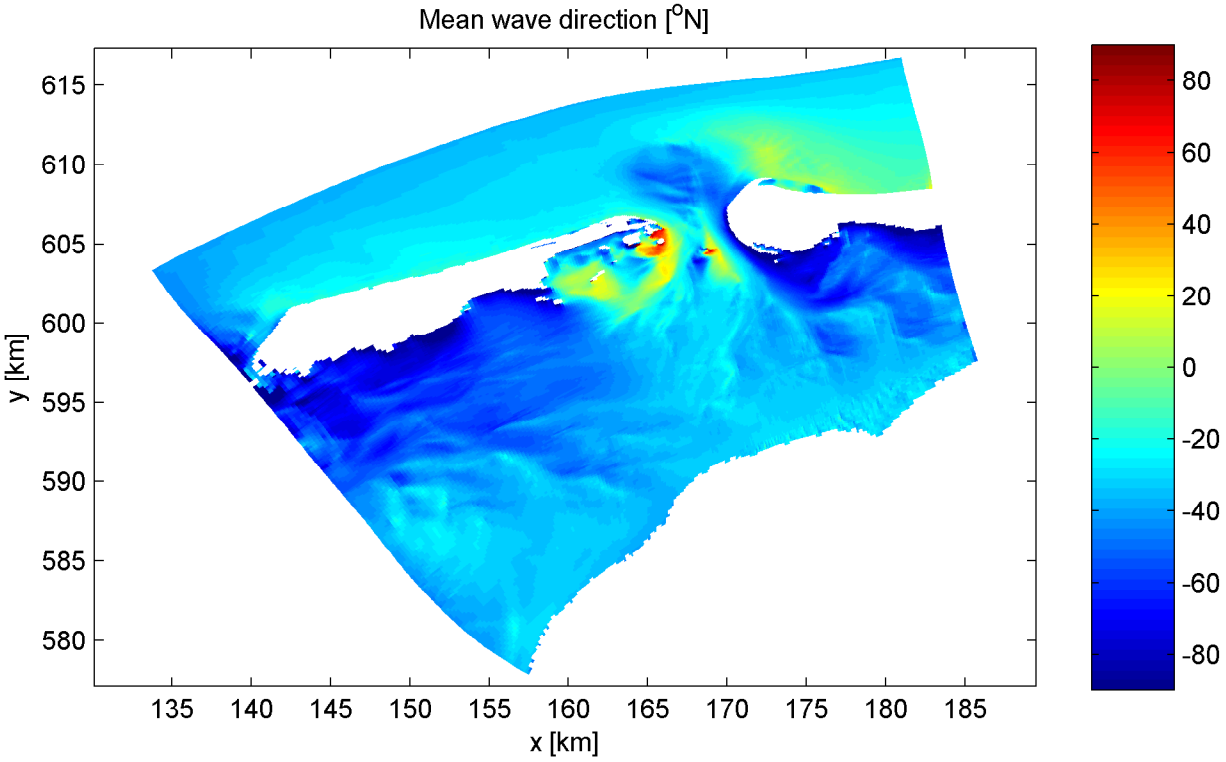

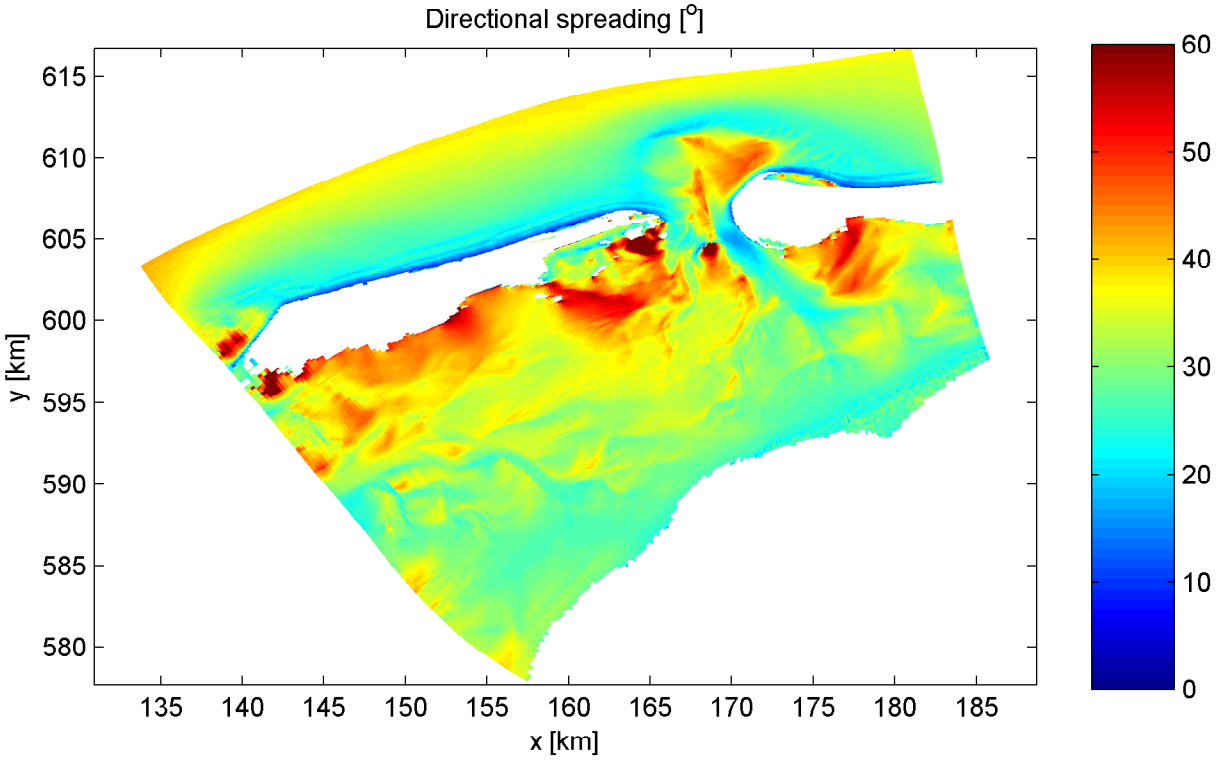

Solution in Amelander Zeegat with $\Delta\theta$ = 10 deg		
WL | DELFT HYDRAULICS	H4918.39	Fig. 3.10b

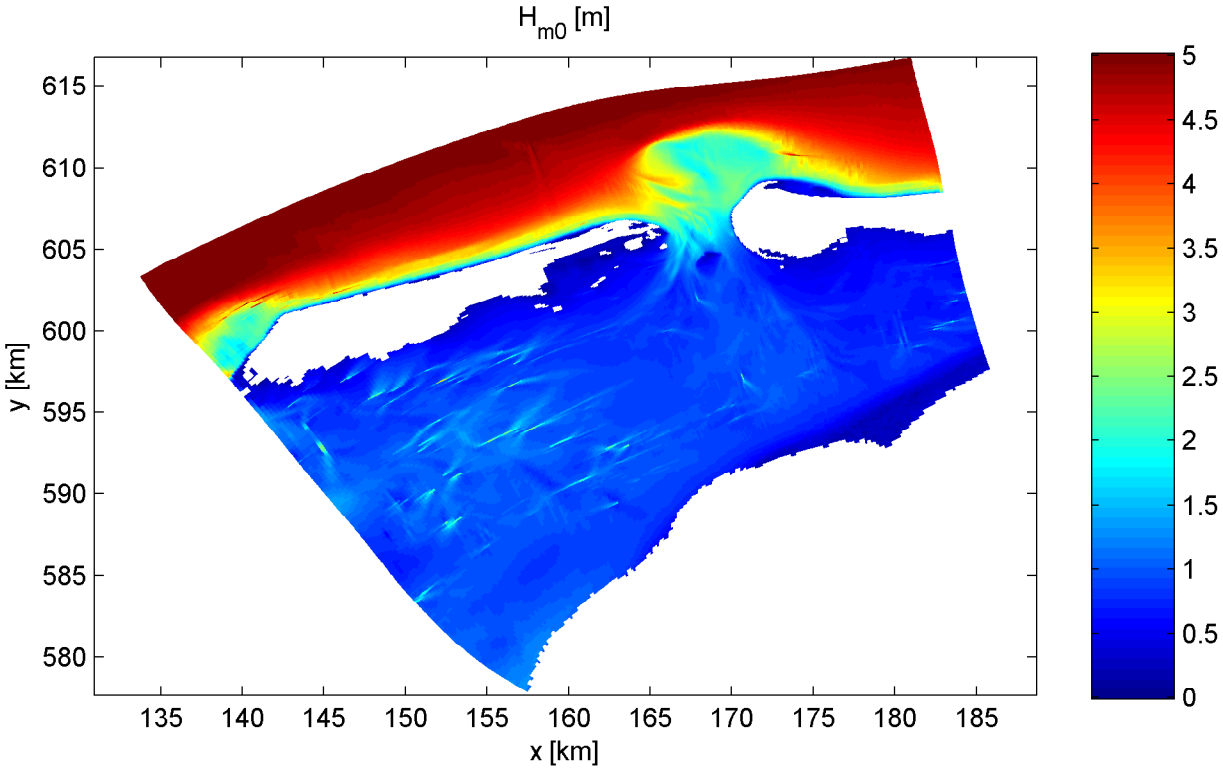

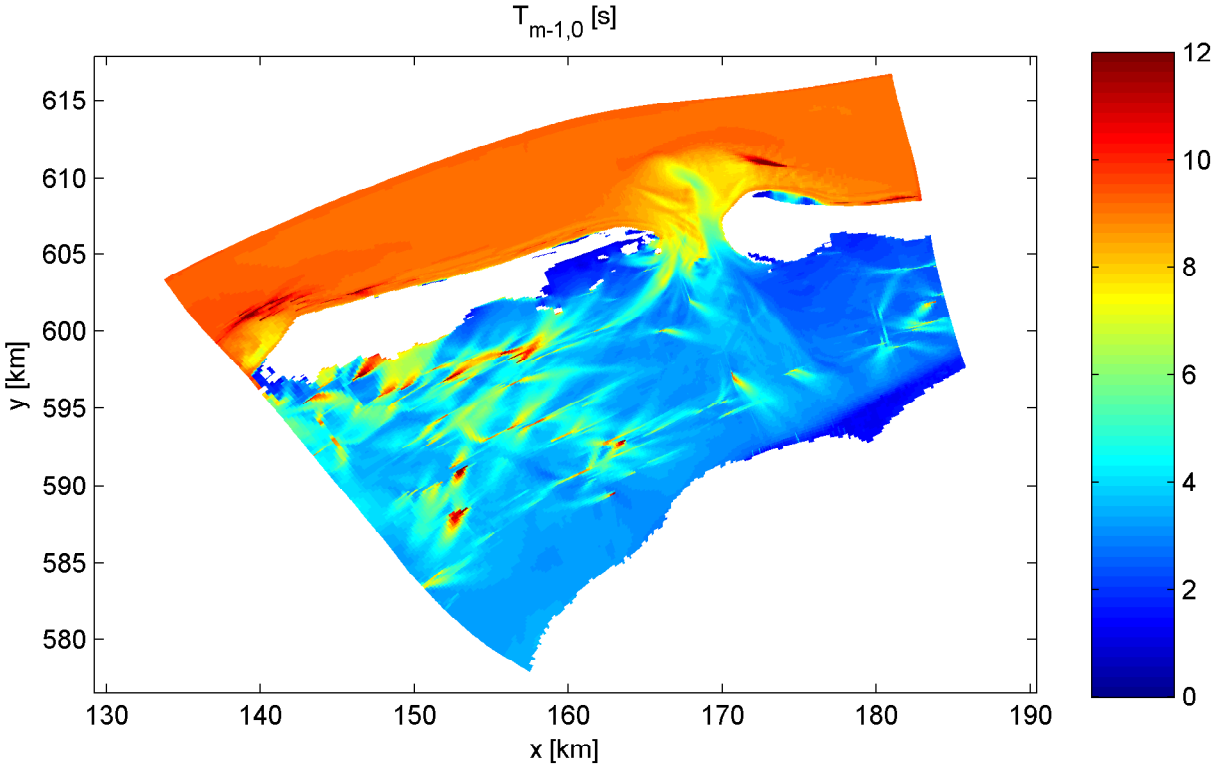

Solution in Amelander Zeegat with $\Delta\theta$ = 2 deg		
WL | DELFT HYDRAULICS	H4918.39	Fig. 3.11a

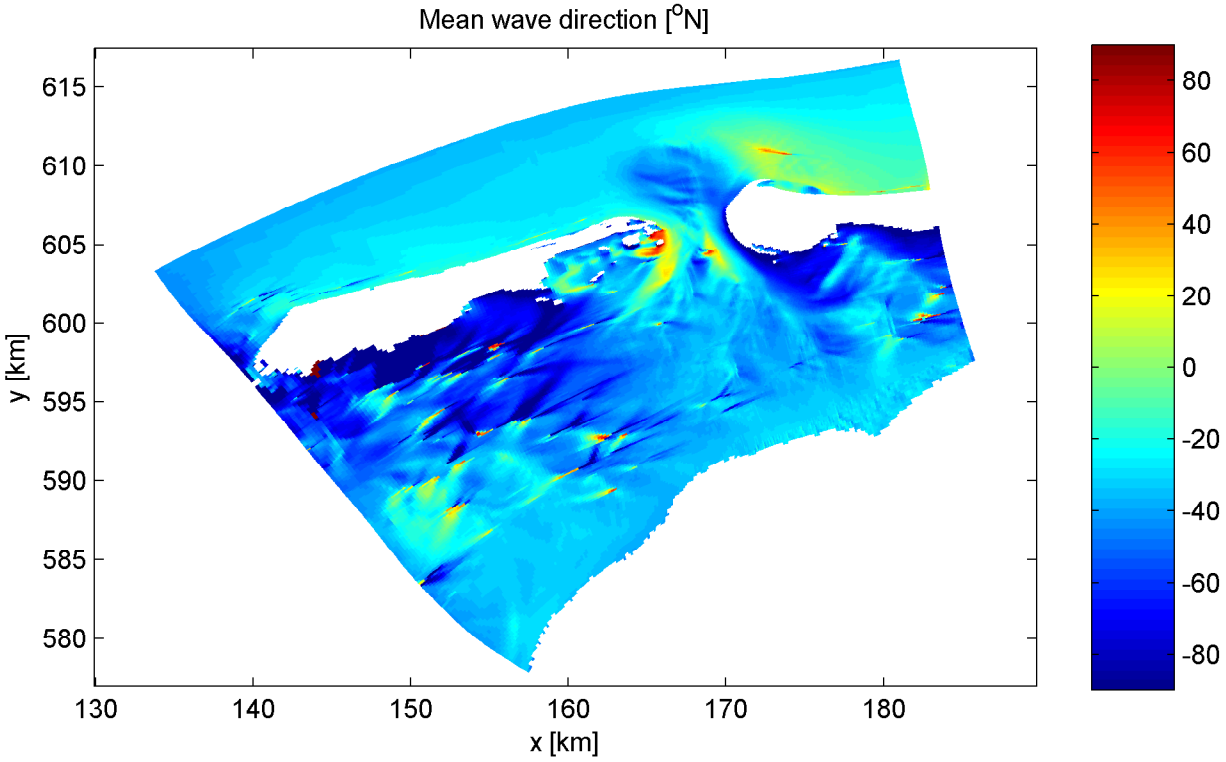

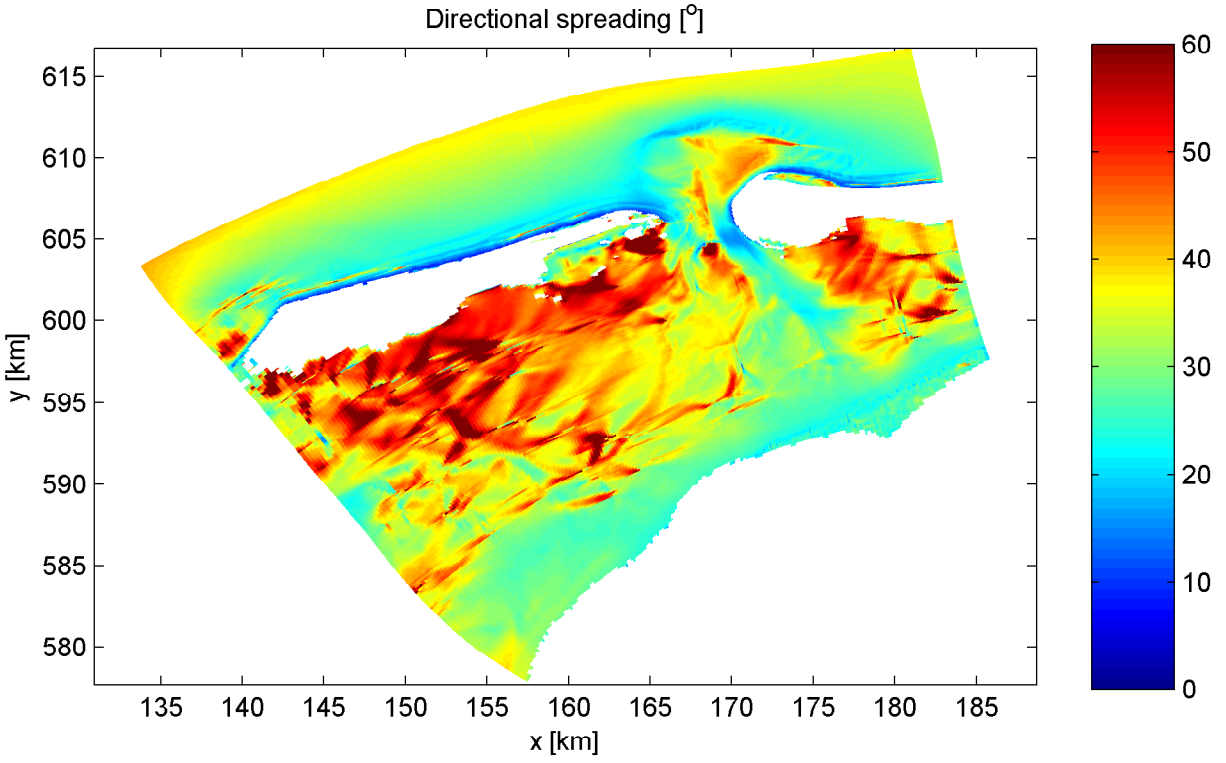

Solution in Amelander Zeegat with $\Delta\theta$ = 2 deg		
WL | DELFT HYDRAULICS	H4918.39	Fig. 3.11b

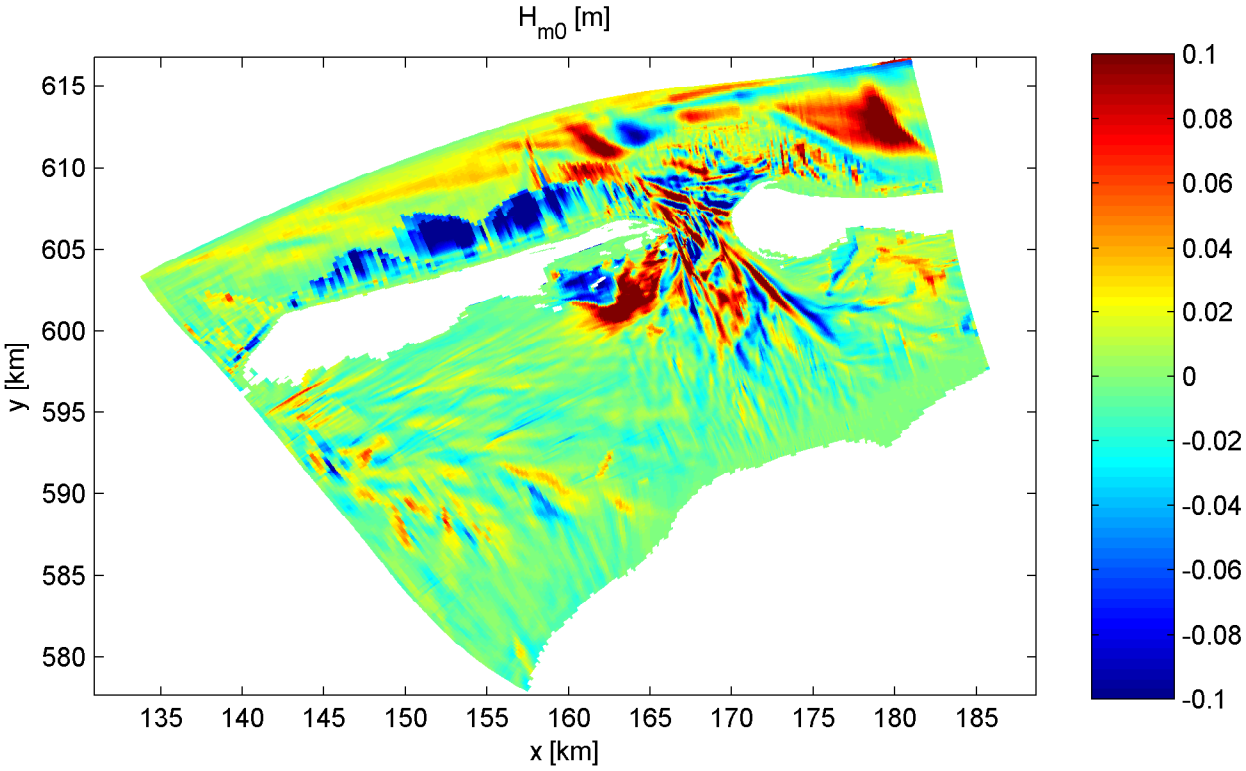

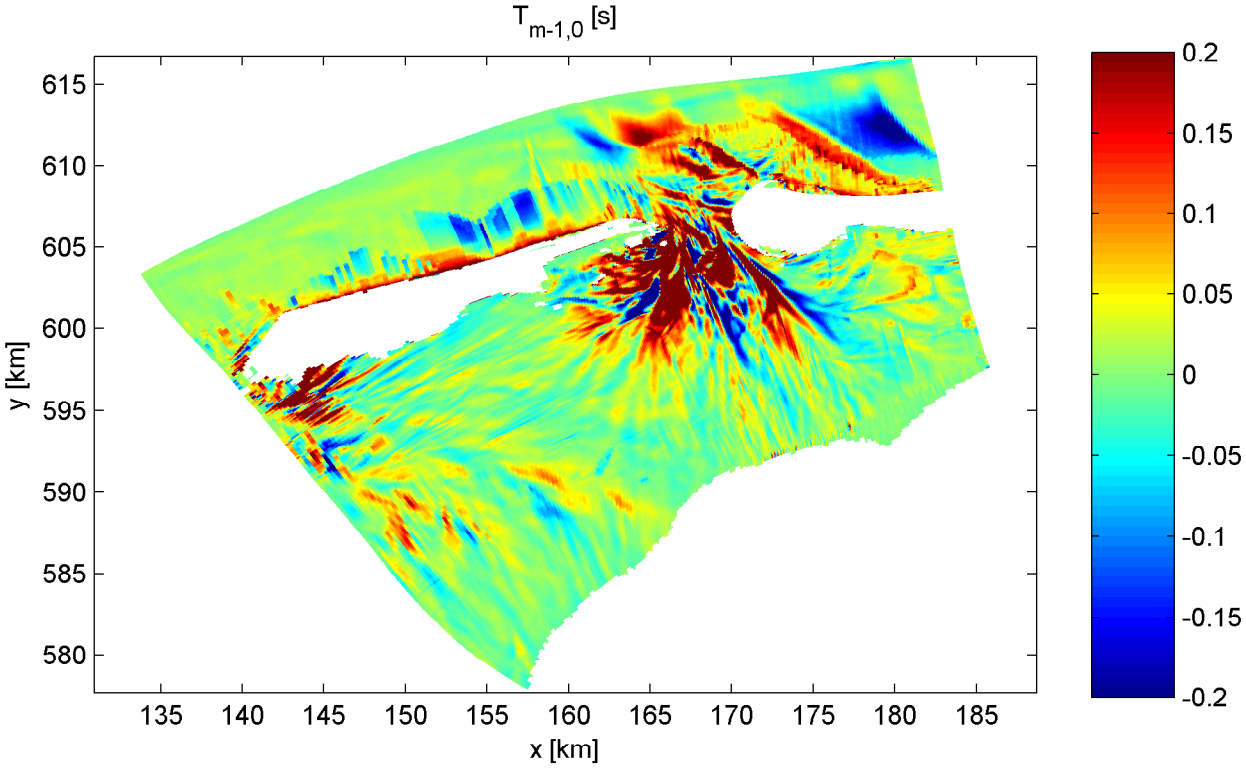

Mesh differences $\phi(\Delta\theta=20)$ - $\phi(\Delta\theta=10)$ in Amelander Zeegat

WL | DELFT HYDRAULICS

H4918.39

Fig. 3.12a

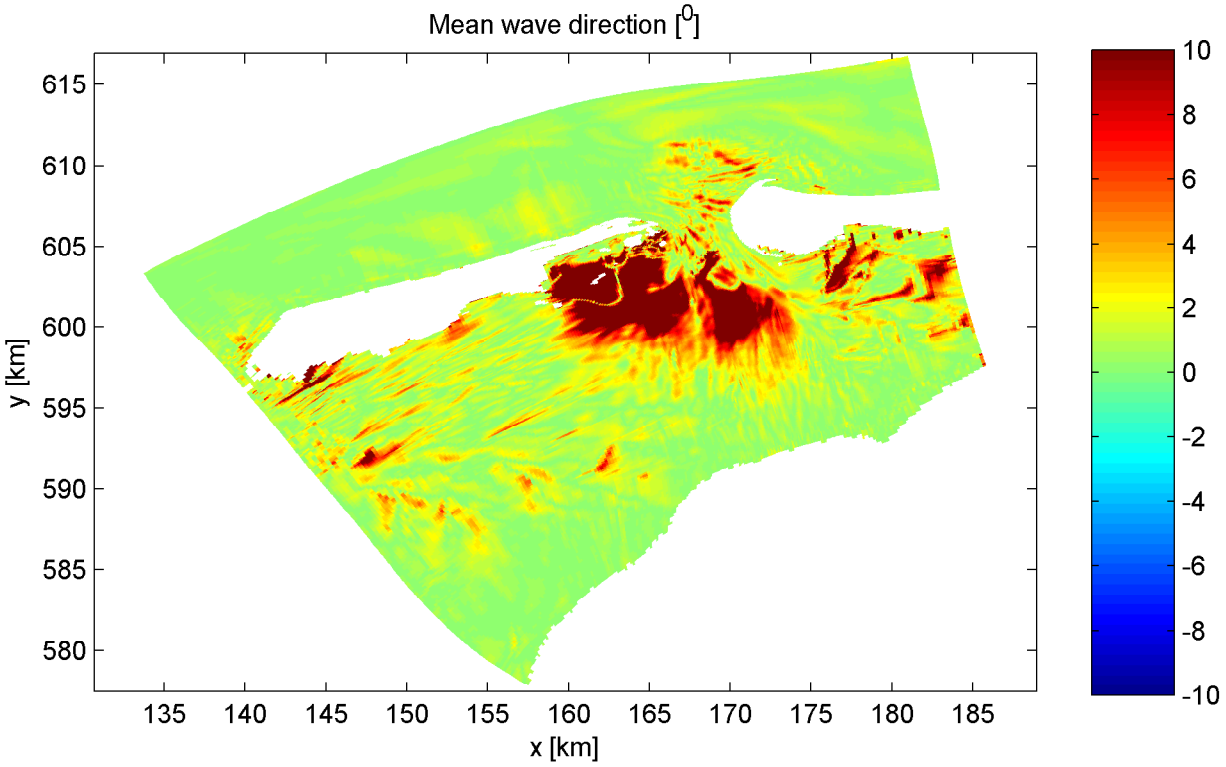

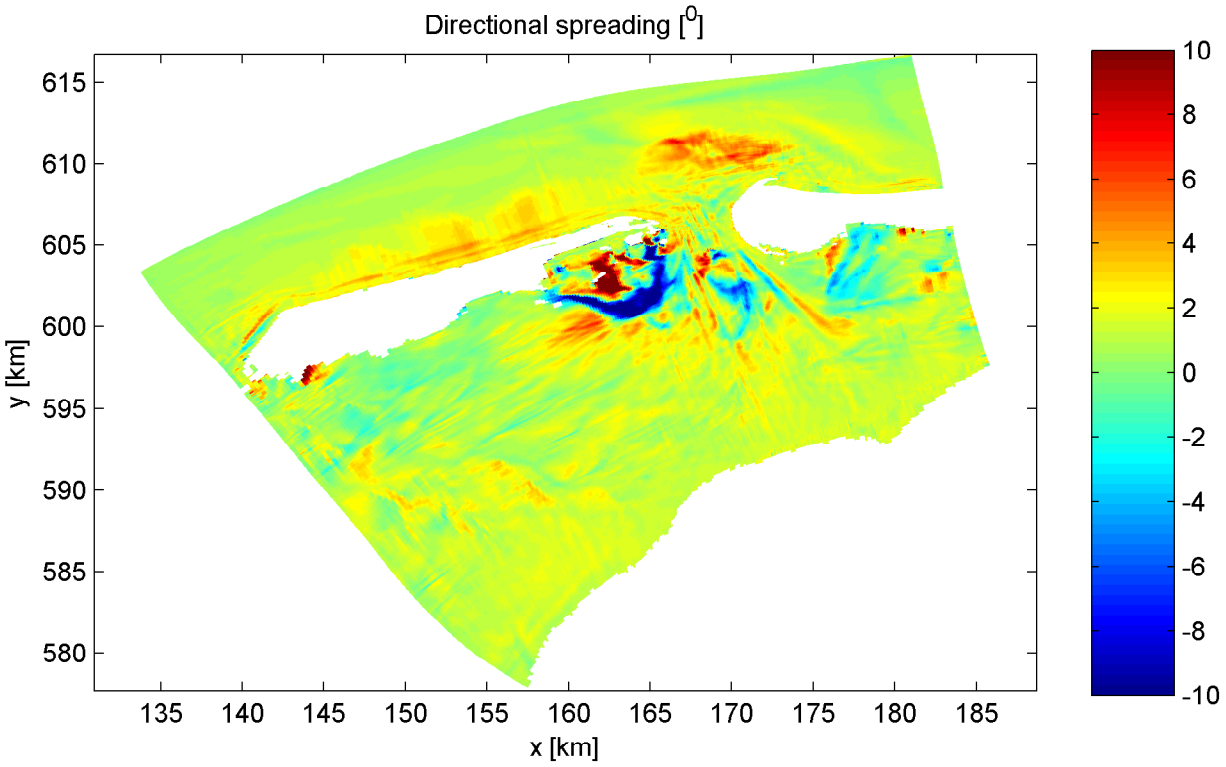

Mesh differences $\phi(\Delta\theta=20)$ - $\phi(\Delta\theta=10)$ in Amelander Zeegat

WL | DELFT HYDRAULICS

H4918.39

Fig. 3.12b

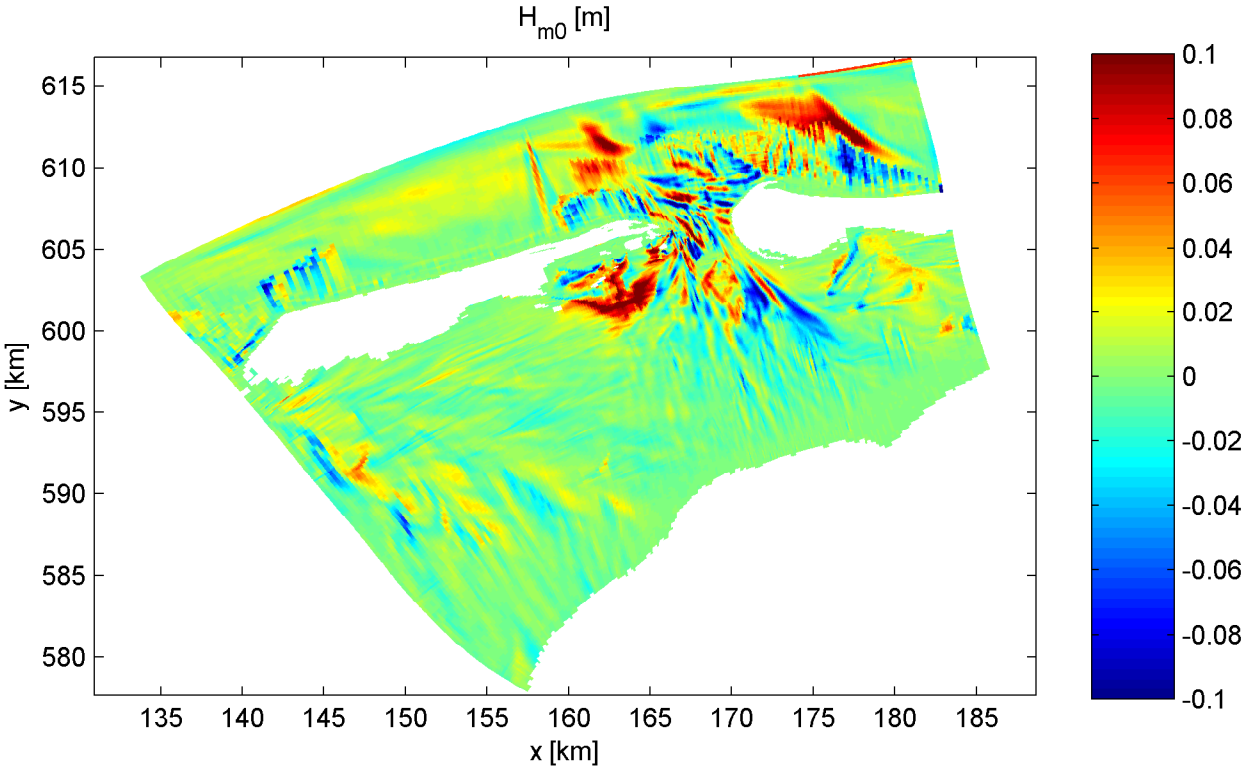

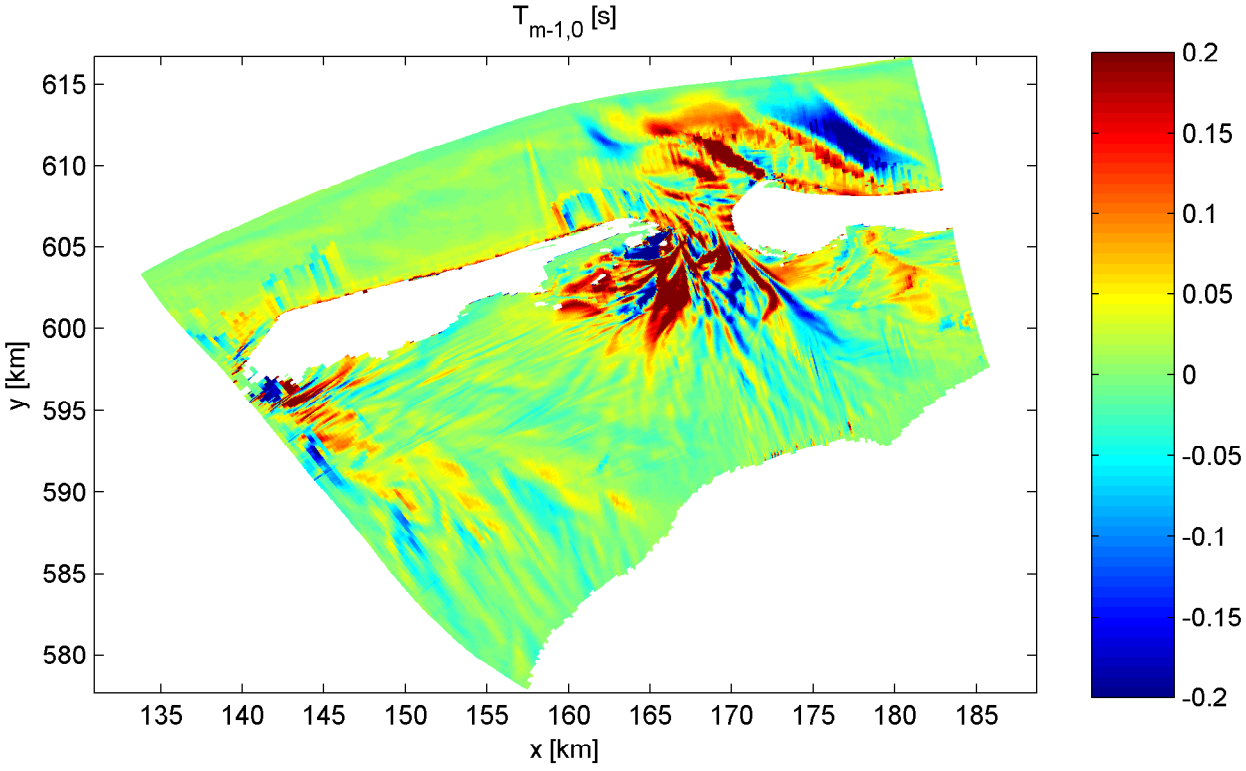

Mesh differences $\phi(\Delta\theta=15)$ - $\phi(\Delta\theta=8)$ in Amelander Zeegat

WL | DELFT HYDRAULICS

H4918.39

Fig. 3.13a

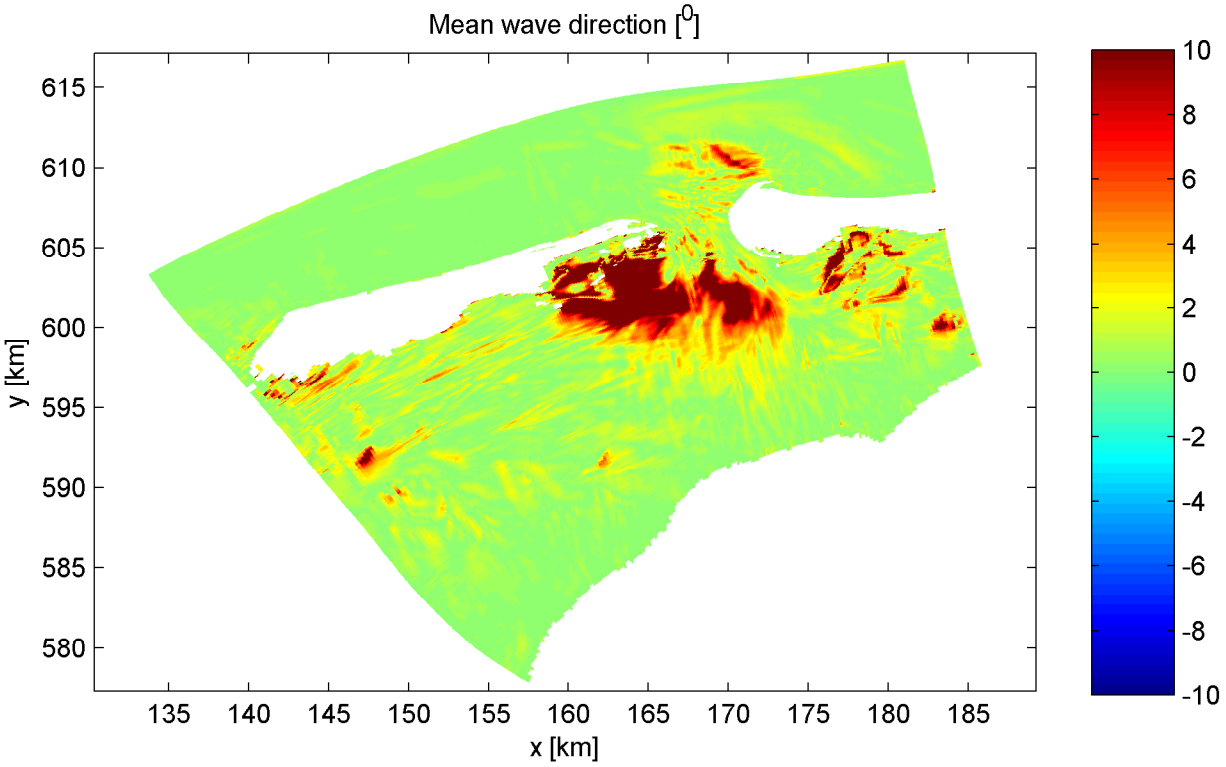

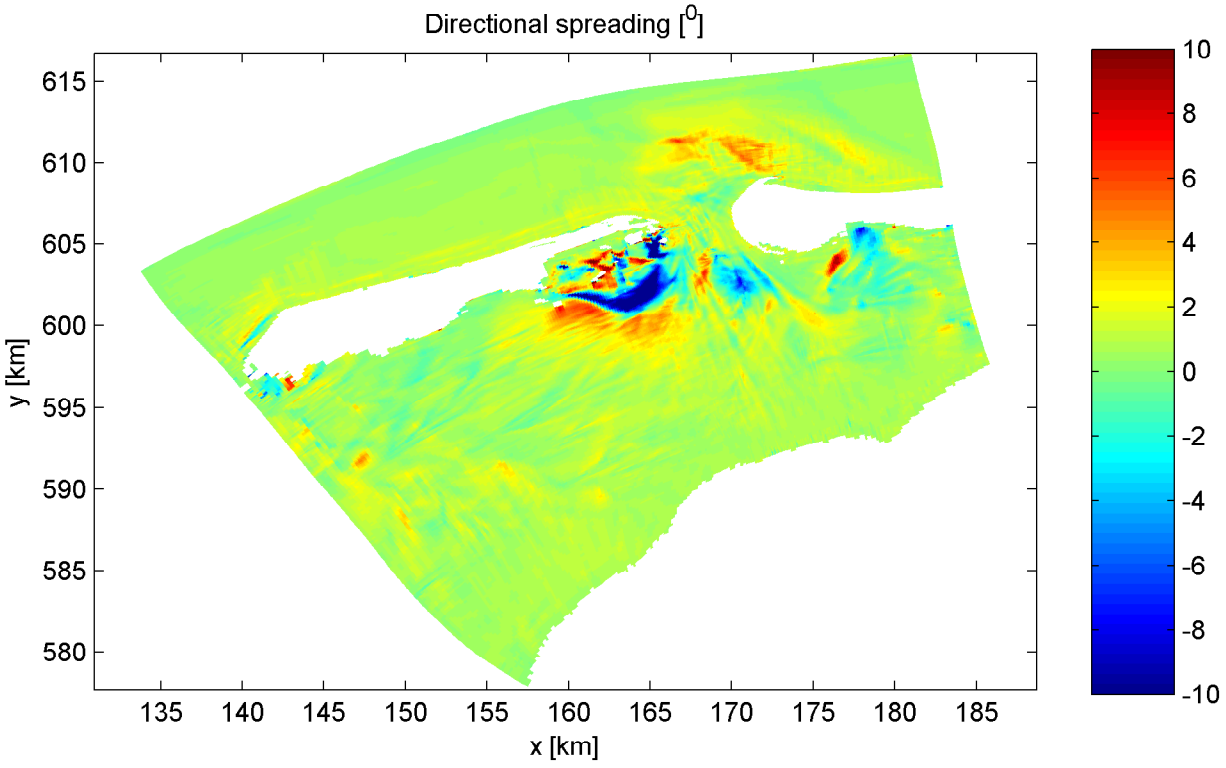

Mesh differences $\phi(\Delta\theta=15)$ - $\phi(\Delta\theta=8)$ in Amelander Zeegat

WL | DELFT HYDRAULICS

H4918.39

Fig. 3.13b

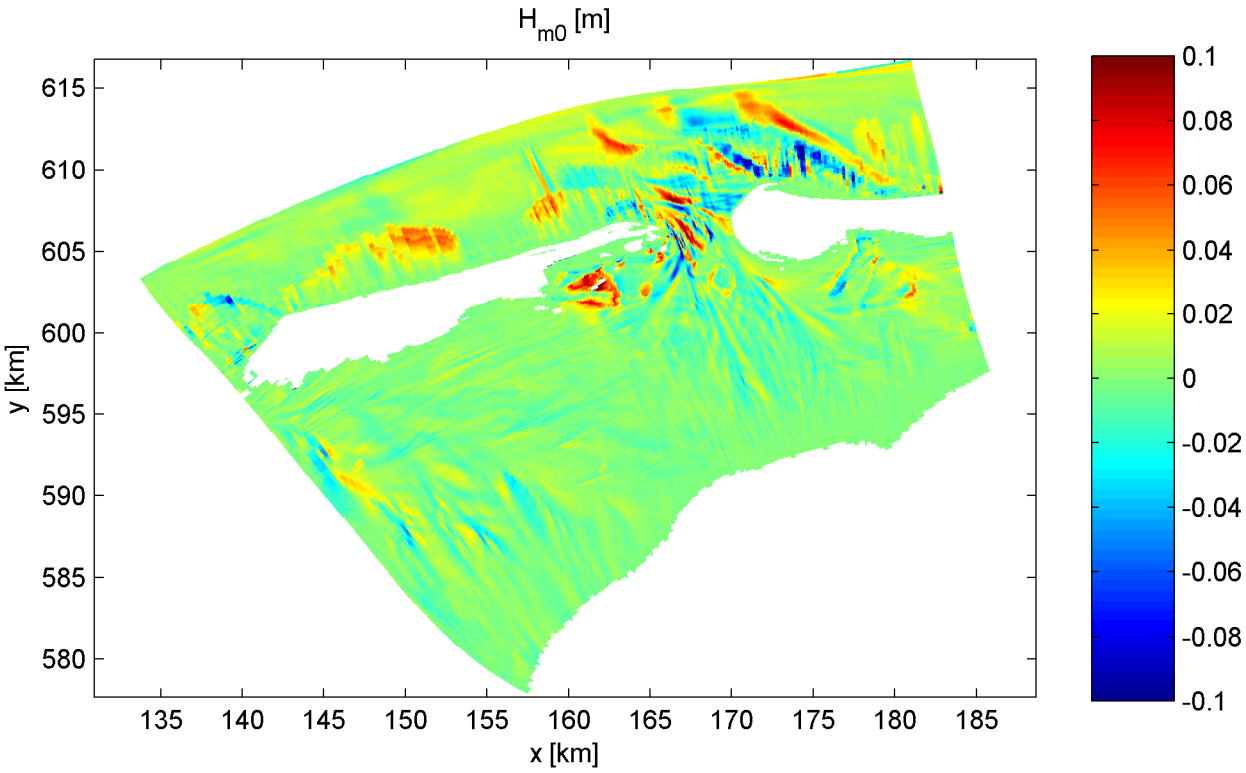

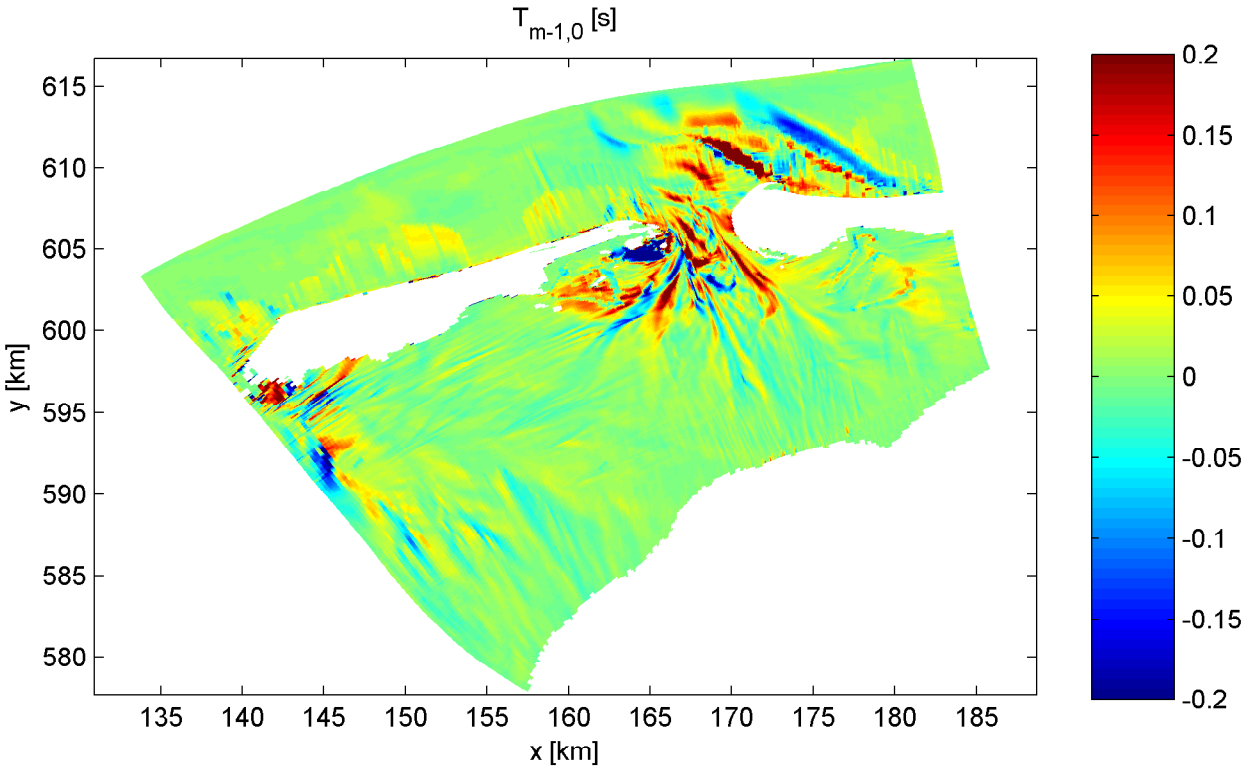

Mesh differences $\phi(\Delta\theta=10)$ - $\phi(\Delta\theta=6)$ in Amelander Zeegat

WL | DELFT HYDRAULICS

H4918.39

Fig. 3.14a

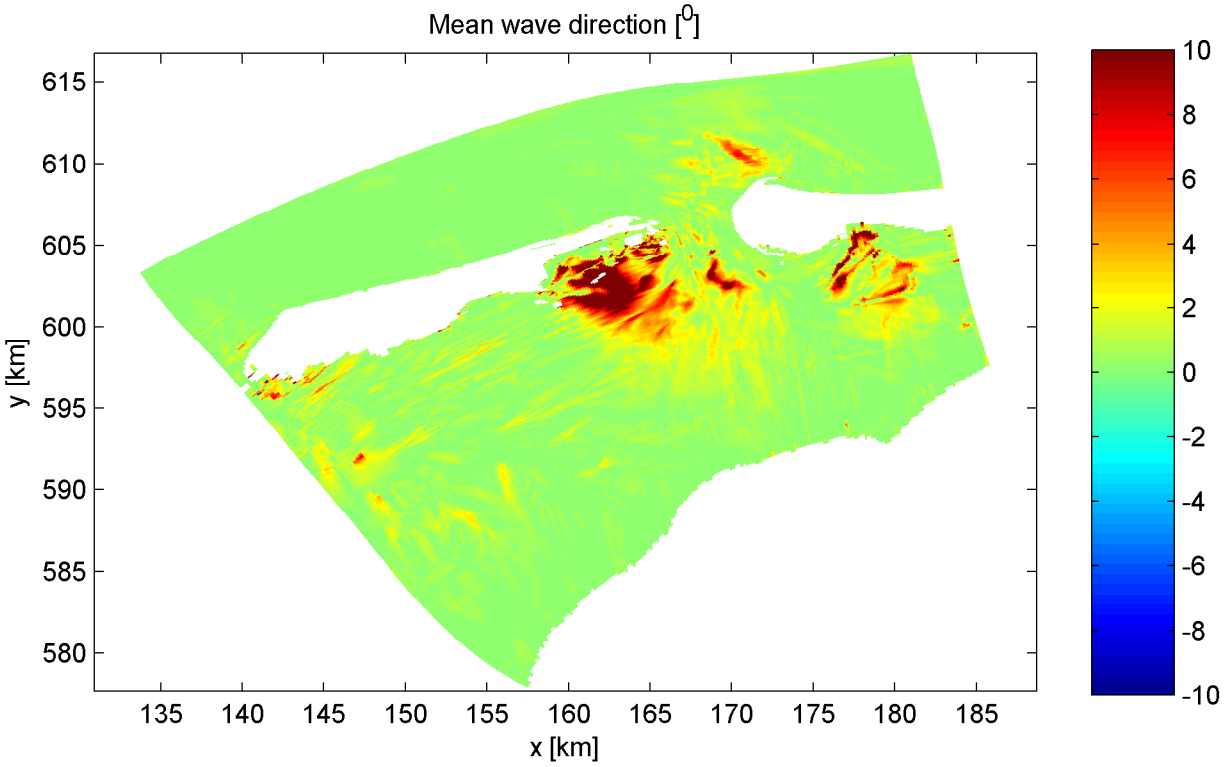

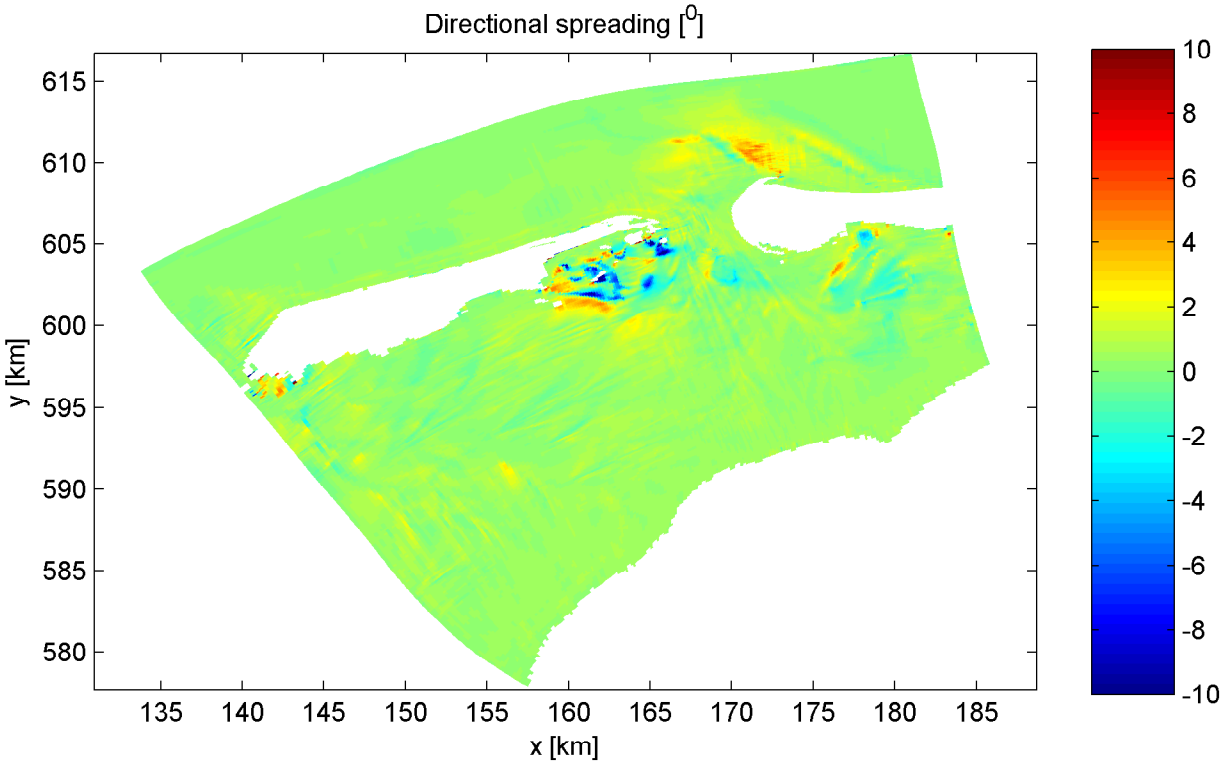

Mesh differences $\phi(\Delta\theta=10)$ - $\phi(\Delta\theta=6)$ in Amelander Zeegat

WL | DELFT HYDRAULICS

H4918.39

Fig. 3.14b

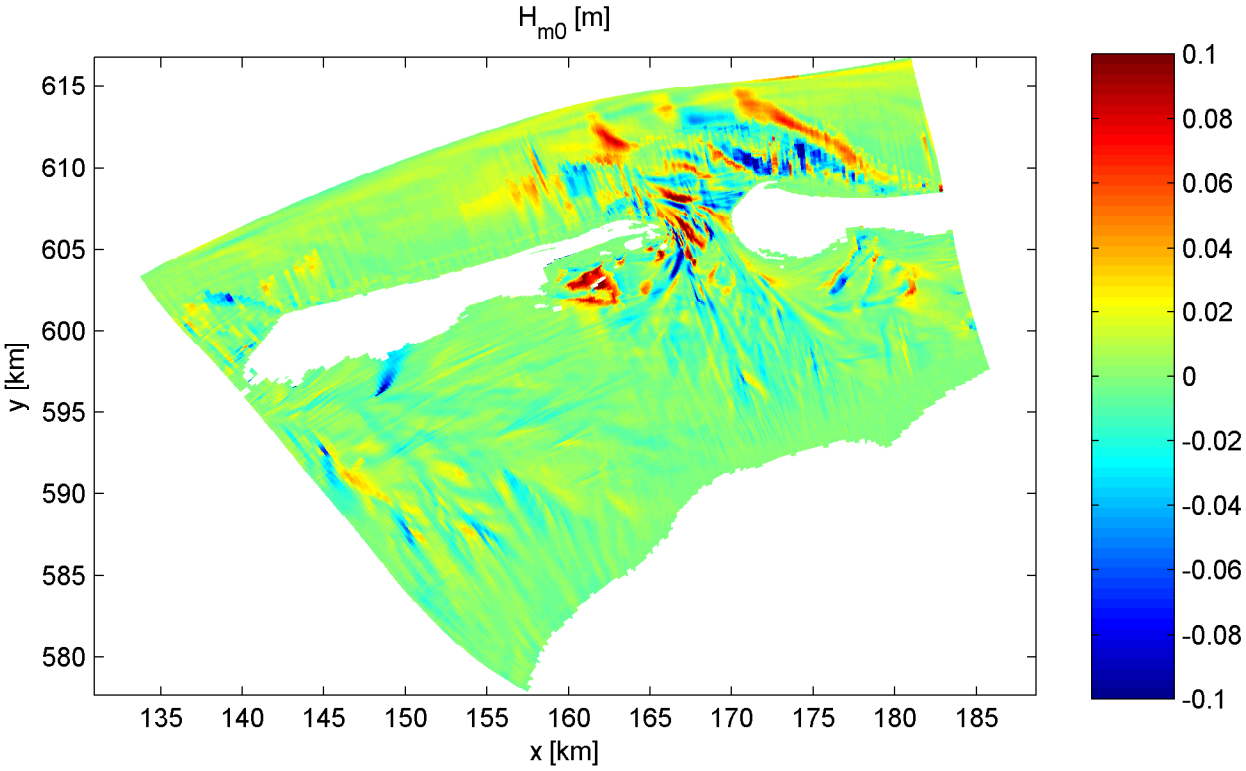

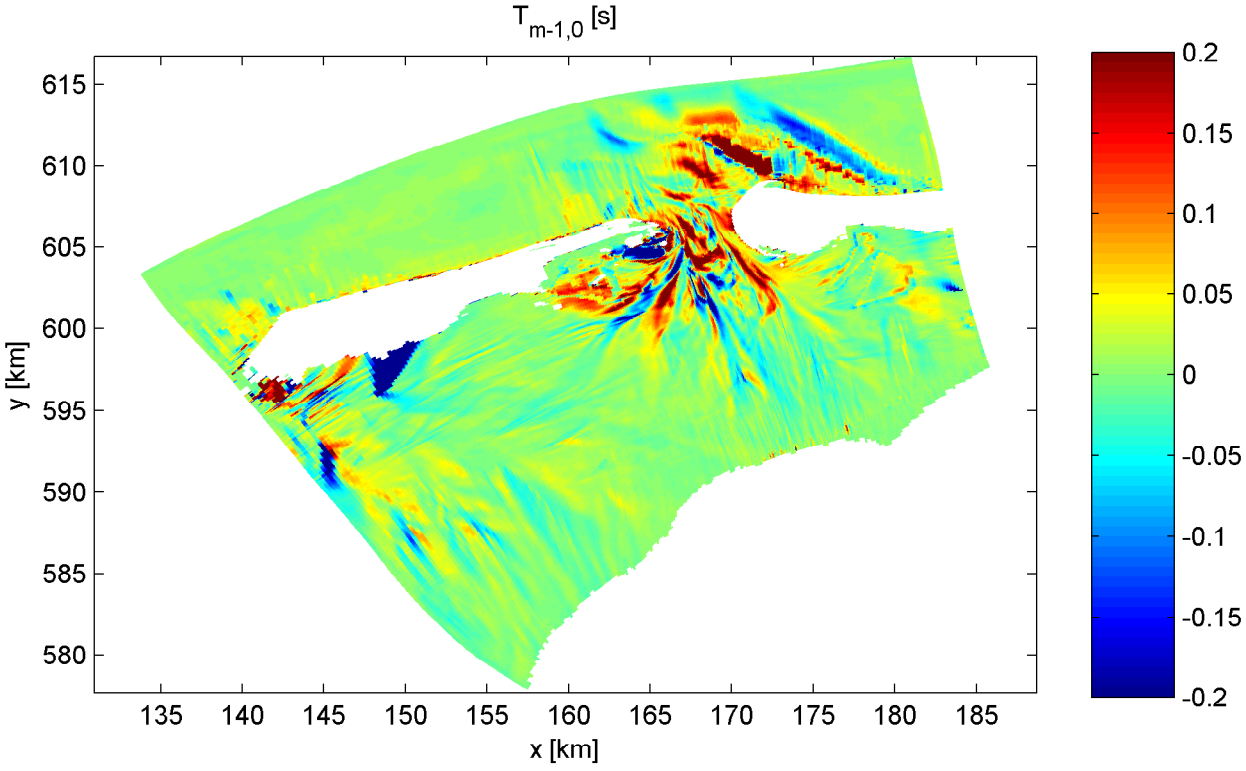

Mesh differences $\phi(\Delta\theta=10)$ - $\phi(\Delta\theta=5)$ in Amelander Zeegat

WL | DELFT HYDRAULICS

H4918.39

Fig. 3.15a

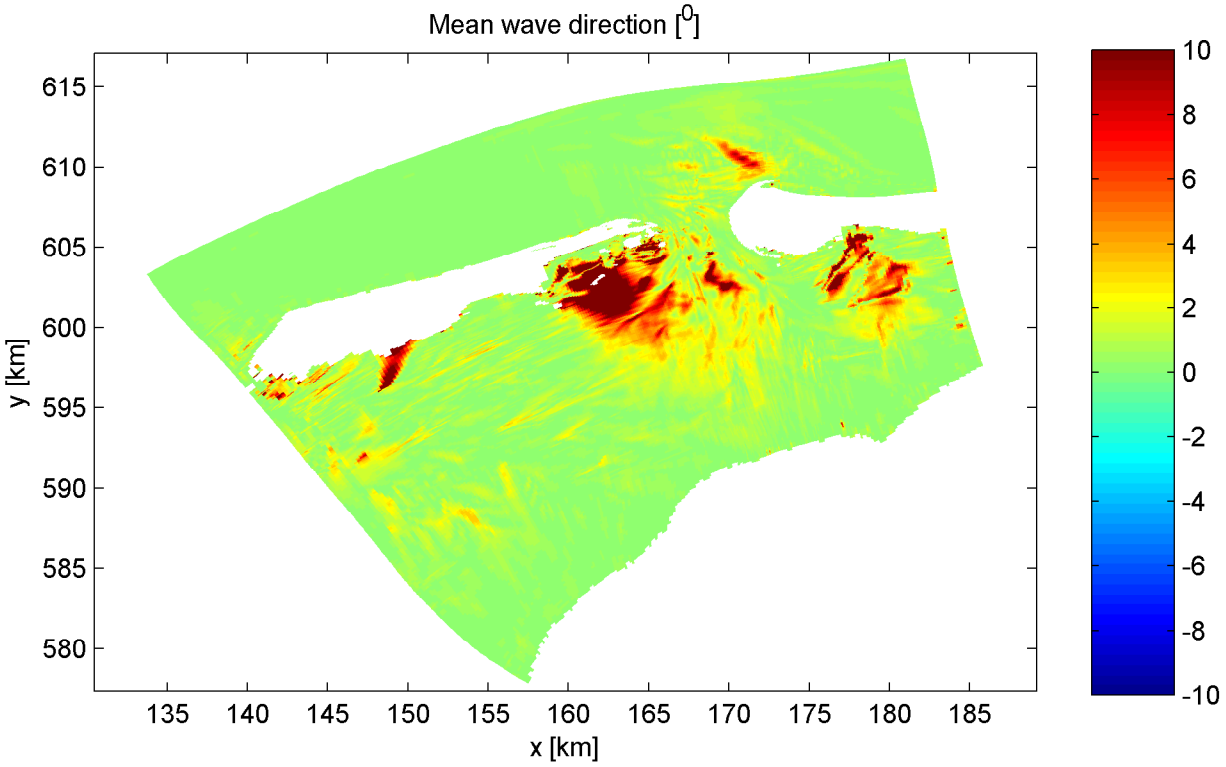

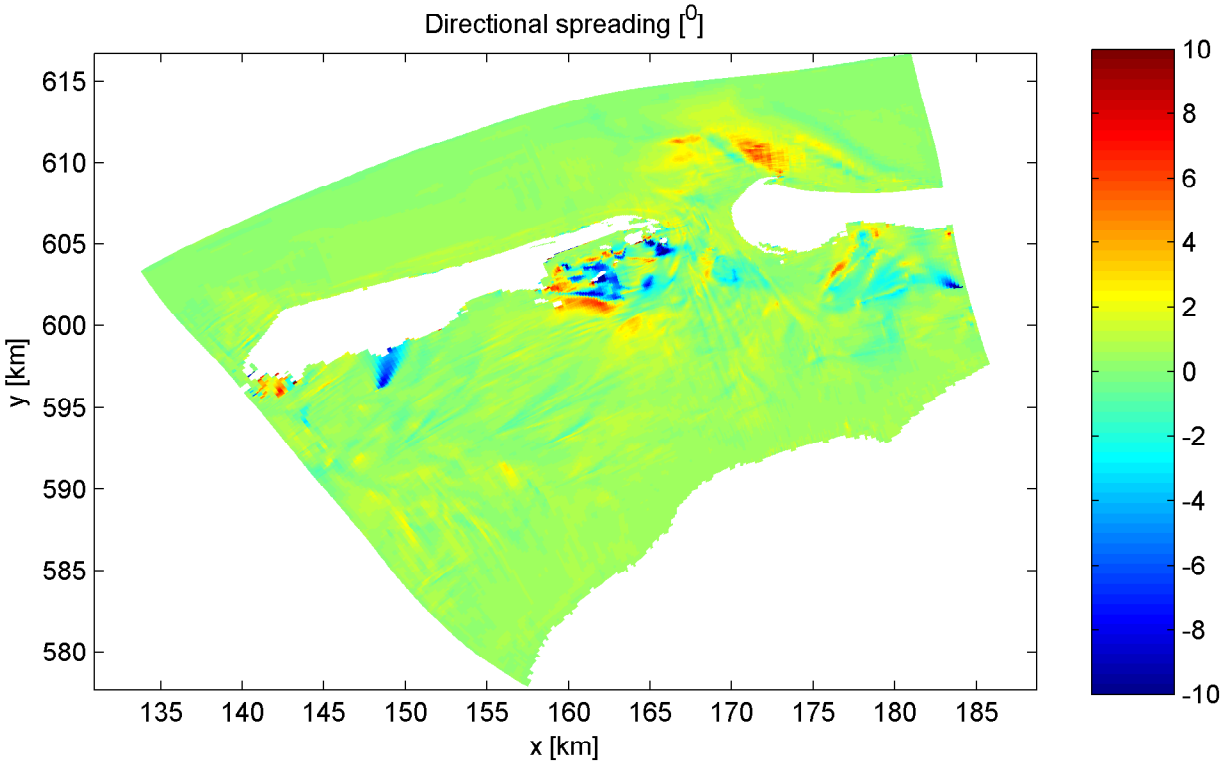

Mesh differences $\phi(\Delta\theta=10)$ - $\phi(\Delta\theta=5)$ in Amelander Zeegat

WL | DELFT HYDRAULICS

H4918.39

Fig. 3.15b

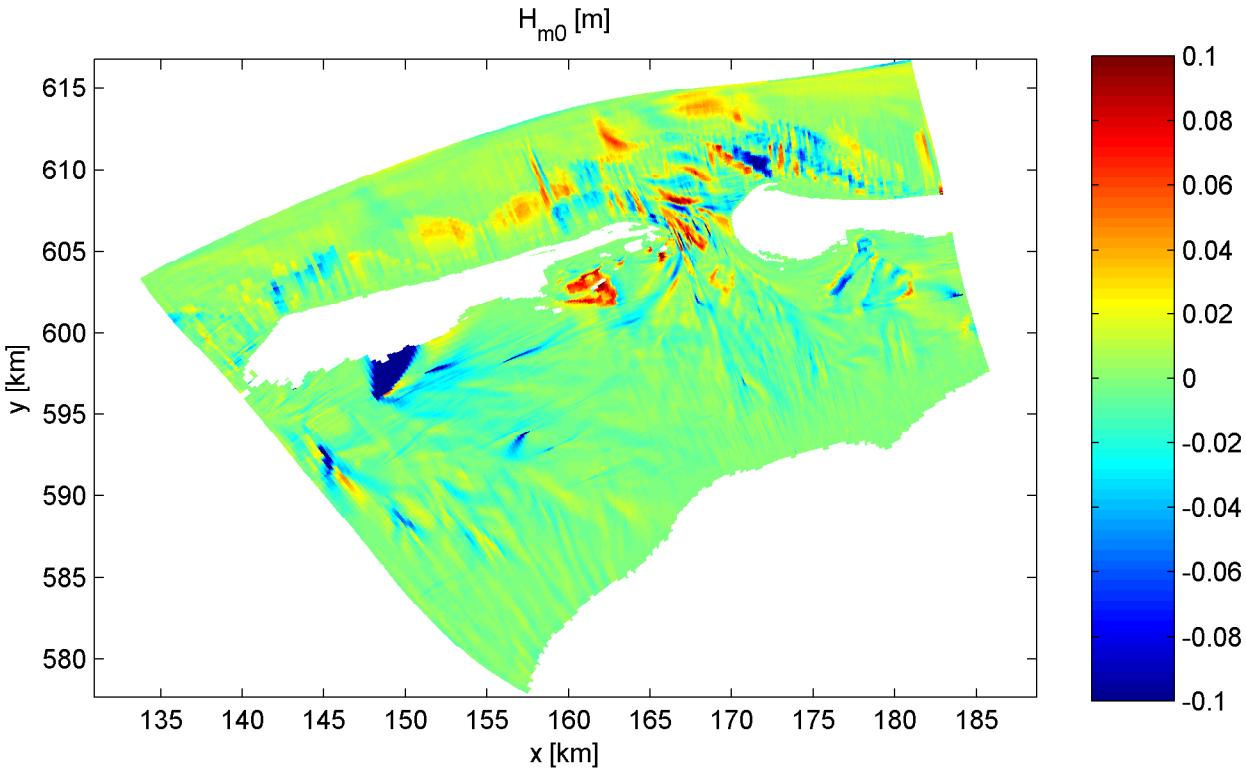

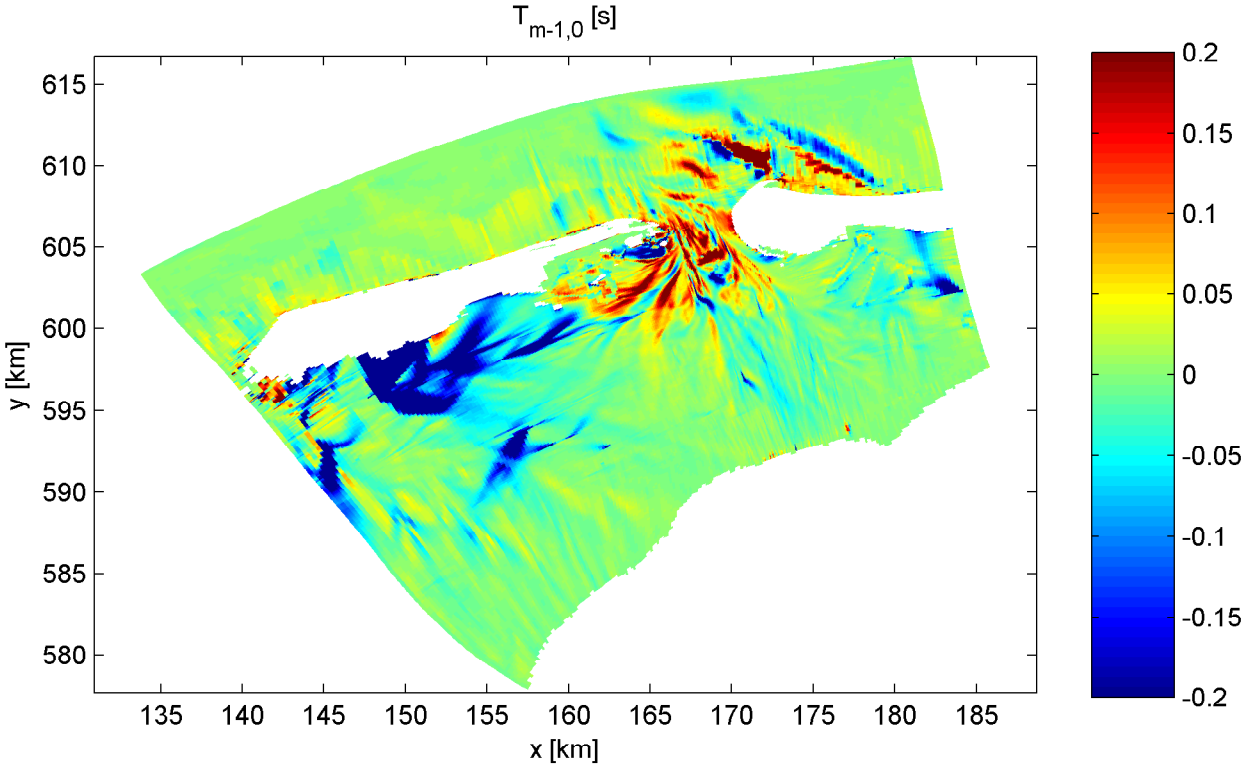

Mesh differences $\phi(\Delta\theta=8)$ - $\phi(\Delta\theta=4)$ in Amelander Zeegat

WL | DELFT HYDRAULICS

H4918.39

Fig. 3.16a

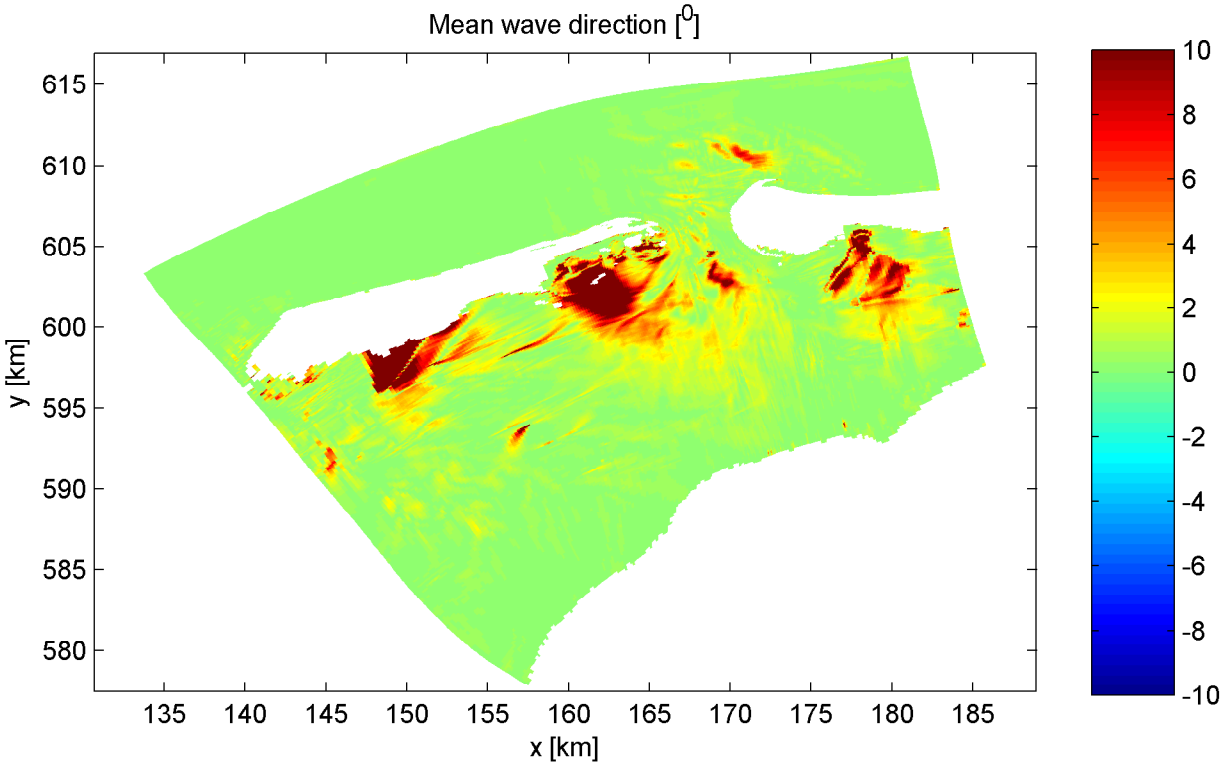

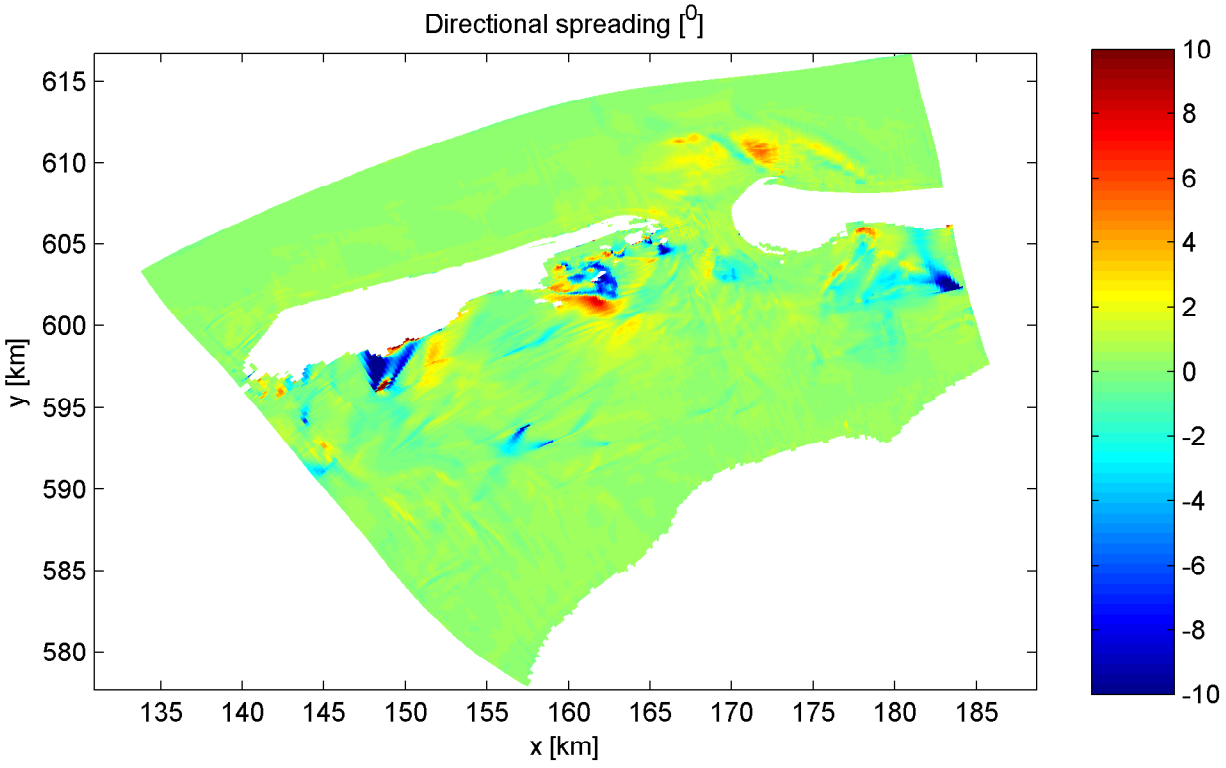

Mesh differences $\phi(\Delta\theta=8)$ - $\phi(\Delta\theta=4)$ in Amelander Zeegat

WL | DELFT HYDRAULICS

H4918.39

Fig. 3.16b

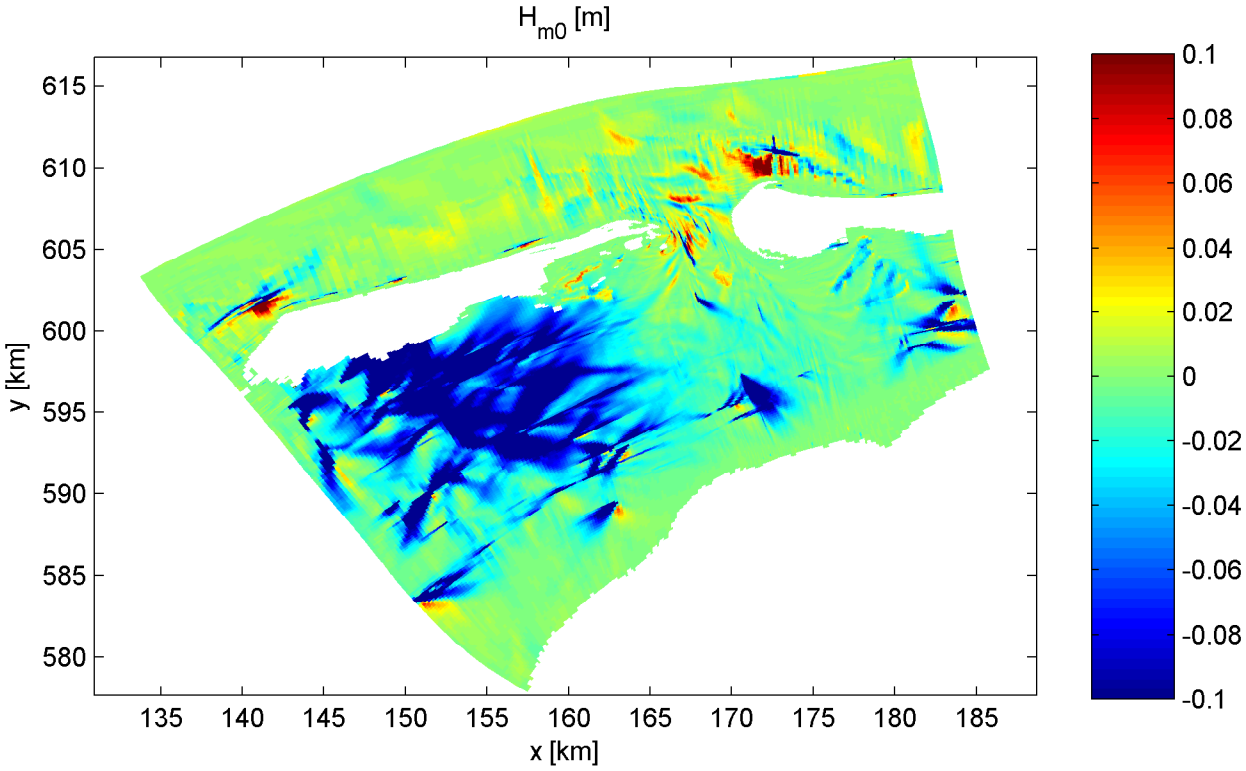

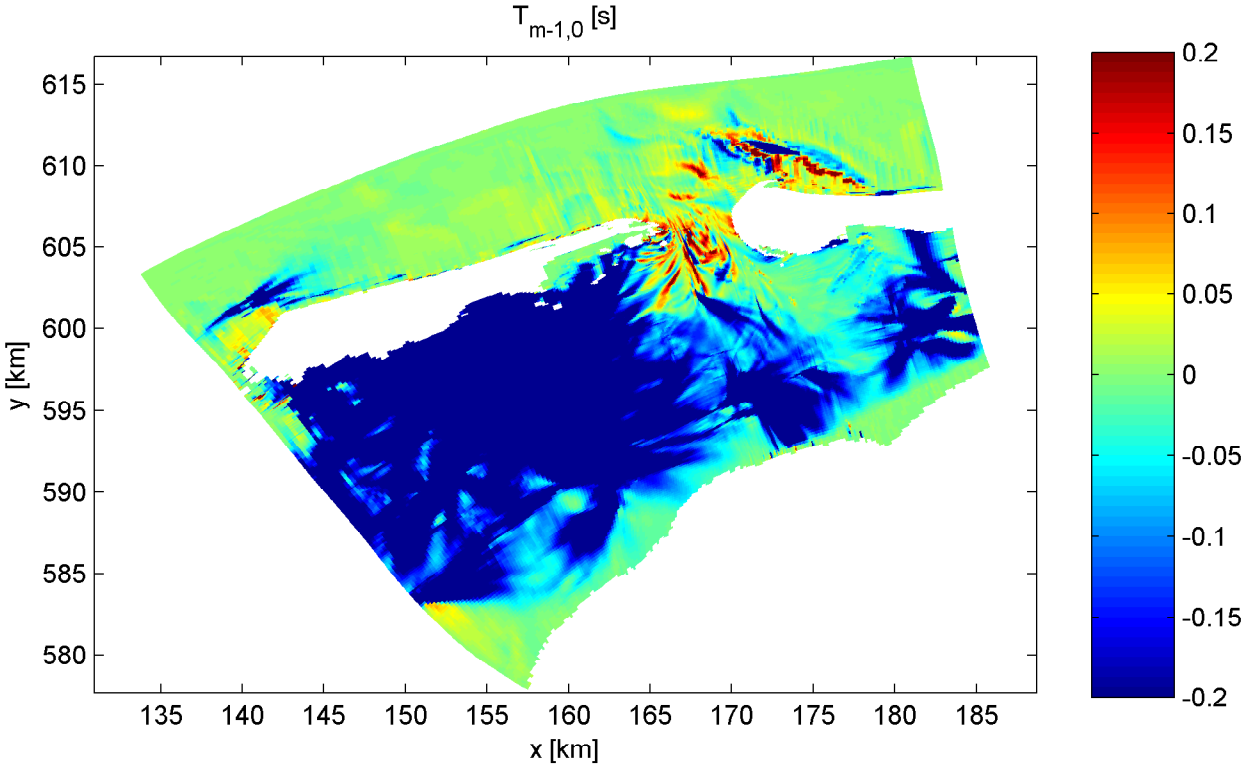

Mesh differences $\phi(\Delta\theta=5)$ - $\phi(\Delta\theta=2.5)$ in Amelander Zeegat

WL | DELFT HYDRAULICS | H4918.39 | Fig. 3.17a

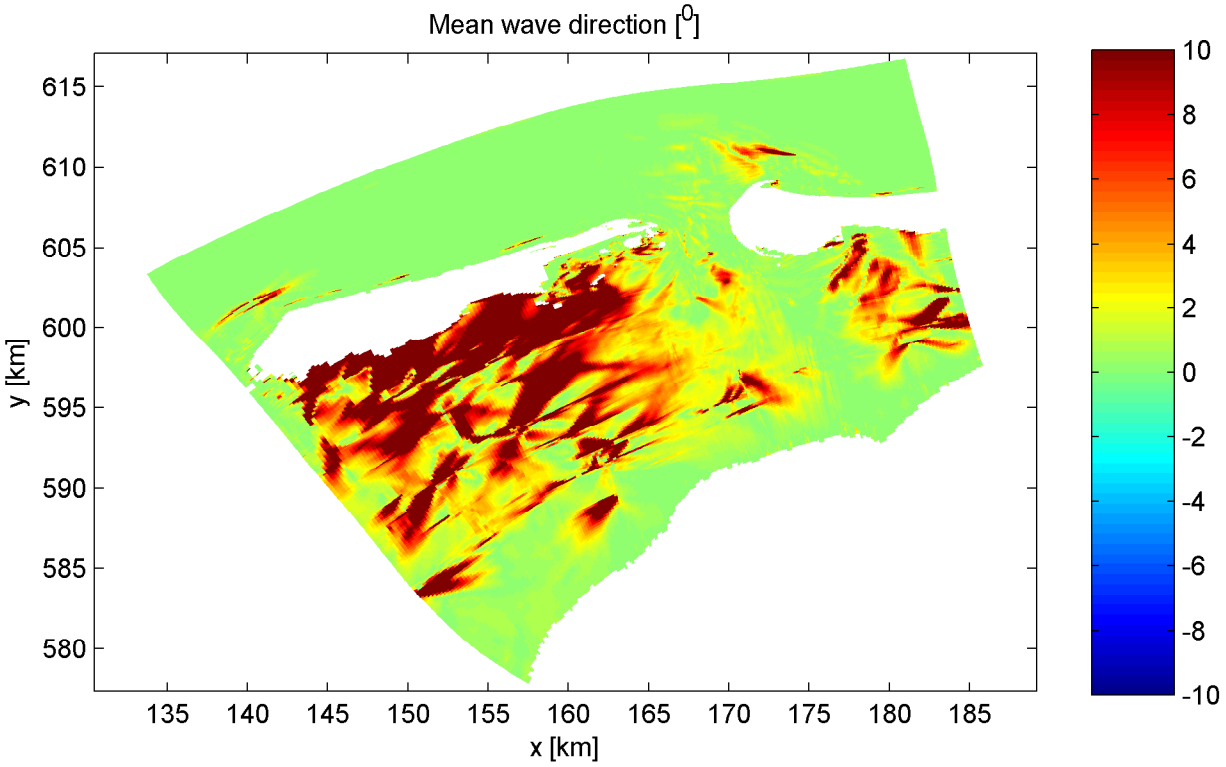

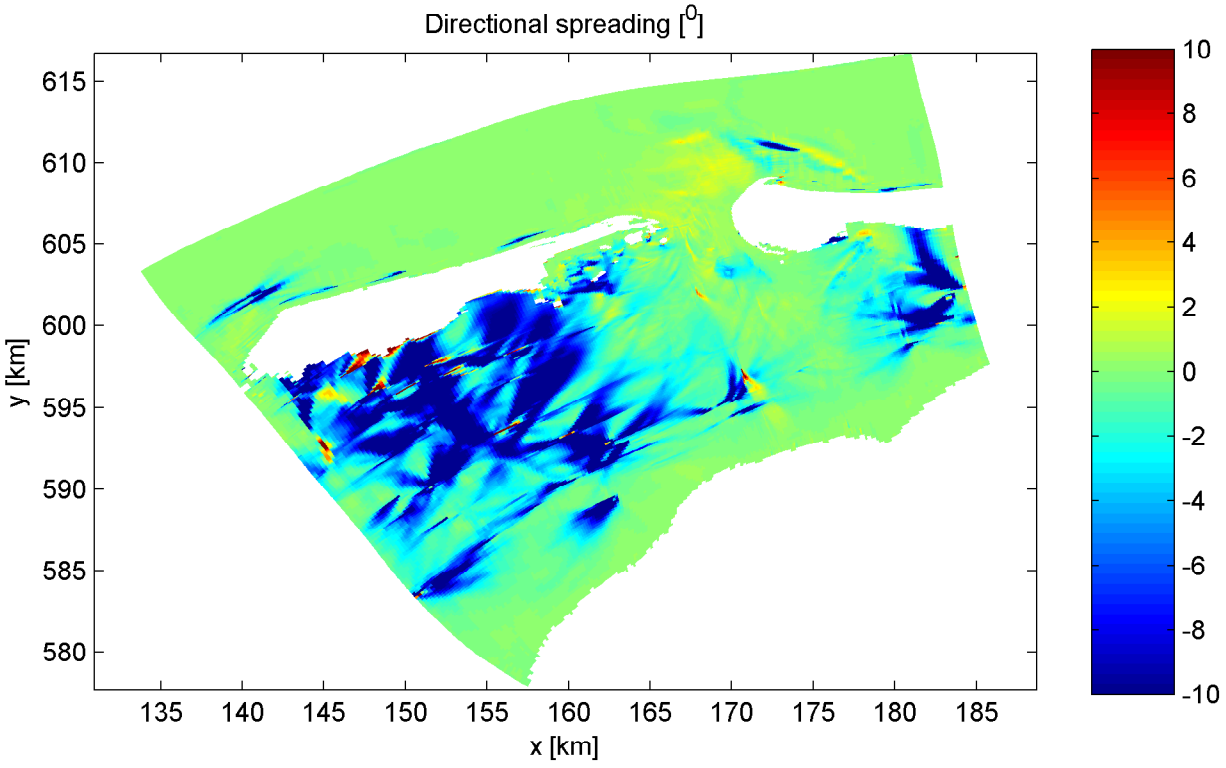

Mesh differences $\phi(\Delta\theta=5)$ - $\phi(\Delta\theta=2.5)$ in Amelander Zeegat

WL | DELFT HYDRAULICS | H4918.39 | Fig. 3.17b

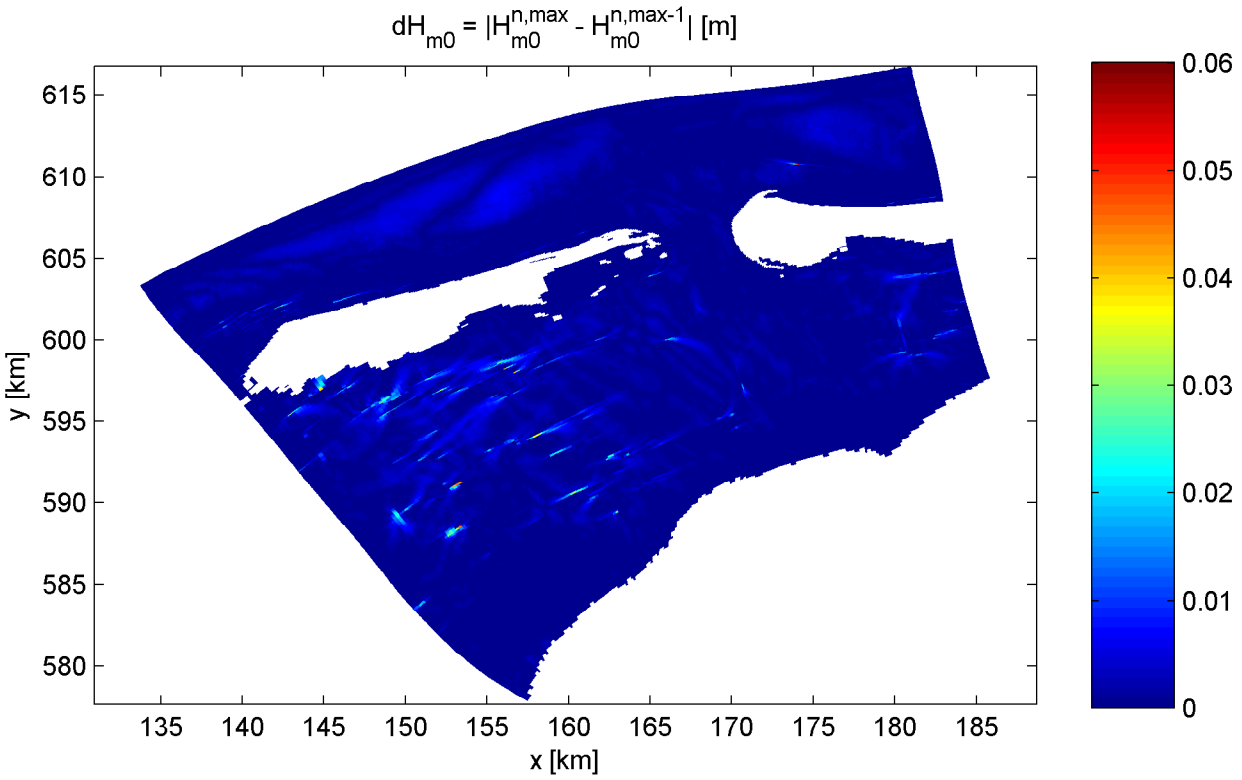

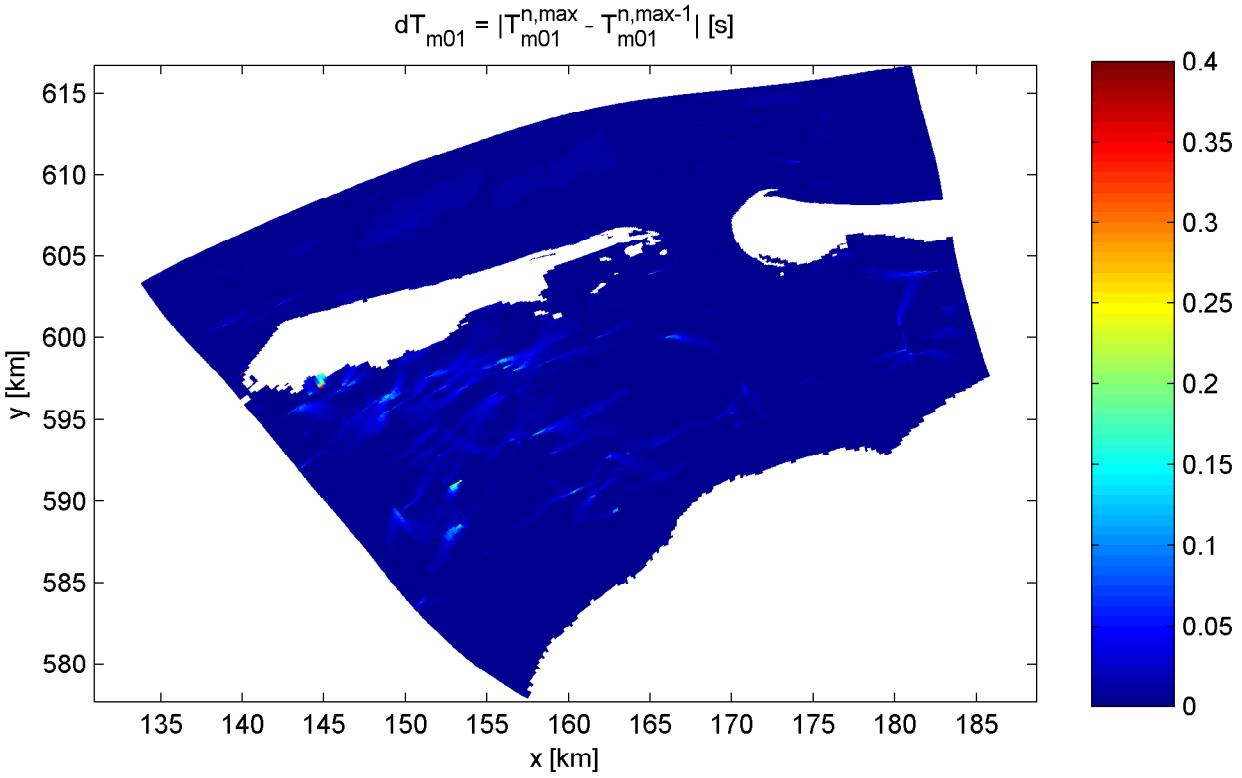

Change in final iteration ($|\phi^{(n,max)} - \phi^{n,max-1}|$) of solution in Amelander Zeegat with $\Delta\theta$ = 2 deg

WL | DELFT HYDRAULICS

H4918.39

Fig. 3.19

WL | Delft Hydraulics

Rotterdamseweg 185
postbus 177
2600 MH Delft
telefoon 015 285 85 85
telefax 015 285 85 82
e-mail info@wldelft.nl
internet www.wldelft.nl

Rotterdamseweg 185
p.o. box 177
2600 MH Delft
The Netherlands
telephone +31 15 285 85 85
telefax +31 15 285 85 82
e-mail info@wldelft.nl
internet www.wldelft.nl